This thesis has been submitted to

Department of Materials Technology

Norwegian University of Science and Technology

in partial fulfilment of the requirements for the degree

Philosophiae Doctor

October 2007

Acknowledgements

The present work was carried out at the Department of Materials Science and Engineering at NTNU as a part of the Strategic University Program – SUP in Light Metals Technology from 2004 till 2007.

I would like to express my gratitude to Professor Geir Martin Haarberg, my main supervisor for the guidance in scientific field as well as for his support, advices and witty approach in practical things regarding my stay in Norway throughout those years.

My sincere thanks belong to Dr. Ana Maria Martinez from SINTEF Materials and Chemistry who co-supervised this work and was anytime willing to share her time and patience in encouraging discussions not only about sulphur.

I would also like to thank to Professor emeritus Jomar Thonstad for all provided information and helpful discussions that walks always hand in hand with his kindness and patience.

I wish to thank to Professor Pavel Fellner, Dr. Marta Ambrová and Associate Professor Ján Cvengroš from STU in Bratislava who provided me with encouradgement that resulted to a decision to arrive to Norway.

Special thanks belong to Professor Yasuhiko Ito and to Associate Professor Masatsugu Morimitsu from Department of Environmental System Science at Doshisha University in Japan for giving me and to my colleague the possibility to carry out the electrochemical experiments of carbon deposition in their laboratories, for showing us the beauty of their country and making our time in Japan unforgettable and enjoyable. I would also like to thank to Associate Professor Masatsugu Morimitsu who took the time to read through my thesis and whose comments and advices were highly appreciated.

Furthermore, I am deeply grateful to all people and colleagues from the department who friendly welcomed me in their group and have become my friends. Especially I am very thankful to Martha Bjerknes and Kjell Røkke who took care of administrative and practical concerns anytime I asked for their help and who never let my Norwegian fade. I also want to thank to Espen Sandnes and Eirin Kvalheim for the lessons about molten salt electrochemistry and for the enthusiasm and good humour they always brought to the laboratory. My gratitude is also given to Sten Yngve Larse, Kristin Vasshaug, Karen Sende Osen, Stein Trygve Briskeby, Lars Erik Owe, Axel Baumann Ofstad, Ingrid Anne Lervik and Dr. Mikhail Tsypkin for all their help. I also appreciate the assistance

from Dr. Arne Petter Ratvik for the effort and countless attempts to make the gas chromatograph work.

The Research Council of Norway is gratefully acknowledged for the financial support.

Finally I would like to thank to my “Czecho-slovak” friends: Martin Keppert, Michal Tkáč, Juraj Chmelár, Marián Palcút, Janka Poplsteinová Jakobsen, Dorota Dudášová and Svatopluk Chytil who always offered their helpful hand, were source of the neverending optimism and support and who became my family here in Norway.

Finally I wish to thank to my family and to Jorge for all their love, understanding and encouragement during these years.

Trondheim, October 2007
Jana Hajasova

Summary

The behaviour of sulphur containing species has been investigated during the last few decades in various molten chloride and fluoride electrolytes but their effect on the performance of the cells producing aluminium still remains a subject of controversy. In the present work the electrochemical behaviour of sulphur containing species was studied in various molten chlorides and fluorides with the aim to contribute to a better understanding of the behaviour of sulphur impurities in the Hall-Héroult process.

The sulphur electrochemistry and chemistry in the systems containing molten electrolytes are of interest for aluminium electrowinning because of the serious impact of the sulphur containing gases on the environment and the effect of sulphur compounds on the efficiency of the electrolysis. The complexity of the sulphur chemistry is briefly summarised in chapter 2.1.

The literature review focused on the electrochemistry of sulphur species in molten salts is discussed in chapter 2 while chapter 3 is dealing with the description of the electrochemical and analytical methods used in this study.

Preliminary experiments in electrolytes consisting of molten NaCl and mixtures of NaF-AlF_3 revealed the necessity to find an inert electrode material for electrochemical studies. Platinum in the chloride melts and gold in the fluoride systems were selected as the most suitable materials for the working electrodes.

The behaviour of the anions containing sulphur in various oxidation states was investigated by means of cyclic voltammetry and chronoamperometry and is described in chapter 4.3. The behaviour of sulphate anions was studied in a single NaCl melt and compared with the molten $CaCl_2$-NaCl (10-90 mol%) mixture at 840 ºC. It was found that the sulphate reduction proceeds differently in these two electrolytes which was ascribed to the difference in the oxoacidity of the melts. The number of electrons transferred during sulphate (S^{VI}) reduction in pure NaCl melt was found to be two with probable sulphite formation which possibly decomposed to sulphur oxide. In the molten $CaCl_2$-NaCl mixture sulphate seemed to be transformed to SO_3 which is further reduced in a one-electron exchange. The electrochemical signals recorded in the voltammograms also suggested that the character of the reduction products involved in those two melts is different. However, the “ec” mechanism, where a charge transfer is followed by a chemical reaction seemed to be the common feature in both electrolytes. The sulphate reduction was also studied in the eutectic LiCl-KCl mixture in the range of temperatures from 450 ºC to 840 ºC. In spite of the fact that the sulphate solubility seemed to rapidly decrease at temperatures below 700 ºC, the possible presence of a chemical reaction taking place after the reduction process of

sulphate anions was suggested to be very similar to that found in molten NaCl. From the analysis of the data obtained by cyclic voltammetry followed that the reduction of sulphate anions to a lower oxidation state is probably diffusion controlled in all the three above mentioned systems at the sweep rates where the effect of the coupled chemical reaction can be neglected. Chapter 4 also includes an additional investigation of the behaviour of the sulphite and sulphide anions in the eutectic LiCl-KCl mixture.

Chapter 5 is devoted to the investigation of the sulphate species in the NaF-AlF_3 mixtures saturated by Al_2O_3 with varying cryolite ratio, i.e. CR = 3, 2, 1.5 and 1.2. It contains a description of sulphate modification at various experimental conditions and revealed its complicated and complex electrochemical behaviour which was monitored by cyclic voltammetry, chronoamperometry and square wave voltammetry. For the electroactive species in the electrolyte with CR equal to 3 two reduction steps were suggested involving three and two electrons respectively. The "ce" reaction mechanism was assumed where a chemical reaction seems to precede a charge transfer. The chemical step might be the partial decomposition of sulphate to SO_2. The sulphate reduction in the electrolyte with CR = 2 appeared to be considerably different. Since the temperature difference in these two systems is only 40 ºC the reason was likely to be due to the higher concentration of AlF_3 in the electrolyte. In this electrolyte only one cathodic process was observed and the reaction mechanism involving three electrons with a preceeding chemical reaction was suggested. Because the production of aluminium metal in the electrolysis cells operating with inert anodes is an attractive idea and have opened a question about the behaviour of sulphur species in very acidic electrolytes (high AlF_3 content) a part of the present studies was devoted to the study of the electrochemical behaviour of the sulphate anions in the electrolytes with CR = 1.5 and 1.2. Cyclic voltammetry and square wave voltammetry revealed that the sulphate is then reduced in two cathodic steps. Simulations and the obtained square wave voltammograms indicated that the cathodic process probably involves more electrons in the very acidic NaF-AlF_3 mixtures than in electrolytes with higher CR equal to 3 or 2. Observation of volatile species formed in the NaF-AlF_3 mixtures with CR = 1.5 and 1.2 was revealed as another important difference. This could be due to the formation of sulphur which at high temperature is present in the gaseous form and thus likely to escape from the laboratory furnace. The difference in the electrochemical behaviour of the sulphate anions in the cryolitic based melts was related to the difference in the bath composition and experimental temperature.

The present study shows the complexity and variability in the electrochemical behaviour of sulphur containing species as well as the difficulties and limitations resulting from the sulphur chemistry in the molten salts at high temperatures.

Table of contents

List of Symbols and abbreviations

Symbols

a_i	activity of species I	
A	area of the electrode	[cm^2]
ΔA	square wave amplitude	[mV]
c_i^0	concentration of species i at the electrode surface	[$mol.cm^{-3}$]
c_i^∞	concentration of species i in the bulk of the solution	[$mol.cm^{-3}$]
dI_p	differential peak current	[A]
D_i	diffusion coefficient of specie I	[$cm^2.s^{-1}$]
E^{rev}	reversible potential	[V]
E^θ	standard potential	[V]
E_d	decomposition potential	[V]
E_p	peak potential	[V]
$E_{p/2}$	half-peak potential	[V]
ΔE	peak separation	[V]
f	frequency	[s^{-1}]
F	Faraday constant	[$C.mol^{-1}$]
ΔG^θ	standard Gibbs energy	[$J.mol^{-1}$]
I	current	[A]
I_{lim}	limiting current	[A]
I_p	peak current	[A]
i	current density	[$A.cm^{-2}$]
i_0	exchange current density	[$A.cm^{-2}$]
i_p	peak current density	[$A.cm^{-2}$]
k	rate konstant	[$cm.s^{-1}$]
k^θ	standard rate konstant	[$cm.s^{-1}$]
n	number of electrons	
R	gas constant	[$J.K^{-1}.mol^{-1}$]
t	time	[s]
T	temperature	[°C]
v	sweep rate	[$V.s^{-1}$]
x	distance	[cm]
$W_{1/2}$	half-width of the peak in SQWV	[V]
z_i	charge number on ion	
α	transfer coefficient	
η	overpotential	[V]

Abbreviations

CA	chronoamperometry
CE	counter electrode
CR	cryolite ratio
CV	cyclic voltammetry
DS	dry scrubber
OCP	open circuit potential
RE	reference electrode
SQWV	square wave voltammetry
WS	wet scrubber
WE	working electrode

1 Introduction

1.1 Aluminium. Characteristics and production

Aluminium is the world's most abundant metal and is the third most common element, comprising 8% of the earth's crust. The versatility of aluminium makes it the most widely used metal after steel. The worldwide demand for aluminium metal has grown to around 29 million tonnes per year. The total world production of primary aluminium was more than 23 million tonnes in 2006 [1]. Approximately 7 million tonnes are annually recycled as the aluminium scrap.

Aluminium is a soft, nonmagnetic, lightweight metal with normally a dull silvery appearance. It is remarkable for its excellent corrosion resistance and durability because of the protective oxide layer. Aluminium is about one-third as dense as steel or copper. It is the second-most malleable metal (after gold) and the sixth-most ductile. It can be easily machined and cast. It has good thermal and electrical properties too.

By utilising various combinations of its advantageous properties such as strength, lightness, corrosion resistance, recyclability and formability, aluminium is being employed in an ever-increasing number of applications in many industries to manufacture a large variety of products. There are also possibilities to readily form alloys with many elements such as copper, zinc, magnesium, manganese and silicon to provide the higher strengths, which makes it very important to the world economy. Structural components made from aluminium and its alloys are vital to the aerospace industry. It is very important in the areas of transportation (car, marine and rail industry) and construction. It is used for a wide range of electrical applications such as overhead lines, electrical energy distribution and transportation cables. Aluminium has found its utilizations also in packaging applications (foils and cans) and in our households or the restaurants as cookware.

Although aluminium compounds have been used for thousands of years, aluminium metal was first produced around 170 years ago. This is because in nature it only exists in very stable combinations with other materials (particularly as silicates and oxides). Nowadays the industrial aluminium production is based upon the Hall-Héroult process which was independently developed and patented in 1886 and named after its inventors: Charles Martin Hall (USA) and Paul Louis Touissaint Héroult (France). The commonly used raw material for aluminium electrowinning is aluminium oxide (alumina). The principle of aluminium production is based on the dissolution of alumina (Al_2O_3) in an electrolyte of fluorides, mainly containing liquid cryolite (Na_3AlF_6), and its instant

electrochemical reduction by carbon. The overall chemical reaction of alumina dissolution and reduction with the reversible decomposition potential is given in Equation 1.1. Liquid aluminium metal is formed on the cathode and the primary anode product is CO_2. At very low current densities CO evolution will occur too [2, 3].

$$1/2Al_2O_{3(dissolved)} + 3/4C_{(s)} = Al_{(l)} + 3/4CO_{2(g)} \qquad E^{rev}_{1250\,K} = -1.18\ V \qquad 1.1$$

The source of the carbon is the anodes which are immersed into the bath. Today, two types of anode design are in use; the prebaked anodes which are more commonly used during the last decades due to their operational advantages and the self baking Söderberg anodes. A schematic drawing of a reduction cell with prebaked anodes is shown in the Figure 1.1. The prebaked anodes are made from a mixture of petroleum coke aggregate and coal tar pitch as a binder and baked in separate anode baking furnaces at about 1100 ºC. The Söderberg anodes are produced from petroleum coke and higher content of coal tar pitch and are continuously baked in the aluminium production cell.

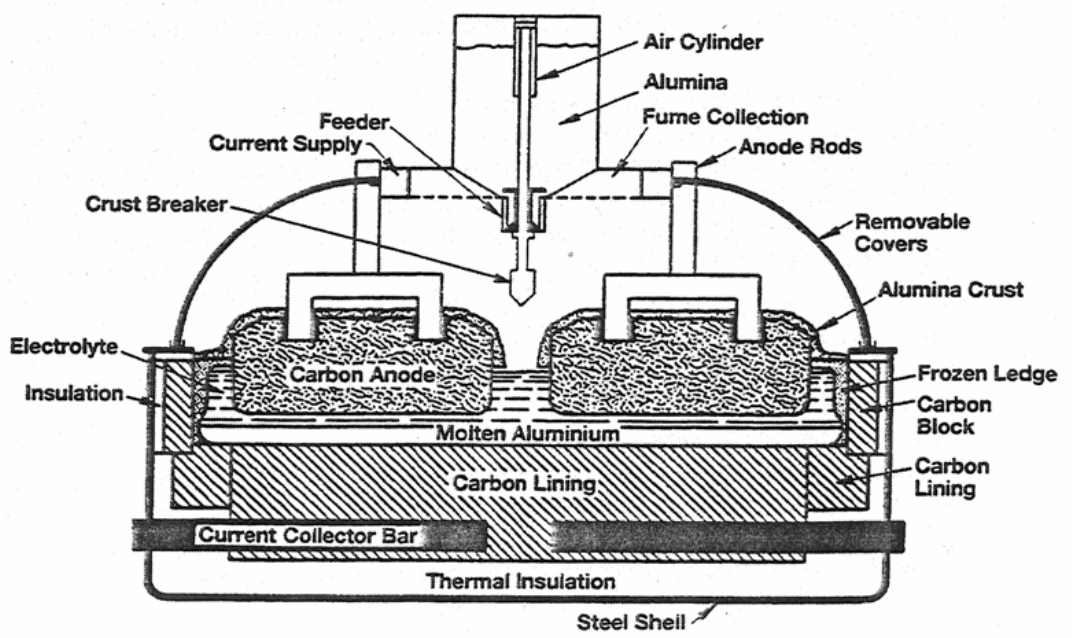

Figure 1.1 Electrolysis cell with prebaked anodes [2]**.**

Modern aluminium plants nowadays operate with 150 to more than 300 cells connected in series mostly side by side to reduce the magnetic effect. Most of them have typically 20 to 40 prebaked anodes per cell positioned horizontally in the bath. Because the anodes are consumed usually after 20-28 days they have to be replaced by new ones. This operation would be avoided if "inert" (not consumable) anodes were introduced to the process. In such case the oxygen would be evolved on the anode instead of CO_2 and the primary cell reaction,

written in Equation 1.2, will take place. Introduction of such anodes into the process will indeed lead to 1 V higher decomposition potential than for a cell with carbon anodes.

$$1/2Al_2O_{3(dissolved)} = Al_{(l)} + 3/4O_{2(g)} \qquad E^{rev}_{1250\ K} = -2.21\ V \qquad 1.2$$

The cathode is in fact a pool of liquid aluminium with a depth of 15-40 cm and placed just below the electrolyte approximately 4-5 cm from the bottom of the anode. It is surrounded by carbon lining which carries the electric current from the metal to the collector bars. It is placed inside a steel shell.

The main component of the industrial electrolyte is cryolite because of its good solvent properties for alumina. Cryolite dissociates in molten phase into Na^+ and AlF_6^{3-} ions. A fraction of the latter complexes dissociate further into F^-, AlF_4^- or AlF_5^{2-}. Aluminium ions bound in such fluoride complexes are transported by diffusion to the cathode and discharged at the electrolyte-metal interface, according to Equations 1.3 and 1.4.

$$AlF_6^{3-} + 3e^- = Al + 6F^- \qquad 1.3$$

$$AlF_4^- + 3e^- = Al + 4F^- \qquad 1.4$$

Sodium cations migrate towards the cathode and NaF diffuses back to the electrolyte. Even though the sodium ions carry most of the charge through the bath, for electrochemical reasons aluminium deposition is favoured over sodium. Besides cryolite the electrolyte is usually modified by additives which improve the physico-chemical properties, such as lower metal solubility, increased electrical conductivity, lower density, vapour pressure and the liquidus temperature. The commonly used additives are aluminium fluoride (AlF_3) used in amount of 6 to 13 weight % and calcium fluoride (CaF_2) 4 to 6 weight %. In some cases also 2 - 4 weight % lithium fluoride (LiF) and/or magnesium fluoride (MgF_2) are added. The surplus of AlF_3 in the melt is normally expressed as cryolite ratio CR (the molar ratio of NaF and AlF_3) or as a bath ratio (the mass ratio of NaF and AlF_3). The electrolyte height in the cell is about 20 cm and the temperature during cell operation is usually between 955 and 965 ºC depending on the bath composition.

Aluminium oxide or alumina can be principally found in bauxite which is the most important and presently dominating ore from which alumina is recovered in a multistep operation called the Bayer process. Bauxite contains largely Al_2O_3 (40-60%) found in the hydrous phases e.g. gibbsite, ($Al(OH)_3$), boehmite, AlO(OH) and diaspore ($Al_2O_3.H_2O$). Alumina seems to be dissolved in the melt in the form of aluminium-oxygen-fluorine anions, $Al_2OF_x^{(4-x)}$ at low alumina

concentrations and $Al_2O_2F_x^{(2-x)}$ at high alumina concentrations. The oxide ions from dissolved alumina complexes are adsorbed and oxidised on the anodes. The product of their discharge further reacts with the carbon of the anodes and thus gradually consumes them forming gaseous carbon dioxide. The discharge of the Al-O-F species at high alumina concentration is described in Equations 1.5 and the reaction at low alumina concentration is written in Equation 1.6.

$$Al_2O_2F_4^{2-} + 4F^- + C = CO_2 + 4e^- + 2AlF_4^- \quad 1.5$$

$$2Al_2OF_8^{4-} + C = CO_2 + 4e^- + 4AlF_4^- \quad 1.6$$

Alumina is fed to the cells through so called “point feeders” in regular intervals to keep its concentration within the range of 2 to 4 wt %. If the amount of added alumina is insufficient, anode effect may occur. It leads to increase of the cell voltage at which the fluoride components of the bath decompose electrochemically, which results in increase of the emissions and reduced current efficiency. Alumina is not only the actual raw material for aluminium production but it also serves as a thermal insulator on the top of the frozen bath. In the dry scrubbers, the gas cleaning facilities, it is used as an adsorbent for the gasses containing fluoride vapours and HF which are harmful for the environment. So it contributes to reduce the emissions and helps to reduce the fluoride losses from the bath when it enters the cell as fluoride enriched “secondary” alumina.

The production capacity for modern cell is about 2000 kgAl/day. Typical material consumption for 1 tonne Al produced is about 400-500 kg of carbon, 1900 kg Al_2O_3 and 20-30 kg AlF_3. Each cell can have individually controlled cell voltage and this is normally between 4.0 and 4.6 V [2]. Cells with prebaked anodes operate with applied current from about 175 kA to 350 kA of the largest ones. The energy consumption values are today close to 14.5 kWh/kg Al although the theoretical energy consumption is only 6.3 kWh/kg Al. The heat losses to the surroundings are responsible for such low energy efficiency below 50 %. Most of the cells operate at 90-96 % current efficiency. The main loss in current efficiency is due to the so-called “back reaction” between dissolved metal and the anode gas, written in Equation 1.7.

$$Al_{(dissolved)} + 3/2CO_{2(g)} = 1/2Al_2O_{3(dissolved)} + 3/2CO_{(g)} \quad 1.7$$

The other main reasons for the decrease of current efficiency are the earlier mentioned anode effect, dissolution of metallic sodium, oxidation of dispersed aluminium droplets in the electrolyte at anode, short circuiting and impurities. The decrease in the current efficiency caused by the impurities can be 2 % in a normal reduction cell [2].

1.2 Impurities in the process of aluminium electrowinning

Primary metal usually has a purity of 99.7 to 99.9 % Al [3]. The rest is species unintentionally introduced to the aluminium cells called impurities. They are fed to the melt together with the raw materials, e.g. alumina, carbon anodes, cryolite and the fluorides. Some of them come up from the cell operation or production equipment, e.g. additional source of iron is corrosion of tools, anode stubs and current leads; silicon can also come from the refractory lining or silicon carbide sidelining.

According to Grjotheim [4] all the impurities, to a varying degree, have an effect on the electrolysis. Impurities more noble than aluminium may tend to decompose electrolytically and deposit on the cathode where they contaminate the produced aluminium or they may be reoxidized at the anode and cause decrease in the current efficiency. Less noble impurities will tend to accumulate in the electrolyte where they can react with the components of the bath and thus modify the chemical composition of the melt. They may also interact with the carbon in the anodes or lining. Other impurities not so detrimental to aluminium production process are those which escape from the cells as harmful gases. They do not accumulate in the bath or in the metal therefore do not decrease the current efficiency neither lower the metal quality but they have negative impact on the environment.

Typical impurity concentrations data from different raw materials for year 2000 are listed in the Table 1.1 and Table1.2.

Table 1.1 Impurity concentrations in raw materials [3].

Impurity	Al_2O_3 [wt %]	Na_3AlF_6 [wt %]	AlF_3 [wt %]
SiO_2	0.007-0.020	0.12-0.13	0.10-0.15
Fe_2O_3	0.008-0.022	0.04-0.11	0.01-0.02
TiO_2	0.002-0.008	0-0.001	0.0008-0.0012
CaO	0.003-0.035		0.06-0.10
ZnO	0.001-0.011		
V_2O_5	0.0012-0.004	0.001-0.005	0.0002-0.0003
P_2O_5	0.0004-0.0011		0.015-0.020
Cr_2O_3	0.002		
Ga_2O_3	0.007-0.008		
Na_2O	0.3-0.45		0.10-0.15
K_2O	0.01-0.08		
H_2O		0.17-0.30	0.2-0.3
Ca		0-0.08	0.009-0.070
SO_4		0.54-0.69	0.9-1.5

Table 1.2 Impurity concentrations in petroleum coke [3].

Impurity	Concentration [ppm]	Impurity	Concentration [ppm]
Si	50-250	B	1
Fe	50-400	Na	30-120
Ti	2-50	Mg	100
Zn	2-20	Ca	20-100
V	30-350	Mn	4
Cr	1-2	Ga	14
Ni	50-220	Pb	3
Cu	1-3	Al	50-250
S	5000-35000	Ash	1000-2000

The major part of the impurities dissolves in the melt and the minor part leaves the cell as outlet in various ways; in the contaminated aluminium metal, as off gases or adsorbed on carbon, alumina or other material that is skimmed off. A substantial amount of the impurities is however recycled back to the process, mainly due to the dry scrubbers where gaseous and particulate impurities are collected and recycled.

All oxide impurities a exhibit certain solubility in molten cryolite and it was assumed that they dissolve according to Equation 1.8. Their concentration in the bath is normally well below their saturation [5].

$$M_xO_y + 2y/3AlF_3 = xMF_{2y/x} + y/3Al_2O_3 \qquad 1.8$$

Grjotheim [4] classified the impurities depending on their nature and divided them into several groups:

1. water as an impurity
2. metal oxides with higher decomposition potential than alumina
3. metal oxides with lower decomposition potential than alumina
4. non-metallic impurities
5. sulphur containing compounds

Water is partly introduced in the form of atmospheric moisture or enters the electrolyte with alumina and fluorides. The result of its reaction with fluoride is gaseous hydrogen fluoride which is harmful for the surrounding environment. Another deleterious effect of water on aluminium electrolysis is decrease of the current efficiency due to the dissolution and contamination of aluminium metal.
Typical metal oxides with higher decomposition potential than alumina are alkali and alkaline earth oxides. Theoretically they should not interfere with the cathodic process, but they can react with the constituent of the electrolyte by reaction 1.9 resulting in corresponding fluoride formation and increasing AlF_3

consumption. However, if the concentration of this type of metal oxide is sufficiently high to reduce the difference between the deposition potentials of the metal and aluminium, co-deposition of such metal is also possible which will decrease the current efficiency of whole process.

$$2Na_3AlF_6 + 3MO = 3MF_2 + 6NaF + Al_2O_3 \qquad 1.9$$

Calcium ions can act as such an example. Ca comes from alumina. Partly it leaves the cell in the gas phase and is deposited in the produced aluminium but some Ca diffuses away through the carbon cathode. After some time Ca level reaches a steady state concentration in the electrolyte. Other examples of this group of oxides are magnesium and lithium oxides. Magnesium oxides reduce the electrical conductivity of aluminium while Li affects the corrosion resistance of the product. Sodium was found to increase its content in the deposited metal with increasing cryolite ratio and operating temperature. It penetrates also into the carbon and causes serious deterioration of the cell lining and contributes to the shorter cell life time.

The third group of the impurities is represented by the metals more noble than aluminium and soluble in it. They will tend to be reduced on the cathode electrochemically according to the Equation 1.10 to the metallic state. Hence they are responsible for most of the aluminium contamination when alloying with it, e.g. Si and Fe being the major contaminants originating from the tools and production equipment.

$$3M^{x+} + xAl = 3M_{inAl} + xAl^{3+} \qquad 1.10$$

For Fe it was shown that it's transport from bath to metal is mass transfer controlled [6]. Iron affects the mechanical properties, deformation, recrystallization and conductance of the final metal. For some impurities, e.g. Ti, V, Cu, and Zn the maximum concentrations in the produced metal are specified and must be strictly met because of their negative influence on the quality of the product. Because of this side alloy formation, some technologically interesting possibilities were suggested to utilize it for direct aluminium alloys production for a few metals. Beside the above mentioned metal contamination, all impurities of this group decrease the current efficiency of the process partly due to the consumption of current which otherwise would be used for aluminium production, or due to the reduction of Al consumed by the reaction 1.10. The impurities of this group, unlike the alkali and alkaline earth oxides, do not accumulate in the electrolyte and they are neither quantitatively transferred to the aluminium as it might be expected. Goodes and Algie [7] in their laboratory study showed that the transfer of these group of impurities between bath and metal is not complete. In fact a large proportion escapes from the furnace in the

form of volatile compounds (see Table 1.3) or they are attached on the carbon dust.

Table 1.3 Impurities mass balance and distribution per unit of metal [8].

Input [ppm]	**Si**	**V**	**Fe**	**P**	**Ti**	**Zn**	**Ga**
Alumina	123	24	348	16	67	60	131
Carbon	173	33	227	4	3	1	2
Bath components	19	2	31	5	1		
Miscellaneous	200		223				
Feed sum	515	59	829	25	71	61	133
Output [ppm]							
Gas	42	38	378	18	41	12	66
Metal	473	20	451	3	25	48	65
Total sum	515	58	829	21	66	60	131

Boron and phosphorus oxides are the main representatives of the non-metallic oxides group. Even though boron decomposes electrochemically it has favourable effect on the quality of Al because it helps to reduce the content of heavy metals. Sometimes it is therefore added to aluminium to remove V and Ti as deposited borides [9]. Phosphorus oxide, on the other hand, is one of the most dangerous impurities. It can be reduced both electrochemically and chemically by aluminium and even at low concentration it lowers the corrosion resistance and increases the brittleness of the metal. The most remarkable negative effect of phosphorus is the decrease in current efficiency. It was reported and generally accepted by several authors [10-13] that 100 ppm of phosphorus can decrease current efficiency of about 1 %. Because this value is too high to be due to only chemical and electrochemical reduction of phosphorus, it was suggested a reduction of P to P^{5+} and its reoxidation in cyclic redox reactions [10, 14]. The explanation for such cyclic processes lies in industrial cells where gaseous P can condense and be reoxidized on the external part of the crust and then after entering the bath be reduced again. One more negative effect of P_2O_5 on the electrolysis is the improvement of wetting of dispersed carbon particles in the electrolyte which may result in overheating of the electrolyte.

The last but quantitatively the most significant impurity in Grjotheim`s classification is sulphur and sulphur containing species. They are introduced into the process together with the raw materials and leave the electrolysis cell as harmful and environmentally polluting gases. Chapter 1.3 discusses this impurity and its effect on the industrial process and serious environmental hazard potential in more detail.

Aluminium reduction cells are normally equipped with dry scrubbing system which was developed in the late 1960s. Beside environmental improvement not only in the neighbourhood of the smelters the major advantage of dry scrubber installation was the possibility to collect and recycle an escaping and expensive fluoride material back to the process. Primary alumina floating through the dry scrubbers acts as sorbent for the removal of gaseous and particulate fluorides from anode gases with a collection efficiency higher than 99 % [2]. Such enriched secondary alumina is then used as feed material. The alumina, however, retains also SO_2 and various polyaromatic hydrocarbons as well as heavy metals in the form of solid particles or gaseous molecules. However, dry scrubbers brought some disadvantages too. After their installation the level of impurities, e.g. P, V, Fe, Ni, Cu, Pb, Ga, Ti, Cr and to a minor extent also Mn, Zn, Zr, Sn and Co increased in the metal and in the electrolyte when they were collected and recycled together with the fluorides. The data showing this effect are given in Table 1.4. Consequently this has lead to a lower current efficiency and decreased metal quality.

Table 1.4 Impurities concentration and the increase in metal contamination caused by dry scrubbers [15].

Impurity source [ppm]	**Fe**	**V**	**Ni**	**Cu**	**Pb**	**Ga**
Fresh alumina	80	30	22	72	13	50
DS alumina	500	105	250	160	70	60
Anodes	600	140				
Bath	40	10	5	25	6	7
Metal without DS	500	52	14	28	20	62
Metal with DS	860	95	44	55	42	85
Increase due to DS	360	46.6	30.3	26.7	21.7	22.7

Presently, a substantial part of impurities concentrated in the finest fraction of secondary alumina is partly removed together with the fines or by the electrostatic precipitators which are installed in front of the dry scrubbers to eliminate the above mentioned problems in current efficiency and metal purity. However, all these cleaning systems reduce the impurities recirculation but still do not remove them all quantitatively.

1.3 Sulphur as an impurity

Sulphur is quantitatively the most dominant impurity in the process of aluminium electrowinning (see Table 1.2). The primary source of sulphur in the aluminium reduction cells are the anodes. They contribute roughly with 80 % of the total S while alumina introduces around 19 % of S depending on the calcination method [16, 17]. The rest comes from other raw materials such as fluorides. In the anodes all of the sulphur is practically organic bound in the form of thiophene, C_4H_4S, and thiols (R-SH) in petroleum coke [18, 19]. Sulphur coming from alumina and fluorides is probably in the form of sulphates.

Sulphur species do not accumulate in the bath or in the metal. This is documented in the Table 1.5 where it is illustrated that the mass balance of sulphur in Söderberg and prebaked cells is satisfied [16]. No serious impact on the metal quality has been reported [20]. Some investigators observed losses in current efficiency as a function of sulphur content in the carbon anode cells [21, 22], while this effect has not been documented by other researchers [20, 23].

Table 1.5 Mass balance for sulphur in Söderberg and prebaked cells [16].

In	**Söderberg [kg/tonne Al]**	**Prebaked [kg/tonne Al]**
Anode	4.39	4.41
AlF_3	0.07	0.06
Al_2O_3	1.04	1.03
Sum	**5.50**	**5.50**
Out		
SO_2	0.10	0.63
COS	0.14	0.15
CS_2	0.01	0.01
H_2S	0.00	0.00
Oxide scales	0.23	
Cyclone	0.25	
Wet scrubbing	2.40	4.63
Cell room gas	0.44	
Sum	**3.57**	**5.42**

The effect of sulphur content on anode consumption was studied and the conclusions derived are also contradictory. While Rhedey [24] claimed decreasing carbon consumption with increasing sulphur content, Bullough et al. [22] and Jones et al. [25] observed increasing rate of anode consumption with increasing sulphur content. Houston and Øye [26] found that the airburn of the carbon anodes increased with increasing sulphur content, but this was in fact ascribed to impurities such as vanadium which is a well-known catalyst for

airburning and which concentration tends to increase with increasing sulphur level. In the studies of Sørlie et al.[27], it was found that the CO_2 reactivity of the anode materials decreases with increasing sulphur content. Similar trend was observed by Hume et al. [28] who related the decreasing air and CO_2 reactivity with higher sulphur level to the ability of sulphur to reduce the so-called "sodium sensitivity", the harmful effect of Na to catalyze the CO_2 reactivity.

It seems that the main impact of sulphur is its contribution to pollution not only in the surrounding area of the aluminium smelters due to the way it leaves the aluminium cells but is also considered to be one of the most serious pollutants in the global range. It escapes from the cells in the form of off gases which are released during the process. Both laboratory and industrial studies showed that during normal electrolysis COS is the dominating sulphurous gas in pure anode gas and is oxidized to SO_2 as the gas becomes burnt with potroom air [16, 29, 30]. The oxidation seems to be governed by the relative concentrations of CO, CO_2 and O_2 and is stated in Equation 1.11 and 1.12.

$$COS + 3/2O_2 = CO_2 + SO_2 \qquad \Delta G^{\theta} = -452.2 \text{ kJ/mol} \qquad 1.11$$

$$COS + 2CO_2 = SO_2 + 3CO \qquad \Delta G^{\theta} = 71.18 \text{ kJ/mol} \qquad 1.12$$

Thus sulphur leaves the aluminium cell predominantly as SO_2 (>95 %) with a minor component as COS (< 5%) which did not become entirely oxidised before being released and very small amounts of CS_2 and H_2S [16, 17]. SO_2 and COS are harmful for the environment and are called greenhouse gases. SO_2 is a major component responsible for acid rain and together with COS contribute to ozone destruction. Although COS is emitted in low levels, due to its long atmospheric lifetime, 5 years, it is considered to be detrimental due to its transport into the stratosphere where it is photochemically transformed into sulphuric acid which is believed to catalyse the ozone depletion [31]. Both gases are lung, skin and eye irritants at low concentration and toxic at higher concentrations.

The sulphur content in the anodes used nowadays is in range from 1 - 4 wt%. Based on the experiments during the industrial operation it was assumed that from the anodes containing 1 wt% S, the total sulphur emissions can be in the order of 5 kg/tonne Al [16, 17]. A smelter with an annual production of 200 000 tonne per year may thus emit 1000 tonne sulphur per year. The real SO_2 values reported from industry varies. Slovalco in Slovak Republic released 1323.807 tonnes SO_2 in 2006 which represents 7.603 kg/tonne Al [32]. For comparison the prebaked series of Hydro Årdal (ÅI and ÅII) released only around 280 tonnes SO_2 in 2006 which is 1.5 kg/tonne Al [33]. Regulations of SO_2 emissions are thus adopted by an increasing number of countries, including Norway where the SO_2 tax is approximately 3 NOK per 1 kg of SO_2.

The reported values for COS emitted during electrolysis vary from 0.28 to 1.6 kg/tonne Al. While Harnish et al. [34] found that a specific emission of 1.6 kg COS/tonne Al was released from anodes containing 1.1 % S, Kimmerle and Noel [17] analysed emissions from cells operating with anodes containing 2.4 % S and reported only 1.1 kg COS/tonne Al. According to Utne et al. [16] the emission of COS is only around 0.27 kg/tonne Al. Based on these data it seems that COS emissions do not follow a linear trend with the sulphur content in the anodes. Despite this fact the emission of sulphur gases from the smelters is expected to rise because the sulphur content in petroleum coke used for anode production is going to increase. At the same time the international protocols and legislation call for a decrease of greenhouse gases emissions and so sulphur off gases and the possibilities to decrease their amount attract presently more and more attention.

Sillinger and Horvath [35] carried out tests in industrial Söderberg cells and found that the upper layer of the bath, which is enriched in carbon dust had considerably higher contents of impurities than the bulk of the electrolyte. The more carbon dust was floating on the top of the bath, the higher content of impurities was present there and the ratio M_{foam}/M_{bath} increased linearly with the ratio C_{foam}/C_{bath}. This linear relationship was found for iron as well as for sulphur and is shown in Table 1.6. Because microscopic analysis of quenched bath samples showed the presence of FeS particles, the reaction of sulphur with iron coming from iron studs offered the explanation for that.

Table 1.6 Impurities distribution in the bath according to [35].

Location	**Impurities concentration [wt%]**			
	C	**Fe**	**Si**	**S**
In the bulk of the bath	0.83	0.014	0.011	0.020
In the upper layer of the bath	3.60	0.029	0.016	0.062
Concentration ratio (upper layer / bulk of bath)	4.3	2.1	1.5	3.1

Ambrová investigated the chemical and electrochemical reactions of sulphur compounds in cryolite melt and found that Al_2S_3 can react with FeO or NiO under formation of FeS, NiS and Ni_3S_2. All these listed sulphides are insoluble in cryolite, and because of their high density they tend to settle on the bottom of the cathode where they can further react with aluminium metal and form Al_2S_3. This may lead to metal contamination with iron or nickel. Besides, Al_2S_3 formed this way can react with cryolite and thus change the composition of the melt. All this can influence the current efficiency.

According to LaCamera et al. [36] sulphur has a big impact on the aluminium electrolysis in cells operating with inert anodes. They found that sulphur adversely affects the current efficiency of such cells. Especially when sulphur is

present as S (+VI) it can be easily reduced to lower valance states, e.g. elemental S or gaseous S_2 and subsequently reoxidized to SO_2 or COS. Then the sulphur species form redox couples between the anode and cathode which consume electricity instead of producing aluminium. Furthermore, present sulphur impurities influence negatively the bath/aluminium interfacial energy and thus uncoalesced aluminium is dispersed in the bath and can be even more easily oxidized. By means of the above mentioned mechanisms caused by sulphur impurities, the current efficiency was dramatically reduced. In some inert anode cells with sulphur level about 500 ppm, the current efficiency was reduced to below 80 % (see Figure 1.2). Even worse was the case when also iron was present in the bath together with sulphur. This combination led to the removal of aluminium produced during cell operation and decreased the current efficiency more rapidly.

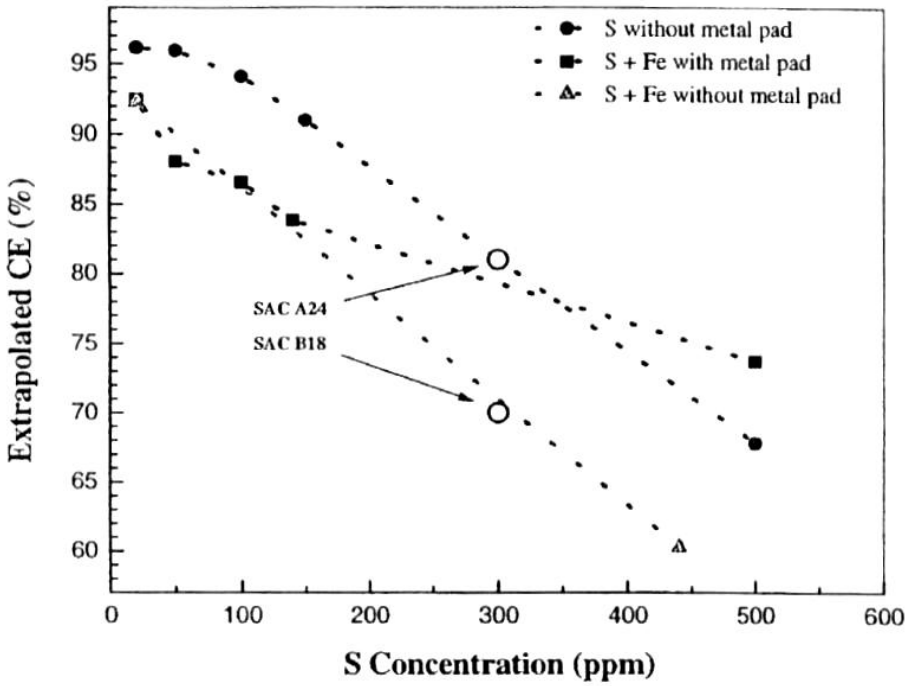

Figure 1.2 Graph of relationship between current efficiency and sulphur concentration in the bath of inert anode cells [36].

Unlike carbon anode cells where sulphur does not remain in the cells but escapes as gaseous COS, in the inert anode cells sulphur was found to build up in the bath and reach values above 500 ppm, often above 1000 ppm. Thus it is desired to maintain the sulphur level below 500 ppm, preferably below 250 ppm.

How the sulphur species enter the electrolysis cell was described in the beginning of this chapter. Their behaviour in the bath is going to be a subject of the next chapters. How sulphur completes its existence in the reduction cells will be written below.

The sulphur cycle in the industrial cell is sketched in the Figure 1.2. Based on the material balance, sulphur leaves the cells without accumulating in the electrolyte. A small amount of sulphur species is trapped in the crust on the top of the electrolyte being skimmed from the cell during the operation, especially in Söderberg cells. A minor part of sulphur reacts with equipment, e.g. gas collecting skirts. The major part of sulphur gases leaves the cell with the off-gases. Presently most of aluminium smelters are equipped with hoods which do not allow the evolved gases to escape to the surrounding but are captured and sucked from the cells and carried to the gas cleaning compartment of the plant, the dry scrubbers (DS). A small amount of sulphur compounds trapped in the DS is recycled back to the cells, mainly as SO_2 adsorbed on alumina and as sulphate. After treatment in the DS, the remaining gas in the form of SO_2 mostly follows to the wet scrubbing system (WS) where it is removed.

The wet scrubbers worldwide are based on a very simple and effective principle. The most used technologies for SO_2 treatment are seawater scrubbing and an alkaline method. Seawater scrubbers are ideal for plants located near the sea. The second mentioned one is convenient for inland smelters.

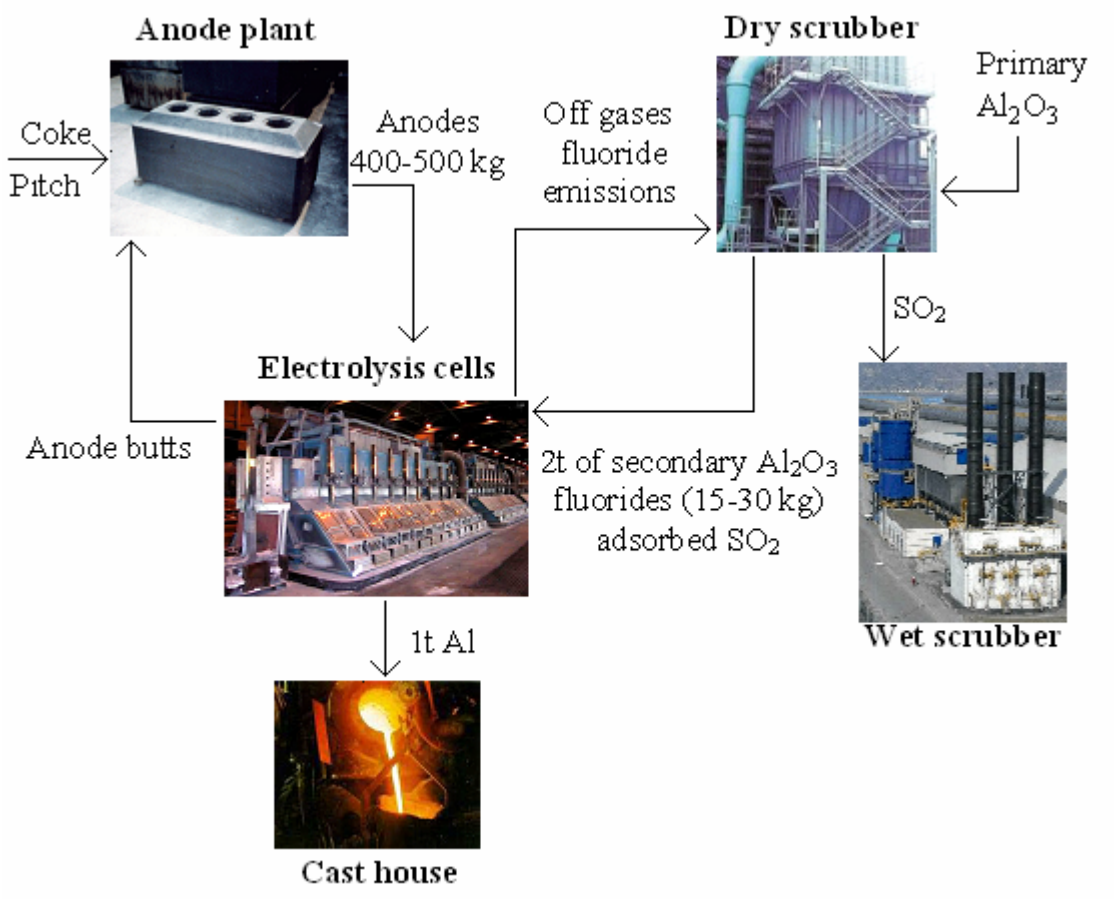

Figure 1.3 Sulphur cycle in the industrial cells.

Sulphur is naturally present in seawater and is a necessary element in the marine environment. Seawater is rich on sulphur and one tonne contains nearly 1 kg of sulphur dissolved as sulphate [37]. Seawater is also naturally alkaline due to the calcium and sodium carbonates content and thus has a capacity to absorb and neutralise acidic gases such as SO_2. Hence desulphurisation by seawater is a very simple process. The seawater and gas flow are one operational step with efficiency above 90 %. No additional chemicals are required. Absorption and neutralisation can be described by Equations 1.13 and 1.14

$$SO_{2(g)} + 1/2O_{2(g)} + H_2O_{(l)} = SO^{2-}_{4(aq)} + 2H^{+}_{(aq)} \quad 1.13$$

$$CO^{2-}_{3(aq)} + 2H^{+}_{(aq)} = H_2O_{(l)} + CO_{2(g)} \quad 1.14$$

With overall reaction 1.15

$$SO_{2(g)} + 1/2O_{2(g)} + CO^{2-}_{3(aq)} = SO^{2-}_{4(aq)} + CO_{2(g)} \quad 1.15$$

This technology has negligible environmental impact and the operational costs are minimal as long as no reagents are used.

Another type of scrubbers works with sodium carbonate and NaOH as absorbing and neutralising agents. Absorption and neutralisation take place according to Equations 1.13 and 1.16

$$SO^{2-}_{4(aq)} + 2H^{+}_{(aq)} + 2Na^{+}_{(aq)} + 2OH^{-}_{(aq)} = Na_2SO_{4(aq)} + 2H_2O_{(l)} \quad 1.16$$

With overall reaction 1.17

$$SO_{2(g)} + 1/2O_{2(g)} + 2NaOH = Na_2SO_{4(aq)} + H_2O_{(l)} \quad 1.17$$

In this type of scrubbers the SO_2 gas is quenched by water. Absorbing liquor is sprayed to the gas in a way that a constant flow of liquid circulates in the system. The absorption liquid must have a constant pH and is regulated by NaOH additions. Correct acidity is necessary to achieve sufficient SO_2 absorption. Formation of Na_2SO_4 is a result of the absorption and the effluent from the scrubber is then pumped to the tanks where evaporation of water takes place during warmer climate and dry disposal of the salt cake is the final result.

2 Literature Survey

2.1 Chemistry of sulphur

Sulphur is known from prehistoric time because it occurs in nature both in elemental form and in compounds, such as H_2S, SO_2 and in a variety of sulphide ores of metals and sulphates. Sulphur occurs naturally near volcanoes. It is also an essential component of proteins in plants, animals and in the cells of human bodies. Each kg of human tissue contains about 2g of sulphur [38].

Sulphur is an element of the VIB group of periodic table, called also chalcogen group. It is the tenth most abundant element in the universe but thermally less stable than oxygen. Naturally occurring sulphur has four isotopes, ^{32}S (95.02 %), ^{33}S (0.75 %), ^{34}S (4.21 %) and ^{36}S (0.02%) but only ^{33}S is active in NMR spectroscopy technique. Sulphur electronegativity is 2.44 and its electronic structure would reach the configuration of the next inert gas atom (Ar) if sulphur filled up remaining 3p orbitals with two more electrons: [Ne] $3s^2$ $3p^4$. Sulphur exhibits allotropism and polymorphism because it exists in several solid, liquid and gaseous forms in which the molecules can have different size (S_n species with n = 2…∞). Each form is stable in a different range of temperatures and pressures. The most common crystalline modifications of sulphur are; the rhombic form which is stable at room temperature but is converted to monoclinic form at 95.6 ºC. Both forms are constructed of S_8 cyclic molecules in the crown line rings and the crystals have a characteristic bright yellow colour which becomes darker as the sulphur is heated and paler as it is cooled. At -200 ºC sulphur becomes colourless [39].

$$S_{\alpha\,(s)} \xleftrightarrow{\text{trans. p. } 95.6\ ^oC} S_{\beta\,(s)} \xleftrightarrow{\text{m.p. } 119.6\ ^oC} S_{(l)} \xleftrightarrow{\text{b.p. } 444.6\ ^oC} S_{n\,(g)}$$

Elemental S_8 sulphur combines, even at moderate temperature, with almost all metals and non-metals; exceptions are gold, platinum, iridium, nitrogen, tellurium, iodine and the noble gases. A particularly characteristic reaction of sulphur is sulfurization; introduction of sulphur into a molecule in any form. Sulphur forms chains not only in its allotropic elemental modifications S_n, but also in compounds such as polysulphides or lower sulphur oxides. Redox reactions are also essential for sulphur behaviour and sulphur thus can be oxidized from its lowest oxidation state S (-II) to the highest S (+VI). In compounds with electropositive elements sulphur is usually found in the -II oxidation state and can be either ionically or covalently bound. However, it can also exist in other negative oxidation levels -2/n; n >1. In compounds with electronegative elements covalently bound sulphur may be present in the

oxidation state 0 or +I, +II, +III, +IV, +V or +VI. Sulphur is inorganically bound primarily in the form of sulphides (S^{2-}) and sulphates (SO_4^{2-}). In organic form it can be found in petroleum and natural gas from which it must be separated.

2.1.1 Sulphides and polysulphides

Sulphides are the salts derived from hydrogen sulphide with the formula M_2S and hydrogensulphides, MHS. Hydrogen polysulphides called also polysulphanes H_2S_n are known as well. Almost all metals form sulphides. Alkali metal sulphides are soluble in water and can be extensively hydrolysed which also applies to aluminium and chromium sulphide. Most of the other metal sulphides do not undergo hydrolysis with water. One of the options to produce sodium sulphide is reduction of sodium sulphate with presence of coal at 700 - 1000 ºC according to Equation 2.1.

$$Na_2SO_4 + 4C \rightarrow Na_2S + 4CO \qquad 2.1$$

Polysulphides can be formed by melting alkali metals or alkali metal sulphides with sulphur in the absence of air at high temperatures. For example Na_2S_n formation has an exothermic character which is used in sulphur batteries to generate electricity. If alkali metal polysulphides are added to polar media as alkali metal halide melts, the solutions become colourful as the result of polysulphides (1-) SS_n^-: e.g. yellow-green colour typical for S_2^-, blue for S_3^- and red for S_4^-.

2.1.2 Sulphur in halogen compounds

Sulphur in reactions with halogens forms halides, e.g. SX_n, S_2X_n, S_nX_2 and S_3F_m. The tendency of sulphur to appear in higher oxidation states and its affinity for halogens decreases with the increasing mass of the halogen. With fluoride atoms sulphur forms disulphur difluoride (S_2F_2), sulphur difluoride (SF_2), sulphur tetrafluoride (SF_4) and sulphur hexafluoride (SF_6). The typical chlorides are disulphur dichloride (S_2Cl_2), sulphur dichloride (SCl_2) and sulphur tetrachloride (SCl_4). Dichloropolysulphides can be prepared by heating S_2Cl_2 to 400-900 ºC in the presence of H_2 with subsequent quenching of the product.

2.1.3 Oxides of sulphur

Sulphur forms many oxides, both molecular with the composition SO_n or S_nO_2 and polymeric with the formula $(S_nO)_x$ and $(SO_{3-4})_x$. Sulphur dioxide SO_2 and sulphur trioxide SO_3 are the best known and industrially most important sulphur oxides. Sulphur monoxide (SO), sulphur tetroxide (SO_4), disulphur monoxide (S_2O) and disulphur dioxide (S_2O_2) are unstable and known only as reaction intermediates.

Sulphur dioxide is industrially produced by burning sulphur or H_2S in air or by heating sulphur containing ore, pyrites for example, in a stream of air or oxygen. SO_2 is a colourless, pungent and corrosive gas soluble in water. It is also very toxic. From the chemical properties it is worth mentioning its activity as a reducing agent. The oxidizing effect of SO_2 is evident only during heating with strong reducing agents such as Mg, Al, K, Na and Ca. In the presence of catalysts such as Pt, vanadium oxide or iron oxide, it reacts with oxygen to form SO_3 at moderate temperature.

$$SO_2 + 1/2O_2 \rightleftharpoons SO_3 \qquad 2.2$$

Sulphur trioxide cannot be produced by direct burning of sulphur in air or oxygen because the heat produced during sulphur burning to SO_2 is sufficient to promote endothermic decomposition of SO_3 so the reaction 2.2 would proceed in reversed order. SO_3 is a strong Lewis acid and forms adducts with Lewis bases such as sodium sulphate. It is also a strong oxidizing agent.

2.1.4 Oxygen acids of sulphur and their salts

Sulphur forms many oxygen acids but only the most relevant to the topic of this thesis and the most known will be mentioned here.

Sulphur exists in three oxygen acids with the formula H_2SO_n (n = 3, 4, 5) and in acids with composition $H_2S_2O_n$ (n = 3, 4, 5, 6, 7 and 8). The most recognised are sulphurous acid (H_2SO_3), sulphuric acid (H_2SO_4), disulphurous acid ($H_2S_2O_5$), dithionic acid ($H_2S_2O_6$) and disulphuric acid ($H_2S_2O_7$). The salts derived from these acids as stated in the order above are then called sulphites, sulphates, disulphites, dithionates and disulphates. The structures of four of them are represented in the following figure.

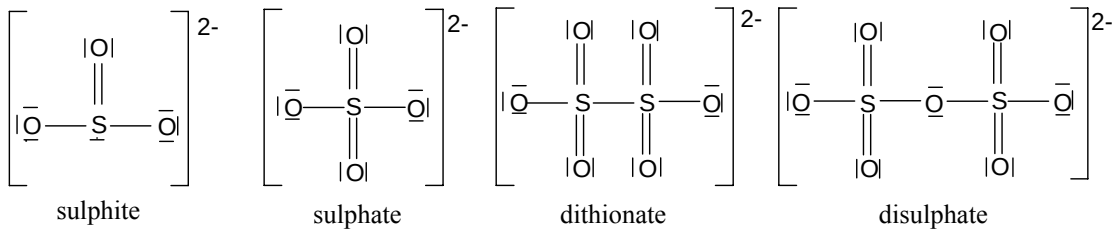

Figure 2.1 Structure of different anions containing sulphur bound with oxygen atoms in the acids or their salts.

The most important acids are sulphurous and sulphuric acids. They are produced from their anhydrides in reactions with water:

$$SO_2 + H_2O \rightarrow H_2SO_3 \qquad 2.3$$

$$SO_3 + H_2O \rightarrow H_2SO_4 \qquad 2.4$$

When these acids are reduced, thionous and thionic acids are formed:

$$2SO_2 + 2e^- \rightarrow S_2O_4^{2-} \qquad 2.5$$

$$2SO_3 + 2e^- \rightarrow S_2O_6^{2-} \qquad 2.6$$

while oxidation gives thionic and peroxodisulphuric acids.

$$2SO_3^{2-} \rightarrow S_2O_6^{2-} + 2e^- \qquad 2.7$$

$$2SO_4^{2-} \rightarrow S_2O_8^{2-} + 2e^- \qquad 2.8$$

The diacids such as disulphurous and disulphuric, are product of condensation:

$$2HSO_3^- \rightarrow S_2O_5^{2-} + H_2O \qquad 2.9$$

$$2HSO_4^- \rightarrow S_2O_7^{2-} + H_2O \qquad 2.10$$

The salts of sulphurous acid (sulphites) can be described as M_2SO_3 or $MHSO_3$ structures. Sulphurous acid and its salts are strong reducing agents especially in alkaline solutions. If sulphites and sulphurous acid are in aqueous solution they can slowly convert to sulphates or sulphuric acid when allowed to stand in the air. In the presence of strong reducing agents sulphurous acid can be reduced to sulphur, hydrogen sulphide or dithionous acid. The hydrogen sulphites are soluble in water unlike sulphites, except alkali metal sulphites. Anhydrous sulphites disproportionate according to Equation 2.11 to sulphides and sulphates when heated.

$$4SO_3^{2-} \rightarrow S^{2-} + 3SO_4^{2-} \qquad 2.11$$

Disulphites can be prepared by mixing the Lewis acid and the Lewis base and are used as reducing agents.

$$SO_3^{2-} + SO_2 \rightarrow S_2O_5^{2-} \qquad 2.12$$

Sulphuric acid is a strong acid and gives two groups of salts: $MHSO_4$ (hydrogensulphates) and M_2SO_4 (sulphates). Sulphates are the most stable oxygen-sulphur compounds. One possible preparation is oxidation of metal oxide or sulphites. The alkali and alkaline earth metal sulphates are very resistant to heat. Hydrogensulphates are primarily formed by the alkali metals. If they are heated and water molecules are substracted, disulphates are created. The salts of disulphuric acid are formed in a reversal of their thermal decomposition.

$$SO_4^{2-} \xrightarrow{+SO_3} S_2O_7^{2-} \xrightarrow{+SO_3} S_3O_{10}^{2-} \xrightarrow{+SO_3} S_4O_{13}^{2-}$$

2.2 Electrochemistry of sulphide and sulphur in molten chlorides

The electrochemical behaviour of sulphide anions in molten chlorides as solvents was extensively studied in the last century mainly in connection with the development of secondary molten salt batteries. The interest was focused on investigation of a system which would utilize sulphur as a cathode material and work with aluminium, sodium or lithium (or lithium alloys) as anodes. In this chapter only a limited selection of the research work which was dealing with sulphide investigation will be mentioned.

Delarue [40, 41] studied the reactions involving sulphur, sulphides, sulphites and sulphates of various metals in molten LiCl-KCl eutectic. He found out that sulphides of Mn (+II), Tl (+I) and alkali and alkaline earth metals were soluble, whereas sulphides of Zn (+II), Cd (+II), Ni (+II), Co (+II), Ag (+I), Sn (+II), Sb (+III), Bi (+III), Pd (+II), Pt (+II), Cu (+I), Fe (+II), Ce (+III) and Pb (+II) were insoluble. Sulphides of Cu (+II), Fe (+III), Au (+I) and Hg (+II) reacted in the melt; the metal ions were reduced and sulphide was oxidized to sulphur.

Bodewig and Plambeck [42] investigated the electrochemical behaviour of sulphide in LiCl-KCl eutectic at 420 ºC. The sulphur-sulphide couple revealed Nernstian behaviour and a two-electron exchange was assumed. Voltammetric studies showed an anodic wave ascribed to the oxidation of sulphur (Equation 2.13) and a cathodic wave was attributed to its reduction to S^{2-}.

$$2S + 2Cl^- \rightarrow S_2Cl_2 + 2e^- \qquad 2.13$$

The observed blue colour of the sulphur-sulphide system was concluded to be a result of polysulphide (S_{x+1}^{2-}) ion formation by reaction of sulphur and sulphide.

Gruen et al. [43] performed spectrophotometric measurements of the same system as studied by Bodewig and Plambeck. On the basis of the absorption spectra they postulated three equilibria between sulphur and sulphide. The observed colour change of the solutions from ultramarine green to ultramarine blue was explained as a result of increasing S_3^-/S_2^- ratio.

Giggenbach [44] on the other hand concluded from his spectrophotometric measurements in LiCl-KCl above 400 ºC when sulphur was added to the melt that S_2^- ions were responsible for the blue colour. When the melt cooled to temperatures below 400 ºC the blue coloration disappeared which was ascribed to dimerization of S_2^- ions to form S_4^{2-} ions.

Kennedy and Adamo [45] studied the electrochemistry of sulphur on gold foil also in LiCl-KCl eutectic. According to them the reduction of sulphur proceeds in two steps, each of them involving the same number of electrons which can be described as:

$$S_n \xrightarrow{+e^-} S_n^- \xrightarrow{+e^-} S_n^{2-} \qquad 2.14$$

where $n \geq 2$. Based on cyclic voltammetry and controlled potential electrolysis they ascribed the blue coloration to the product of the first reduction step of sulphur.

Cleaver et al. [46] studied oxidation of alkali metal polysulphides in fused KSCN and LiCl-KCl eutectic. Sulphur was found to be the final oxidation product. Contrary to the above stated authors they found that Na_2S was practically insoluble in the LiCl-KCl eutectic at 420 ºC and no voltammetric waves were observed. When $Na_2S_{2.2}$ was added, cyclic voltammetry on the gold electrode showed two redox couples. One wave was attributed to a one-electron process $S_2^{2-} \rightarrow S_2^- + e^-$ while the second one was probably result of sulphur deposition: $S^{2-} \rightarrow 2S + e^-$.

Weaver and Inman [47] studied polysulphides solutions in LiCl-KCl eutectic by potentiometric and chronopotentiometric techniques. It was shown that the predominant solute species were polysulphide ions S_x^{2-}, which was in harmony with earlier studies. The oxidation of the sulphide ion in the melt seemed to be complex and controlled by the extensive formation of a polymeric sulphur film.

Marassi and co-workers [48] examined the behaviour of sulphur and sulphide in $AlCl_3$-NaCl melt on different electrodes. In melts containing sulphur one reduction and one oxidation wave were seen at tungsten and glassy carbon electrodes. At platinum two reduction waves were observed. The oxidation peaks were similar for all electrode materials. Reduction of sulphur led to the formation of sulphide, the oxidation led to formation of S (+I) and S (+II) depending on the temperature; the higher oxidation state was preferred at higher temperature. They assumed that the mechanism for the electrochemical oxidation of sulphur involves a complex set of charge transfer and chemical steps.

Paulsen and Osteryoung [49] reduced coulometrically liquid sulphur in $AlCl_3$-NaCl melts at 175 ºC. The reduction was a two-electron process giving S^{2-}. The solubility of metal sulphides was found to increase rapidly with increasing acidity of the melt (higher $AlCl_3$ concentration). From the slope of the Nernst plot for the sulphur-sulphide couple four electrons were calculated to give the following reaction:

$$S_2 + 4e^- = 2S^{2-} \qquad 2.15$$

The oxidation of sulphur gave cations in oxidation state +I or higher.

2.2.1 The role of sulphide in an alternative process for aluminium electrowinning

Except for studies of sulphur species for utilization in batteries, scientists during past two decades also tried to find an application of sulphides from a metallurgical viewpoint. Thus a possibility of metal electrowinning via a sulphide intermediate became an interesting idea. The attractive idea of metal extraction from corresponding metal sulphides is based on a fact, that many metal sulphides have lower decomposition potentials than their chlorides or oxides. Especially production of metallic aluminium by electrolysis of aluminium sulphide (Al_2S_3) from molten bath offers a remarkable option from the viewpoint of energy utilization; Al_2S_3 has lower theoretical decomposition potential (about 1V at 1023 K [50]), compared to that of Al_2O_3.

The main idea of this new way of aluminium production is based on the conversion of Al_2O_3 into Al_2S_3 as an intermediate which would be further decomposed involving cathodic reduction of aluminium cations and anodic oxidation of sulphide anions. The electrolyte would consist purely of $MgCl_2$-NaCl-KCl eutectic or alternatively of the eutectic of $AlCl_3$- $MgCl_2$-NaCl-KCl and operation would run at temperature range between 700-850 ºC. The simplified reactions of the process are written in the following equations.

Cathode: $Al^{3+} + 3e^- \rightarrow Al$ 2.16

Anode: $2S^{2-} \rightarrow S_{2\,(g)} + 4e^-$ 2.17

Overall: $Al_2S_3 \rightarrow 2Al + 3/2S_{2\,(g)}$ 2.18

Still the first operational step which is also additional when it comes to comparison with conventional Al production is the conversion of alumina to aluminium sulphide. This can be realised by two methods. The first one is patented by Loutfy et al. [51], using pure carbon and sulphur at temperature above the melting point of aluminium sulphide:

$$Al_2O_3 + 3C + 3S \rightarrow Al_2S_3 + 3CO \quad 2.19$$

Because the reaction proceeds only at temperatures higher than 1400 K it leads to high energy requirements [52]. In the second option Al_2S_3 is produced by the reaction of CS_2 and alumina [53]. Xiao et al. and Lans et al. [54, 55] showed that the optimal temperature for this way of sulphidization of α-Al_2O_3 is about 850 ºC. After 5 hours a maximal conversion only about 40 % was obtained. From this follows that conversion of alumina to Al_2S_3 could be a complicated procedure and only if it becomes technically feasible and effective the aluminium metal electrolysis from a mixture of molten chloride melts could be realized.

Minh et al. [56] studied the electrochemical behaviour of Al_2S_3 in $MgCl_2$-NaCl-KCl eutectic on graphite electrodes at 1023 K. They revealed that the oxidation is a diffusion controlled reversible process and sulphide ion is involved in a two-electron discharge. The electrochemical reduction is consequently followed by a fast dimerization of sulphur atoms to S_2 formation. Based on their investigation they assumed that the sulphur product is soluble in the melt. Aluminium cations were reduced by a three-electron exchange transfer to Al in a reversible diffusion controlled step and an insoluble product was formed on the cathode. The same authors investigated Al_2S_3 reduction also in $MgCl_2$-NaCl-KCl melts enriched by $AlCl_3$ [50, 57]. They proved that $AlCl_3$ addition enhances the solubility of aluminium sulphide but does not affect the electrochemical behaviour of Al_2S_3. Thus the reduction of aluminium ions and oxidation of sulphide proceed the same way as in the melt without $AlCl_3$. The researchers also suggested that Al_2S_3 is dissolved in the melt in the form of AlS^+ species. The current efficiencies in the range from 75 % to 85 % were obtained at the used current densities and produced aluminium achieved purity better than 99 %.

Minh and Yao [58] performed Al_2S_3 electrolysis on graphite by cyclic voltammetry in a mixture of molten LiF-NaF eutectic at 1023 K and in cryolite at 1323 K [59, 60]. In this molten fluoride mixture the reduction of sulphide was

found to be reversible and diffusion controlled involving elemental sulphur generation at the anode. The reaction mechanism can take place in one step

$$2S^{2-} \rightleftharpoons S_2^{2-} + 2e^- \qquad 2.20$$

or proceed via two steps as described in Equations 2.21 and 2.22

$$S^{2-} \rightleftharpoons S + 2e^- \qquad 2.21$$
$$S + S^{2-} \rightleftharpoons S_2^{2-} \qquad 2.22$$

When saturation of S_2^{2-} ions is reached, sulphur atoms formed by reaction 2.21 after being dissolved in the melt combines to give sulphur. The experiments showed that the current efficiency in the fluoride melt was much lower than that in the chloride electrolyte. Unlike in chloride melts where the sulphide was observed to behave similarly, the sulphide reduction varies in cryolite and in mixture of fluorides. In cryolite melts Minh and Yao revealed that sulphide added in the form of Al_2S_3 was oxidized to sulphur in a two-electron exchange quasi-reversible reaction, where the rate is controlled by both diffusion and charge transfer kinetics.

$$S^{2-} \rightleftharpoons S + 2e^- \qquad 2.23$$

They also remarked that the mechanism is simplified since at the experimental temperature besides the formation of sulphur gas, the formation of CS_2 is probable on the graphite substrate.

The method of aluminium production from sulphides offers several advantages compared to the classical reduction of aluminium. In this alternative process, sulphide is oxidized on the graphite anodes which stay relatively inert and remain dimensionally stable unlike carbon anodes in the present industrial process. The fluoride gas emissions from the traditional Hall-Héroult process would be eliminated because the electrolyte is basically a mixture of chlorides. This type of electrolyte would also operate at a lower temperature. The produced sulphur gas could be recycled and utilized for Al_2S_3 production. If the current efficiency is increased, and ohmic drop reduced due to a better and optimised cells design and suitable electrolyte, the electrical energy requirement could approach to 8 kWh/kg Al which would favour the aluminium electrolysis from sulphide in comparison with the conventional Hall-Héroult process (14 kWh/kg Al) [58, 61]. The main disadvantages of electrowinning from sulphides are the low current efficiency and the extra operational step to convert the alumina to sulphide.

2.3 Electrochemical studies of sulphate anions in molten chloride melts

Pushkareva [62] studied the effect of sulphates on the current efficiency of magnesium production from carnallite melts at 700 ºC using a carbonaceous iron cathode. Results of qualitative chemical analysis showed that in the presence of liquid magnesium in the electrolyte, introduction of sulphate yielded elemental sulphur. Thus dissolved magnesium probably acts as reducing agent. She also suggested possible reactions between sulphide and atmospheric oxygen or chlorine with liberation of elemental sulphur.

Liu [63] electrolyzed Li_2SO_4-K_2SO_4 eutectic mixture on platinum electrodes at 625 ºC. He suggested reaction 2.24 to be the limited process on the anode.

$$SO_4^{2-} \rightarrow 1/2O_2 + SO_3 + 2e^- \qquad 2.24$$

The chemical analysis of the product formed in the cathode compartment revealed the presence of both sulphite and sulphide but unsure formation of sulphur. Thus he assumed that the cathodic process probably involve the total reactions written below.

$$SO_4^{2-} + 2e^- \rightarrow SO_3^{2-} + O^{2-} \qquad 2.25$$

$$SO_4^{2-} + 6e^- \rightarrow S + 4O^{2-} \qquad 2.26$$

$$SO_4^{2-} + 8e^- \rightarrow S^{2-} + 4O^{2-} \qquad 2.27$$

Liu also pointed out that acid-base equilibria play an important role in molten sulphates. He observed that some metals, e.g. Ni react with sulphur species and forms sulphides unlike others, e.g. Bi which precipitates as oxide and releases SO_3.

Johnson and Laitinen [64] carried out electrolysis of the Li_2SO_4-Na_2SO_4-K_2SO_4 mixture on Pt electrodes at 550 ºC and observed mainly sulphur and oxides but only a small amount of sulphite. They confirmed the same anodic process as Liu described by reaction 2.24. After addition of magnesium powder to the solution, sulphide and a little sulphur were found in the cooled product. They claimed that if a large quantity of metal was the reducing agent, sulphide became the most likely product. They also tried to reduce the solvent by other metals such as Fe, Cd, Ni, Zn, Tl and Pb but the reduction did not proceed rapidly.

According to Senderoff [65] and Woodall [66] the sulphate anion could be directly reduced at a cathode in molten LiCl-KCl. The chronopotentiometric transition times indicated that the electrode process was a diffusion controlled

two-electron reduction with a thermally unstable product from the primary reaction.

Wrench and Inman [67] performed a chronopotentiometric investigation of sulphate species in equimolar NaCl-KCl at 750 ºC. They found that the sulphate ion was not directly reduced to a lower-valent sulphur compound unless the metaphosphate ion was added to the melt. Because the equilibrium constant for the Lux-Flood acid-base equilibrium reaction $SO_3 + O^{2-} \rightleftharpoons SO_4^{2-}$ is very high ($K > 10^2$) the presence of a very strong acid is necessary to remove the oxide ions according to the reaction 2.28

$$SO_4^{2-} + 2PO_3^- \rightarrow SO_3 + P_2O_7^{4-} \qquad 2.28$$

Thus the chronopotentiometric waves were assigned to the one-electron diffusion controlled reduction of free or complex sulphur trioxide ($S_2O_7^{2-}$) involving soluble but probably unstable products, so that the electrochemical step was followed by a chemical step. In the effluent gases sulphide was detected and the platinum crucible also appeared to be covered by sulphide after the experiment. However, gold, which served as a working electrode was untouched.

Burrows and Hills [68] made electrochemical studies in the same melt as Liu [63] using various metal electrodes, such as Fe, Co, Cu, Pd, Au, W. The anodic peak was found to be due to the oxidation of O^{2-} ions and the products of prolonged cathodic electrolysis were elementary sulphur, oxide ion and SO_2. Burrows [69] also tried to reduce sulphate ion on an inert metal cathode in LiCl-KCl eutectic but did not observe any cathodic wave attributable to sulphate. It was suggested that when the sulphate anion is not directly reducible then the oxidizing character of sulphate melts must result from the promotion or acceleration of the dissociation of the sulphate ion. Furthermore, during the experiment, the platinum electrode became tarnished by a film of oxides (most likely PtO) so the discharge of sulphate ion was suggested through a mechanism with intermediate formation of PtO_2 (Equation 2.29).

$$PtO + SO_4^{2-} \rightleftharpoons PtO_2 + SO_3 + 2e^- \qquad 2.29$$

Hoa, Welch and Jenkins [70, 71] examined lead deposition on graphite electrodes from dissolved $PbSO_4$ in molten salt solutions. Two different solvents were used for the experiments: LiCl-KCl eutectic and Li_2SO_4-Na_2SO_4-K_2SO_4 eutectic in a broad temperature range. The current efficiency was found to decrease with increasing lead sulphate concentration. From studies of the reaction of lead with the melt and chronopotentiometric studies of the cathodic process, the decrease in current efficiency was connected with the non-electrochemical formation of

lead sulphide (Equation 2.30).

$$4Pb + 5PbSO_4 \rightarrow PbS + 4PbO.PbSO_4 \qquad 2.30$$

After examination of the anode products formed on a carbonaceous anode during lead electrowinning from lead sulphate dissolved in LiCl-KCl, the overall reaction for electrolytic decomposition given in Equation 2.31 was suggested. At low current densities the CO_2 content was observed to increase according to reaction 2.32.

$$PbSO_4 + C \rightarrow Pb + CO_2 + SO_2 \qquad 2.31$$

$$C + SO_2 \rightleftharpoons CO_2 + 1/xS_x \qquad 2.32$$

Based on the experiments a possibility of an intermediate step involving a chemical reaction in the overall anode process was suggested. The mechanism of sulphate anion discharge is summed up in equations below.

$$SO_4^{2-} + C_s \rightleftharpoons C_sO + SO_{3\,(ads)} + 2e^- \qquad 2.33$$

$$C_sO + SO_{3\,(ads)} \rightleftharpoons CO_{2\,(ads)} + SO_{2\,(ads)} \qquad 2.34$$

$$CO_{2\,(ads)} \rightleftharpoons CO_{2\,(g)} \qquad 2.35$$

$$SO_{2\,(ads)} \rightarrow SO_{2\,(g)} \qquad 2.36$$

Sequeira and Hocking [72] examined Na_2SO_4-NaCl melts by using platinum electrodes at 900 ºC. The observed eight-electron reduction of SO_3 to S^{2-} and O^{2-} as a product of limiting cathodic process. Reduction of SO_3 to SO_2 in a two-electron exchange step appeared to play a considerable role at more anodic potentials and at lower current densities too. They also proved that platinum underwent anodic attack in sulphate melts. The two-electron discharge of sulphate anions to SO_3 and oxygen is probably accompanied by the oxidation of platinum (Equation 2.37) and its passivation.

$$Pt + SO_4^{2-} \rightleftharpoons Pt\text{-}O + SO_3 + 2e^- \qquad 2.37$$

When platinum was used as cathode, corrosion was observed. This probably resulted from the reaction of Pt with one or more products from the sulphate reduction.

Rapp and Goto [73] in relation to studies of hot corrosion proposed the electrolytic reduction of sodium sulphate at 927 ºC through a sequence of two-electron transfer steps resulting in the formation of sodium sulphide and sodium oxide.

Fang and Rapp [74] concluded that in a pure sodium sulphate melt at 900 ºC using platinum electrodes, a variety of electrochemical reactions can take place. The occurrence of a particular reaction will be depending on the gas composition, the electrode potential and material. In a basic Na_2SO_4 melt in argon or oxygen atmosphere, reactions involving oxide ions or its related species could occur. If the anodic or cathodic overpotentials are high enough, the sulphate anions can decompose electrochemically to form SO_3, O_2, O_2^- and sulphites on the anode and S^{2-} and O_2^{2-} on the cathode. In atmospheres containing SO_2 or SO_3, the primary electrochemical reactions involving gas species are the reduction of pyrosulphate ions according to reaction 2.38 followed by a chemical combination or by a further electrochemical reaction.

$$S_2O_7^{2-} + e^- \rightleftharpoons SO_4^{2-} + SO_3^- \qquad 2.38$$

Park and Rapp [75] made polarization studies also in a Na_2SO_4 melt at 900 ºC on platinum foil and porous Pt electrodes. Based on their basicity and oxygen measurements (Figure 2.2) during cathodic polarization of a porous Pt electrode and cyclic voltammetry, they found that a single electrochemical reaction of pyrosulphate ions (Equation 2.39) must be coupled with a chemical reaction (Equation 2.40).

$$S_2O_7^{2-} + 2e^- \rightarrow SO_4^{2-} + SO_3^{2-} \qquad 2.39$$

$$SO_4^{2-} + SO_3 \rightarrow S_2O_7^{2-} \qquad 2.40$$

The sulphite ions may subsequently establish an equilibrium with superoxide ions and dissolved oxygen and produce SO_3 according to Equation 2.41. Additionally, superoxide ions would maintain equilibrium with dissolved oxygen and oxide ions by reaction 2.42.

$$SO_3^{2-} + 2O_2 \rightleftharpoons SO_3 + 2O_2^- \qquad 2.41$$

$$2O^{2-} + 3O_2 \rightleftharpoons 4O_2^- \qquad 2.42$$

Also spontaneous decomposition of sulphate into sulphide ions was assumed for the reduction step connected with increasing basicity.

$$SO_4^{2-} + 8e^- \rightleftharpoons S^{2-} + 4O^{2-} \qquad 2.43$$

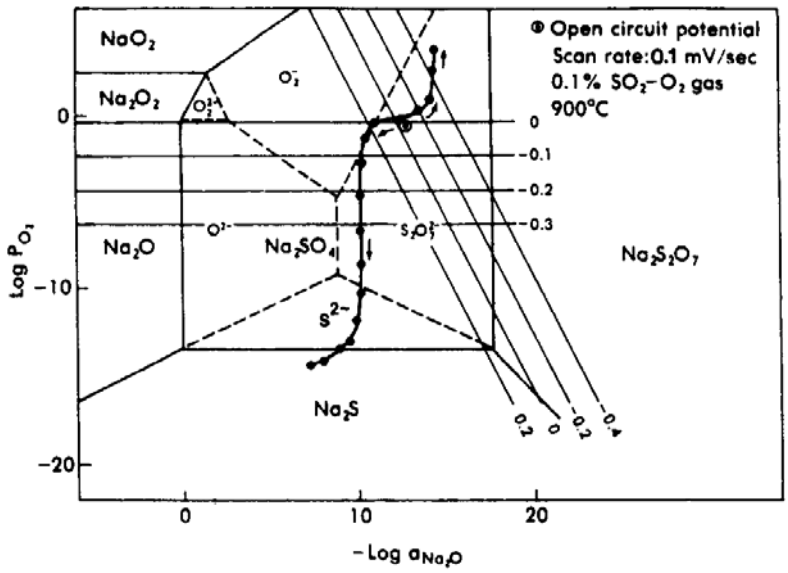

Figure 2.2 Trace of basicity and oxygen activity measured for porous Pt working electrode according to [75].

In connection with glass production technology Tilquin et. al. [76] examined the electrochemical behaviour of sulphate in $Na_2O{\cdot}2.5SiO_2$ at 1000 ºC by means of cyclic voltammetry, square wave voltammetry and impedance spectroscopy. It appeared that the sulphate decomposed to sulphite ions and oxygen completely and fast providing a melt containing S (+IV). The voltammograms showed two reduction peaks attributed to the reduction of sulphite ions to the observed elementary sulphur via the reaction path described in Equations 2.44 and 2.45. The first peak on the voltammograms corresponded with a reduction involving strong adsorption of sulphur on the electrode.

$$SO_3^{2-} + 4e^- \rightleftharpoons S(0)_{ads} + 3O^{2-} \qquad 2.44$$

$$SO_3^{2-} + 4e^- \rightleftharpoons S(0) + 3O^{2-} \qquad 2.45$$

Rasmussen and co-workers [77] explored by potentiometric measurements the coordination of SO_4^{2-} to vanadium (+IV) and (+V) in $M_2S_2O_7$-M_2SO_4-V_2O_5 (M = K, Cs) melts, respectively under $SO_{2\,(g)}$ and $O_{2\,(g)}$ atmospheres at 450 - 470 ºC on a gold electrode. They found that in the $M_2S_2O_7$-M_2SO_4 system probably a layer containing $O_{2\,(g)}$ was formed on the gold electrode surface due to the possible decomposition reaction 2.46 catalyzed by gold metal.

$$S_2O_7^{2-} = O_2 + 2SO_2 + O^{2-} \qquad 2.46$$

Wartena et al. [78] investigated an unusual option for the efficient recycling of wood pulping chemicals by means of electrolysis of mixtures containing sodium carbonate and sodium sulphate at 860 ºC on gold and nickel electrodes. They

elucidated the complimentary reaction of sulphate ions as an eight-electron reduction resulting as sulphide and oxide ions formation with the sulfoxylate ion, SO_2^{2-} as an intermediate which chemically reacts with carbonate to give the overall reaction 2.47

$$SO_4^{2-} + 2CO_3^{2-} + 12e^- \rightarrow S^{2-} + 8O^{2-} + 2CO \qquad 2.47$$

2.4 Sulphur compounds in cryolite melts

The effect of sulphur containing compounds on industrial aluminium production was the subject of interest mainly in the 60`s-80`s of the previous century. The experimental research of the behaviour of sulphur species in cryolite melts has not been performed in such extent as in the chloride melts. It means that the behaviour of sulphur compounds in the electrolyte for industrial aluminium production still remains a topic for further investigation because it has not yet been well understood. Most of the listed summary of earlier results in this chapter comes from the work done and discussed by Russian researchers. Unfortunately many of their hypothesis and assumptions are only hypothetical without experimental research.

As mentioned earlier in chapter 1, sulphur enters aluminium electrolysis cells mostly in the form of thiophene and sulphates. Baimakov and Vetyukov [79] postulated that the direct reaction of sulphates with cryolite is possible as shown in Equation 2.48 in which formation of NaF leads to the increased basicity of the melt. Sulphate can be also reduced to sulphide by dissolved aluminium metal present in the melt according to Equation 2.49.

$$3Na_2SO_4 + 2Na_3AlF_6 \rightleftharpoons Al_2(SO_4)_3 + 12NaF \qquad 2.48$$
$$3Na_2SO_4 + 8Al \rightleftharpoons 4Al_2O_3 + 3Na_2S \qquad 2.49$$

Part of the sulphide can be absorbed in the carbon lining [80] and the rest being dissolved in the melt can be transported to the anode where it is reoxidized to sulphur dioxide

$$S + 2CO_2 \rightleftharpoons SO_2 + 2CO \qquad 2.50$$

Abramov et al. [81] stated in their book that sulphates can react with cryolite only in the presence of carbon in the temperature range from 850 - 900 ºC:

$$3Na_2SO_4 + 2Na_3AlF_6 + 3C \rightleftharpoons Al_2O_3 + 12NaF + 3SO_2 + 3CO \qquad 2.51$$
$$Na_2SO_4 + 4C \rightleftharpoons 4CO + Na_2S \qquad 2.52$$

In the presence of aluminium reactions between sulphate and cryolite are limited due to the interaction of sulphates with aluminium resulting in aluminium sulphide formation. They also claimed that sulphates can be reduced according to reaction 2.53 so that sulphur dioxide is released. Sulphides may undergo electrochemical oxidation to sulphur and further by oxygen to sulphur dioxide as given in reactions 2.54 and 2.55.

$$SO_4^{2-} + C \rightleftharpoons SO_2 + CO_2 + 2e^- \quad 2.53$$

$$S^{2-} \rightleftharpoons S + 2e^- \quad 2.54$$

$$S + O_2 \rightleftharpoons SO_2 \quad 2.55$$

Burnakin and co-workers [21, 82-85] studied the effect of sulphur on the anode performance in an industrial electrolyte. Anodes made of petroleum coke with the sulphur content from 0.6 to 3.7 wt % were tested in a melt with cryolite ratio 2.7 and 6 wt % alumina at 980 ºC. They showed that the magnitude of the anodic overvoltage decreased with increasing sulphur content within the current density range from 0.1-0.6 $A.cm^{-2}$. The relationship between the anodic overvoltage ($\Delta\eta$ in mV) and sulphur content in the anode (c_s in wt %) was described in the form of the following equation:

$$\Delta\eta = 38.2\ c_s \quad 2.56$$

They found that 1 wt % higher sulphur content leads to a decrease in the anode voltage by 35-40 mV. Besides they found that the ohmic resistance increased considerably with higher sulphur content. Other observations revealed that a higher sulphur content is connected with increasing sulphur content in anode gases, e.g. H_2S and COS as well as the anode consumption due to the reactions between sulphur and carbon from the anodes. They concluded that such observations could be a result of electrochemical reactions of sulphur bound in thiophene, as the main sulphur containing compound in the anode mass. In Table 2.1 the reactions where thiophene reacts with alumina are summarized. They also suggested that higher concentration of sulphur gases could speed up the corrosion rate of metal parts and equipment of the electrolysis cell.

Table 2.1 Possible electrochemical reactions between alumina and thiophene, T = 1273 K [82].

Reaction	E_d [V]
$4Al_2O_3 + C_4H_4S \rightleftharpoons 8Al + 4CO_2 + SO_2 + 2H_2O$	0.74
$2Al_2O_3 + C_4H_4S \rightleftharpoons 4Al + 4CO + S + 2H_2O$	0.98
$3Al_2O_3 + C_4H_4S \rightleftharpoons 6Al + 3CO_2 + COS + 2H_2O$	1.06
$3Al_2O_3 + C_4H_4S \rightleftharpoons 6Al + 3CO_2 + CH_4 + SO_3$	1.20
$3Al_2O_3 + C_4H_4S \rightleftharpoons 6Al + 4CO + SO_3 + 2H_2O$	1.21

During the investigation of the behaviour of sulphate ions in the same melt as described above, Burnakin [21] observed increase of metal losses with increasing sodium sulphate concentration up to 3 wt % in the electrolyte. The reduction in the current efficiency was reported to be not more than 0.2-0.3 %. However small this number is, it is in contradiction with the investigations of Barillon and Gilmore [20, 23] who claimed that sulphur has no effect on operation of aluminium cells equipped with prebaked or Söderberg anodes. Because sulphate ions were fairly stable in cryolite in the absence of aluminium, Burnakin ascribed the metal losses to the reactions between sulphate and aluminium listed in Table 2.2. Sulphides can further react with anode carbon to produce SO_2 according reaction 3 in Table 2.2. The increasing rate of sulphide concentration was supported by analysis of the samples.

Table 2.2 Possible reaction of sodium sulphate and sodium sulphide with aluminium and alumina respectively, T = 1250 K [21].

No.	Reaction	ΔG^{θ} [kJ.mol^{-1}]
1	$3Na_2SO_4 + 2AlF_3 + 8Al \rightleftharpoons 6NaF + 4Al_2O_3 + Al_2S_3$	-3615.5
2	$3Na_2SO_4 + 2Na_3AlF_6 + 8Al \rightleftharpoons 12NaF + 4Al_2O_3 + Al_2S_3$	-3540.9
3	$3Na_2SO_4 + 8Al \rightleftharpoons Na_2S + 4Al_2O_3$	-3670.3
4	$3Na_2SO_4 + 8Al \rightleftharpoons 3Na_2O + 3Al_2O_3 + Al_2S_3$	-2677.0
5	$Na_2S + Al_2O_3 \rightarrow 2Al + SO_2 + Na_2O$	-992.9
6	$2Na_2S + 4Al_2O_3 + 3C \rightarrow 8Al + 2SO_2 + 2Na_2O + 3CO_2$	-2969.8

The study of the effect of sulphates on anodic overvoltage tested by adding sodium sulphate to the melt revealed a dramatic drop in overvoltage upon additions of sulphate up to 2.5 wt %. This was attributed to the participation of sulphate in the reactions according to Equations 2.57 and 2.58 but since sulphide was detected in the melt the preference was given to Equation 2.58.

$$Na_2SO_4 + 2Na_3AlF_6 + C \rightleftharpoons 12NaF + Al_2O_3 + 3SO_2 + 3CO \qquad 2.57$$

$$Na_2SO_4 + 2C \rightleftharpoons Na_2S + 2CO_2 \qquad 2.58$$

It was observed that regardless of the sulphur content of the anode mass, the amount of sulphates added to the cell during electrolysis reached a constant value which could be determined by recycling of the fluorides from the escaping gases. Burnakin also compared the temperature of crystallisation of the melt with and without additions of sodium sulphate. He observed that the crystallisation temperature decreased linearly with increasing sulphate concentration and this effect was more pronounced when aluminium was present in the melt.

The laboratory experiment in cryolite with 6 wt % alumina performed by Burnakin et al. [85] at 1000 ºC confirmed their previous observations. After electrolysing in the electrolyte containing 2 wt % sodium sulphate a rapid decrease in sulphate concentration in the melt was observed during first 20 min, whereas the concentration of sulphide reached a maximum during this period and then decreases sharply. After 40-50 min both sulphur forms established a stable level. Thus the depletion of sulphate from the electrolyte was a result of the reduction of sulphate by aluminium and carbon to form sulphides where the reduction by aluminium was demonstrated to happen faster than by carbon.

Recently Ambrová [86] studied chemical and electrochemical reactions of dissolved sodium sulphate in molten chloride and fluoride melts. Based on the chemical analysis of the samples she found that the chemical reduction of sodium sulphate to sulphides proceeds in a similar way in chloride, fluoride and cryolite melts. In chloride melts sulphate was reduced in the presence of liquid aluminium metal or solid carbon according to reactions 2.49 and 2.52 But because only a low content of sulphides was detected in chloride melt, it was assumed that the chemical reaction took place only on the surface of the reducing agent: liquid Al or solid C particles. In cryolite melts higher concentrations of sulphide were formed by reactions 2 and 4 listed in Table 2.2 and also higher losses of aluminium metal were detected in fluoride and cryolite melts. Investigation of the mutual reactions between aluminium sulphide and metal oxides such as FeO and NiO revealed that metal sulphides insoluble in cryolite were formed. If such sulphides react with aluminium under formation aluminium sulphide, they can contribute to metal contamination and decreased current efficiency. Based on chronopotentiometry and simulation it was assumed that sodium sulphate is not stable and decomposes into Na_2O and SO_3. Thus the electroactive species are sulphur trioxide which is reduced to sulphur dioxide and at the same time it thermally decomposes in the range of the experimental temperature (820-1000 ºC) to sulphide, which presence was confirmed by chemical analysis, and sulphate.

From the summary of the research activities dealing with investigations of the sulphur species behaviour in molten salts it is obvious that the chemistry and electrochemistry of sulphur in such media is rather complicated and complex.

2.5 Theoretical considerations and thermodynamics

Sulphates are generally considered as stable compounds. When metallic sulphates are heated in vacuum or in a neutral atmosphere, they can primary decompose to oxides and SO_3 according to the following equations:

$$MSO_4 \rightleftharpoons MO + SO_3 \quad 2.59$$

$$M_2(SO_4)_3 \rightleftharpoons M_2O_3 + 3SO_3 \quad 2.60$$

accompanied by further decomposition of SO_3 to SO_2 and O_2.

The kinetics of this decomposition varies widely with the different metallic cations. The stability decreases with increasing polarizing power of the cations. Thus small cationic size and high charge promote decomposition [87]. Na_2SO_4, Na_2S, Al_2S_3 should all be stable compounds even at high temperature.

Because sodium sulphate is the most important refining agent in the glass industry, its thermal stability was the subject of a few investigations. Lee et al. [88] stated that thermal decomposition of sodium sulphate is significant in the presence of molten glass from 1100 ºC whereas only a very small weight loss is observed for pure Na_2SO_4 below 1200 ºC. Its decomposition causes evolution of gaseous products:

$$Na_2SO_4 \rightarrow Na_2O + SO_2 + 1/2O_2 \quad 2.61$$

Castro et al. [89] examined the thermal transformation of alkaline and alkaline earth metal sulphates on a graphite platform over the temperature range from 200-2000 ºC and identified samples of the solid residues. Their results led to the conclusions that sodium and potassium sulphates exhibit a higher thermal stability than calcium, magnesium and beryllium sulphates. Sodium sulphate was found to be stable compound up to 900 ºC. Above this temperature some amount of it was possibly converted to another sulphur containing species (Na_2S) and above 1200 ºC sulphate fully decomposed to Na_2O and oxygenated sulphur species were released to the gas phase.

On the other hand it has been reported in the literature [90] and it is known from thermodynamic data that Al_2SO_3 is not stable at high temperature (over 800 ºC), the decomposition products being Al_2O_3 and SO_3. At temperatures above 500 ºC SO_3 will decompose to lower sulphur oxide and oxygen.

The phase diagram NaCl-Na_2SO_4 was determined by Gabčová and Malinovský [91], Na_3AlF_6-Na_2SO_4 was studied by Grjotheim et al. [92] and the ternary system Na_3AlF_6-Al_2O_3-Na_2SO_4 was investigated by Matiašovský and Malinovský [93] who showed that there is a considerable solid solubility of sodium sulphate in cryolite which was in agreement with Grjotheim et al. [92]. All the above mentioned phase diagrams are illustrated in Figure 2.3. Koštenská and Malinovský [94] established the NaF-Na_2SO_4 diagram pointing to the presence of the intermediate compound Na_3FSO_4.

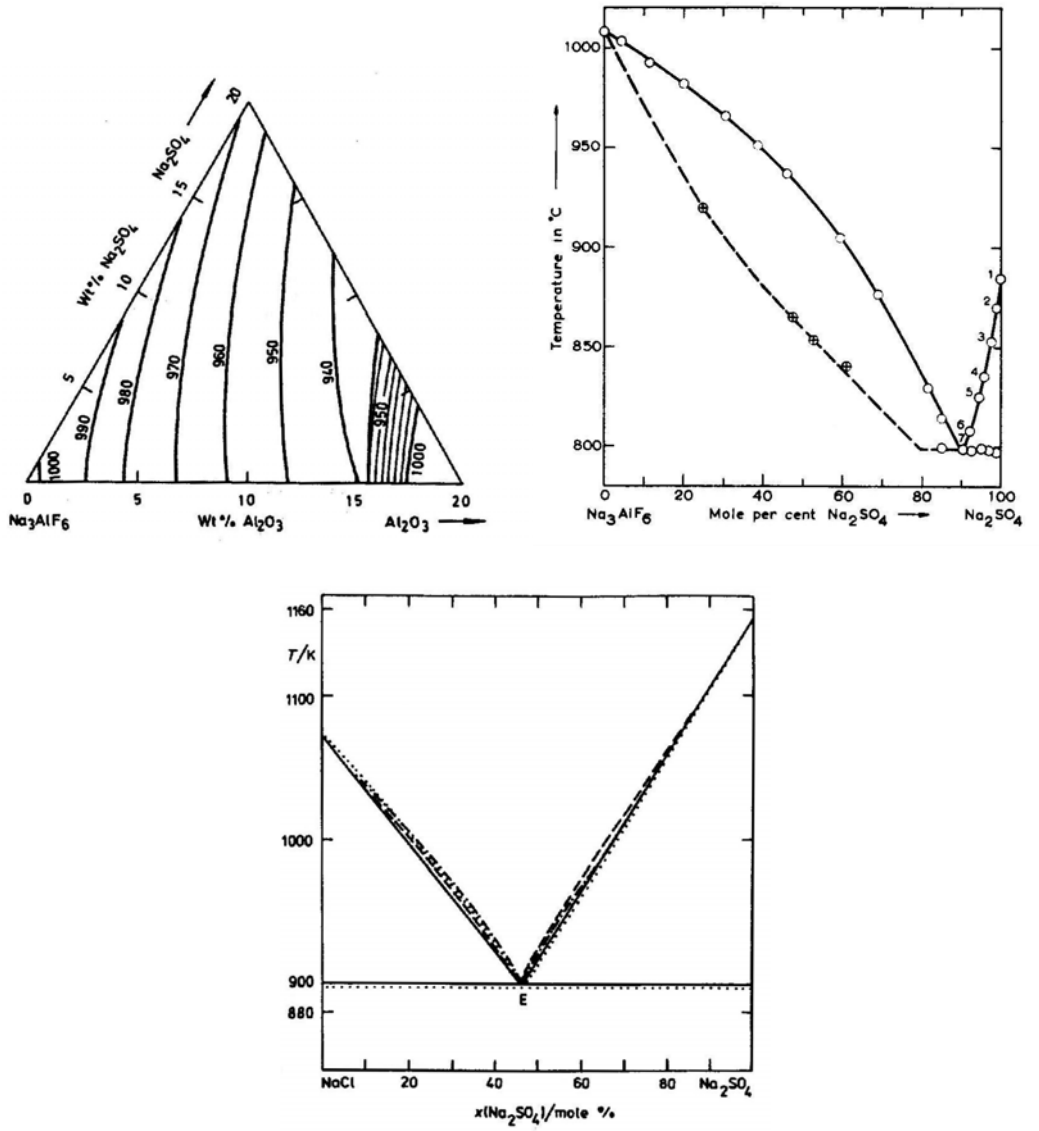

Figure 2.3 The phase diagrams of systems Na_3AlF_6-Al_2O_3-Na_2SO_4, Na_3AlF_6-Na_2SO_4 and NaCl-Na_2SO_4 according to [91-93].

Pourbaix diagrams or potential-pH graphs exist for some of the oxidation states of sulphur species. Such diagrams present the reversible potentials of sulphur redox couples normally in water solutions for different pH values. From these one can see how the oxidizing power of the sulphur-oxygen acids and their anions is greater in acid solutions, while the reducing power is greater in alkaline solution. Unfortunately it is not possible to use those potential diagrams as a reference point for comparing the potentials of sulphur compounds obtained in molten salts with the potentials in water solutions. This is because the properties of aqueous solvents vary from molten salt electrolytes and the solution properties influence the behaviour of the dissolved species.

It was reported by Neumann and Bergve [95] that the decomposition potential of pure Na_2SO_4 electrolysed between two platinum electrodes at 890 ºC and 914 ºC was -2.5 V and -2.45 V, respectively. They indicated that it could be SO_3 reduction to S^{2-} involving an eight electrons exchange. Some possible redox reactions of sodium sulphate with the calculated potentials versus chlorine evolution in chloride melts and oxygen evolution in fluoride melts are given in Tables 2.3 and 2.4. The Gibbs energies for calculations of the potentials in the tables were obtained by the thermodynamic calculation programme FactSage [96]. The components of the reactions were considered to be in the standard states; pure compounds in liquid state at the referred temperature while SO_3, SO_2, O_2 as well as S as gaseous species having a partial pressure of 1 atm.

Table 2.3 Possible reduction reactions of sodium sulphate in sodium chloride melt versus chlorine evolution $Cl^- = 1/2Cl_2 + e^-$, T = 840 ºC.

Overall electrode reaction	$E^{\theta}_{840\ ^oC}$ [V]
$2SO_4^{2-} + 2e^- = SO_2 + SO_3 + 3O^{2-}$	-3.03
$SO_4^{2-} + 2e^- = 2O^{2-} + SO_2$	-3.96
$SO_4^{2-} + 2e^- = O^{2-} + SO_3^{2-}$	-2.96
$SO_4^{2-} + 6e^- = 4O^{2-} + 1/2S_2$	-3.07
$SO_4^{2-} + 8e^- = 4O^{2-} + S^{2-}$	-2.74
$2SO_4^{2-} + 8e^- = 1/2S_2 + 6O^{2-} + SO_2$	-2.19
$2SO_4^{2-} + 6e^- = 1/2S_2 + 5O^{2-} + SO_3$	-1.88
$2SO_4^{2-} + 8e^- = SO_3 + 5O^{2-} + S^{2-}$	-1.63

Table 2.4 Possible reduction reactions of sodium sulphate in fluoride melts versus oxygen evolution $O^{2-} = 1/2O_2 + 2e^-$, T = 1000 ºC.

Overall electrode reaction	$E^{\theta}_{1000\ ^oC}$ [V]
$SO_4^{2-} + 8e^- = S^-$	-0.75
$3SO_4^{2-} + 6e^- = 6O^{2-} + 3SO_2$	-0.34
$SO_4^{2-} + 6e^- = O^{2-} + 1/2S_2$	-0.58
$SO_4^{2-} + 8e^- = O^{2-} + S^{2-}$	-1.13

From the data in the tables follow that sulphate reduction S(+VI) to oxidation states S(0) or S(-II) probably can proceed easier than to the valence state S(+IV). However, it is difficult to draw any conclusion or prediction about the electrochemical behaviour of sulphate based on the data above. For the complete picture of the sulphur behaviour in such systems the kinetics of the process is necessary to take into account.

3 Theory of measurements

The behaviour of sulphur containing species was studied in high temperature molten salts by means of electrochemical experiments. Techniques such as cyclic voltammetry, chronoamperometry and square wave voltammetry commonly used in electrochemistry of molten salts were applied on the systems of interest in order to obtain information about the activity of sulphur compounds which would contribute to a better understanding of their reactivity and reaction mechanism in such media. Because the literature dealing with the theory of electrochemistry is widely available only basic principles and a brief description of applied methods are given in following section of this chapter.

3.1 Electrochemical methods

The electrochemical reduction of species in an electrolyte can be expressed as the sequence of three steps; mass transport of the electroactive species from the bulk of the electrolyte to the electrode, charge transfer of the species in the vicinity of the electrode which happens in a boundary layer called the Helmholtz layer and the mass transport of the product from the electrode to the bulk. The rate of reduction and hence the cathodic current is thus dependent on the rate of the slowest step.

$$O_{bulk} \xrightarrow[\text{transport}]{\text{mass}} O_{electrode} \qquad 3.1$$

$$O_{electrode} \xrightarrow[\text{transfer}]{\text{charge}} R_{electrode} \qquad 3.2$$

$$R_{electrode} \xrightarrow[\text{transport}]{\text{mass}} R_{bulk} \qquad 3.3$$

In an electrochemical system mass transport of species can be due to migration, diffusion or convection. The flux of the species "i" is then the sum of all of their contributions:

$$\underset{}{Flux_i} = \underbrace{-z_i u_i F c_i \nabla\Phi}_{\text{migration}} \; \underbrace{- D_i \nabla c_i}_{\text{diffusion}} + \underbrace{c_i v}_{\text{convection}} \qquad 3.4$$

Migration is the movement of charged species caused by a potential gradient. If a large excess of an inert electrolyte is used, $\nabla\Phi$ becomes small and the migration term can be neglected. Convection is the movement of a species due to mechanical forces. It can be avoided at least for a short period of time if the experiments are performed without stirring or vibration. Besides close to the electrode surface it can be assumed as negligible. However, natural convection arising from density differences occurs when time >10s. Thus diffusion becomes the only mass transport in the studied system. Diffusion is the transport of the

species due to a concentration gradient which is the driving force. If the mass transport is only one dimensional, perpendicular to the electrode surface, then the diffusion is called linear or planar diffusion. It is described by the Fick`s first and second laws given in Equations 3.5 and 3.6 respectively.

$$\text{Flux}_i = - D_i \frac{dc_i}{dx} \qquad 3.5$$

$$\frac{\partial c_i}{\partial t} = D_i \frac{\partial^2 c_i}{\partial x^2} \qquad 3.6$$

The first law expresses the steady state diffusion. The second equation (3.6) describes the variations of concentration with time. In electrochemical context the correlation between the flux and current is given by following equation:

$$\text{Flux}_i = \frac{I_i}{nFA} \qquad 3.7$$

If the reduction of species O to a new compound R is the subject of interest, then the electrochemical process on the electrode can be described:

$$O + n\, e^- \underset{\overleftarrow{k}}{\overset{\overrightarrow{k}}{\rightleftharpoons}} R \qquad 3.8$$

The potential of the working electrode is then expressed in the form of the Nernst equation 3.9 where the electrode potential is related to the standard potential of the species O and R and their activities. If the activity coefficients of oxidized and reduced forms are unity, the concentrations instead of activities can be used.

$$E^{rev} = E^{\theta} + \frac{RT}{nF} \ln \frac{a_O}{a_R} \qquad 3.9$$

The rate of reaction 3.2 can be measured through current or current density and at any potential the measured current density is given by the sum of the partial current densities of forward and reverse reaction 3.2 and depends on a rate constant k and the concentration of the electroactive species.

$$i_{tot} = \vec{i} + \overleftarrow{i} = -nF\vec{k}c_O + nF\overleftarrow{k}c_R \qquad 3.10$$

The rate constants vary with the applied potential according to Equations 3.11 and 3.12 where α_c and $(1- \alpha_c)$ are the cathodic and anodic transfer coefficients.

$$\vec{k} = k^{\theta} \exp\left(-\frac{\alpha_c nF(E-E^{\theta})}{RT}\right) \quad 3.11$$

$$\overleftarrow{k} = k^{\theta} \exp\left(\frac{(1-\alpha_c)nF(E-E^{\theta})}{RT}\right) \quad 3.12$$

At the reversible potential $E = E^{rev}$ when zero current is flowing, both processes reduction and oxidation occur at an equal rate. In such a situation the anodic and cathodic currents sum up to become zero and their magnitudes are equal to the exchange current density defined by Equation 3.13

$$i_0 = nFc_O^0 k^{\theta} \exp\left(-\frac{\alpha_c nF(E^{rev}-E^{\theta})}{RT}\right) = nFc_R^0 k^{\theta} \exp\left(\frac{(1-\alpha_c)nF(E^{rev}-E^{\theta})}{RT}\right) \quad 3.13$$

For the situation when the system is not in equilibrium the overpotential can be defined as the deviation of the measured potential from the reversible potential. In such a case the total current density can be obtained from the Butler-Volmer equation (3.14) and represents the theoretical description of the electrode kinetics. The current density thus varies with the exchange current density i_0, the overpotential η and the transfer coefficients α. The terms in the square brackets are then the anodic and cathodic contributions to the net current.

$$i = \vec{i} + \overleftarrow{i} = i_0 \left[\exp\left(\frac{(1-\alpha_c)nF\eta}{RT}\right) - \exp\left(-\frac{\alpha_c nF\eta}{RT}\right)\right] \quad 3.14$$

If the rate constants $\vec{k}$ and $\overleftarrow{k}$ are both large then the slowest and rate determining step may be diffusion, and the Nernst equation can be applied to calculate the surface concentrations. Such electrode reactions can be called as reversible. If the rate constants are not both large, the process is termed irreversible. At high negative overpotentials the cathodic current density is given by Equation 3.15 and at high positive overpotentials the anodic current density is given by Equation 3.16.

$$\log|i| = \log i_0 - \frac{\alpha_c nF}{2.3RT}\eta \quad 3.15$$

$$\log|i| = \log i_0 + \frac{(1-\alpha_c)nF}{2.3RT}\eta \quad 3.16$$

In practice many studied systems do not exhibit straight reversible or irreversible behaviour but perform quasi-reversibility, an intermediate stage between the earlier mentioned cases.

3.1.1 Cyclic voltammetry

Cyclic voltammetry (CV) is a potential sweep technique widely used for qualitative description of unknown systems. The potential is swept from an initial potential E_1 to the first vertex potential E_2 where the sweep is reversed. When the potential sweep is reaching E_1 value in the reverse scan it can be halted, again reversed or alternatively the sweep can continue to a new value of the second vertex potential E_3. A typical cyclic voltammogram of a reversible system with one electron exchanged is in Figure 3.1.

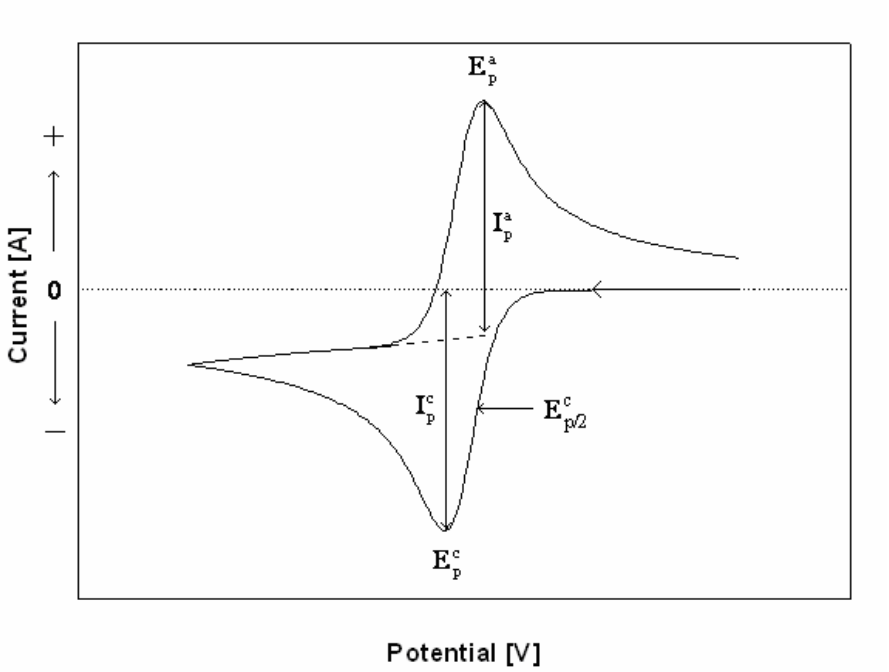

Figure 3.1 Cyclic voltammogram simulated by the FactSage computer program for a reversible system exchanging one electron at 25 ºC.

The solution of Fick`s 2nd law with applied appropriate initial and boundary conditions for oxidized and reduced species represents the mathematical description of the cyclic voltammogram. Assuming that only the oxidized species is initially present in solution and the diffusion coefficients of both forms: O and R are equal, the initial and boundary conditions are:

$$c_O(x,0) = c_O^\infty \qquad c_R(x,0) = 0$$

$$c_O(\infty,t) = c_O^\infty \qquad c_R(\infty,t) = 0$$

$$D\left(\frac{\partial c_O}{\partial x}\right) + D\left(\frac{\partial c_R}{\partial x}\right) = 0 \qquad \text{if } t \rangle 0 \text{ and } x = 0$$

The detailed description of the solution for the current function is complicated because of the time potential dependence and can be found in many publications [97-99]. It has been shown that for a reversible system with soluble reactant and soluble product considering only planar diffusion such a solution is given by the Randles-Sevčik equation (Equation 3.17). The peak current is then proportional to the concentration of the electroactive species, diffusion coefficient and to the square root of the sweep rate.

$$i_p^c = -0.4463\frac{(nF)^{3/2}}{(RT)^{1/2}}c_O^{\infty}D_O^{1/2}v^{1/2} \qquad 3.17$$

A plot of i_p as a function of $v^{1/2}$ should be linear and pass through the origin. The diffusion coefficient can then be calculated from the slope of the straight line. The peak potential for such a system can be defined by means of the half-peak potential $E_{p/2}$ (the potential where the current reaches half of the peak current value):

$$E_p = E_{p/2} - 2.2\left(\frac{RT}{nF}\right) \qquad 3.18$$

Other diagnostic criteria for cyclic voltammograms of a reversible process involving soluble species are as follows:

- $\Delta E_p = E_p^a - E_p^c = 2.2\left(\frac{RT}{nF}\right)$
- $\left|i_p^a/i_p^c\right| = 1$ when the diffusion coefficients of both the reduced and oxidized species are equal
- E_p is independent of sweep rate
- at potentials beyond E_p, the current is proportional to $t^{-1/2}$

If an insoluble product is formed, the peak current is given by the Berzins-Delahay equation 3.19 and the peak potential is expressed by Equation 3.20.

$$i_p^c = -0.610\frac{(nF)^{3/2}}{(RT)^{1/2}}c_O^{\infty}D_O^{1/2}v^{/2} \qquad 3.19$$

$$E_p = E_{p/2} - 0.77\left(\frac{RT}{nF}\right) \qquad 3.20$$

As it was mentioned earlier in the high temperature molten salts it is more

common to deal with quasi-reversible systems than with reversible processes. Such a quasi-reversibility of a system can be recognised by the following criteria:

- the peak current is proportional to $v^{1/2}$, but from a certain sweep rate the relationship deviates from linearity
- $\left|i_p^a/i_p^c\right| = 1$ if the transfer coefficients α_a and α_c are equal to 0.5
- ΔE_p increases with increasing sweep rate
- E_p^c shifts to more negative values with increasing sweep rate

When the electron transfer rates are not greater than the rate of the mass transport, the Nernstian equilibrium cannot be maintained at the electrode surface and the system behaves irreversibly. In the most extreme case the absence of a reverse peak is the most significant feature that serves to recognise irreversible systems. Since this can be also due to a fast following chemical reaction other characteristics which serve to recognise irreversible behaviour must be fulfilled:

- E_p^c shifts with increasing sweep rate and is linearly proportional to log sweep rate. Then the number of exchanged electrons and á can be determined from: $\frac{dE_p^c}{d\log v} = -1.15\frac{RT}{\alpha nF}$
- i_p^c must be proportional to $v^{1/2}$
- $E_p - E_{p/2} = 1.86\left(\frac{RT}{\alpha nF}\right)$

3.1.2 Chronoamperometry

Chronoamperometry (CA) is a potential step technique in which the potential of the working electrode is changed instantaneously from the initial potential E_1 to a new step potential E_2 and is held at this potential for a sufficient time so that the reduction of the O species can occur at a diffusion controlled rate. E_1 is chosen at a potential value at which no electrode reaction occurs. In this technique the current is monitored as a function of time. Such a CA potential-time profile is shown in Figure 3.2. The equation which describes this current-time response for a planar electrode represents the solution of the Fick`s 2nd law with the boundary conditions: $c_O(x,0) = c_O^\infty$; $\lim_{x\to\infty} c_O(x,t) = c_O^\infty$; $c_O(0,t) = 0$ and is called the Cottrell equation:

$$\left|I_{lim}\right| = \frac{nFAD_O^{1/2}c_O^{\infty}}{\pi^{1/2}t^{1/2}} \qquad 3.21$$

A plot of current versus $t^{-1/2}$ should be linear and pass through the origin if the process is diffusion controlled and the diffusion coefficient of the electroactive species is directly proportional to the slope of the curve.

During the first period of the potential change the current will be influenced by double layer charging while the current at long time is affected by natural convection. Hence the data in the range of 1ms to 10 s are usually collected.

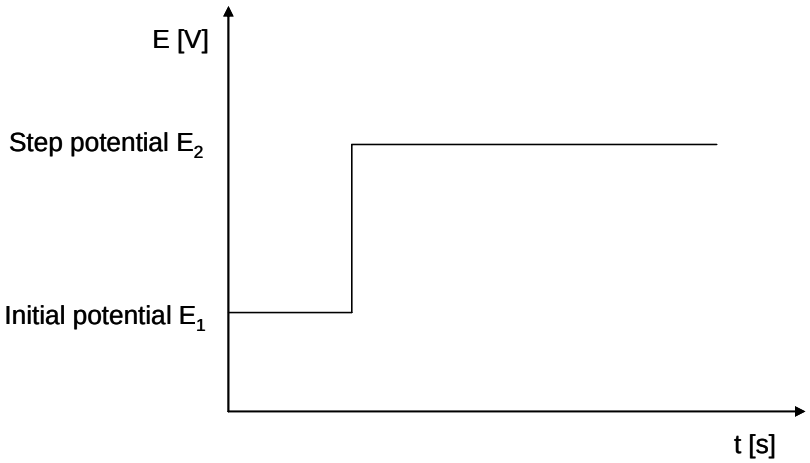

Figure 3.2 The potential-time profile for a single chronoamperometric potential step.

CA can also be applied to determine the number of exchanged electrons in a redox process. If the overpotential of diffusion controlled reversible reduction is defined as a function of the limiting current, then from the slope of such a relationship one can obtain the number of electrons participating in the process. For a reduction reaction involving soluble reactant and insoluble product the equation can be written as:

$$\eta = E - E^{rev} = \frac{RT}{nF}\ln\left(\frac{I_{lim}-I}{I}\right) \qquad 3.22$$

If reactant and product are both soluble species the equation has the following form:

$$\eta = E - E^{rev} = \frac{RT}{nF}\ln\left(\frac{I_{lim}-I}{I_{lim}+I}\right) \qquad 3.23$$

3.1.3 Square wave voltammetry

Square wave voltammetry (SQWV) is a pulse method and its potential-time waveform applied to the electrode is shown in Figure 3.3. During each period of the square wave the pairs of current measurements are performed: $I_{forward}$, $I_{reverse}$ and $I_{difference}$. A SQW voltammogram is then a plot of the differential current as a function of the potential and the sweep rate is altered by changing the square wave frequency or the amplitude of the staircase waveform.

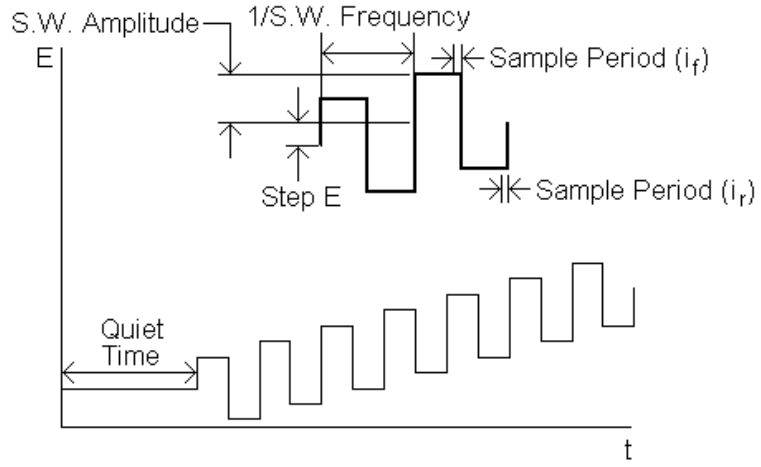

Figure 3.3 Potential wave form for square wave voltammetry [100].

The advantage of this technique is that when the sum of synchronized square wave and staircase potential is applied to a stationary electrode, the double layer charging current will become negligible when measuring at a suitable time after the pulses occur. The resulting current-time response for a reversible system involving soluble species is a symmetrical Gaussian shaped peak at $E_{1/2}$ [98, 101].

Such a bell-shaped peak has following main characteristics:

- The width of the SQWV peak $W_{1/2}$ at half of its height varies with the peak-to-peak square wave amplitude ΔA and is a function of the exchanged electrons and temperature as written in the following equation

$$W_{1/2} = 3.52\frac{RT}{nF} \qquad 3.24$$

- The differential current is a linear function of the bulk concentration of the electroactive species and is directly proportional to the square root of the square wave frequency f [102]

$$dI_p = nFAc_O \frac{1-\Gamma}{1+\Gamma}\sqrt{\frac{Df}{\pi}} \qquad 3.25$$

where Γ is defined as:

$$\Gamma = \exp\left(\frac{nF}{RT}\frac{\Delta A}{2}\right) \qquad 3.26$$

This method is suitable for any electrochemical system as long as the differential peak current varies linearly with the concentration of the electroactive species and the square root of the frequency of the staircase signal.

3.2 Analytical methods

3.2.1 Determination of sulphides and sulphites

Sulphides and sulphites can be determined by titrimetric analysis with iodine which is called iodimetry [103, 104]. Iodimetric titrations are based on reaction 3.27 in which iodine can be employed in two ways. It may be used as a standard solution and titrated into the reducing solution or it may be liberated from iodine compound by an oxidising agent in solution and consequently titrated with thiosulphate solution or some other standardised reducing solutions.

$$I_2 + 2e^- \rightleftharpoons 2I^- \qquad 3.27$$

Sulphites SO_3^{2-} react with I_2 in slightly acidic solution according Equation 3.28. The surplus of iodine solution is then determined by back titration with $Na_2S_2O_3$.

$$SO_3^{2-} + H_2O + I_2 \rightleftharpoons SO_4^{2-} + 2H^+ + 2I^- \qquad 3.28$$

Reaction of suphides with iodine in acidic solution can be expressed by Equation 3.29. Similarly as in case of sulphites, the surplus of iodine solution is titrated by sodium thiosulphate.

$$S^{2-} + I_2 \rightleftharpoons S + 2I^- \qquad 3.29$$

During the titrimetry HCl is added to the solutions of analysed sulphur compounds to prevent evolution of SO_2 or H_2S and thus eliminate sulphur losses.

For the analysis the commercial solution of $Na_2S_2O_3$ was used (0.1 mol.dm^{-3}, Titrisol® Merck KGaA). The rest of the solutions were prepared according to the description in the literature [105].

3.2.2 Determination of sulphur dioxide

Presence of sulphur dioxide SO_2 (or sulphur trioxide SO_3) may be determined by oxidation of SO_2 with solution of hydrogen peroxide H_2O_2 to H_2SO_4 and subsequent acid-base titration with NaOH [106]. The off gases from the laboratory furnace were bubbled through the solution of H_2O_2 (3%) where SO_2 (SO_3) was converted by oxidation to H_2SO_4. This was further neutralized by titration with 0.1 mol.dm^{-3} solution of NaOH (Dilut-It® J.T.Baker) on phenolphthalein indicator. The reaction can be represented by Equation 3.30

$$H_2SO_4 + 2NaOH = Na_2SO_4 + 2H_2O \qquad 3.30$$

4 Experimental measurements

4.1 Experimental set-up

Experiments were carried out in a closed, vertical, electrically heated furnace with water-cooling system, shown in Figure 4.1

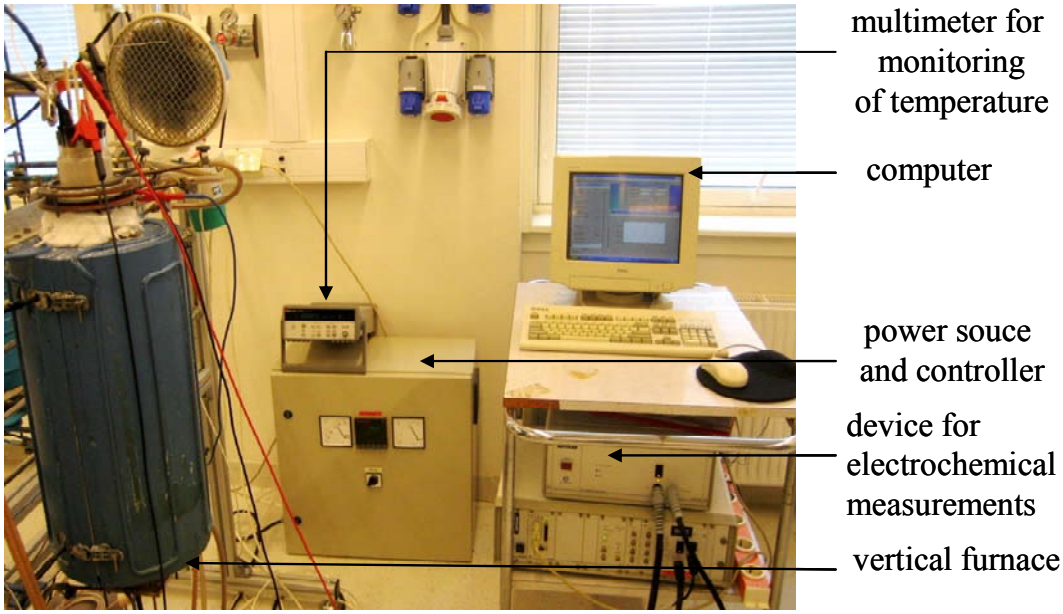

Figure 4.1 Laboratory furnace with electrochemical device.

The electrochemical response of the system was mainly measured by Autolab potentiostats PGSTAT 20 operating with GPES software (General Purpose Electrochemical system) except the preliminary experiments that were monitored by Zahner IM6e electrochemical device equipped with Thales software. The temperature of the electrolyte varied with the melt composition from 450 ºC to 1000 ºC and was measured by a Pt-Pt10%Rh thermocouple placed in an Alsint (sintered Al_2O_3) tube which was immersed in the bath. The temperature of the furnace was controlled by another thermocouple of the same type inserted horizontally through the steel frame of the furnace to be in contact with the Pythagoras tube placed inside the furnace and connected to a Eurotherm controller.

A three-electrode arrangement was used for all the electrochemical experiments with working (WE), counter (CE) and reference (RE) electrodes. The CE was made of a platinum wire that was coiled to ensure a larger area compared to the WE. Platinum served as the CE in all experiments in the chloride and fluoride melts except the preliminary investigations focused on examining the material

inertness and its suitability for further studies. The specification of other CE`s used in such experiments is given in the chapter 4.3.1 in context with each system. In the chloride melts $Ag/AgCl_{(diss.)}$ sealed in a Pythagoras tube was used as RE. In the experiments with fluoride melts an aluminium electrode was made in order to give a well-defined reference potential. It was constructed from a tungsten wire whose bottom part was covered by a layer of liquid aluminium and from the electrolyte it was protected by an Alsint tube. The contact of such an aluminium reference electrode with the melt was realized through a small hole in the lower part of the protecting tube close to its bottom. The WE was a metal wire with 1 mm in diameter and immersed to the electrolyte in the depth of 1 or 1.5 cm. The contact of the WE with the electrolyte was monitored by the change of resistance or potential and thus the immersion depth was controlled. All the studied electrolytes were placed in Alsint crucibles and together with the electrodes and the thermocouple they were sealed in the glass or steel cell equipped with Alsint radiation shields to maintain equal heat distribution. Argon gas (99.999 %) was flushed through the cell at a constant rate during all the measurements to ensure an inert atmosphere. A picture of the experimental set-up is shown in Figure 4.2.

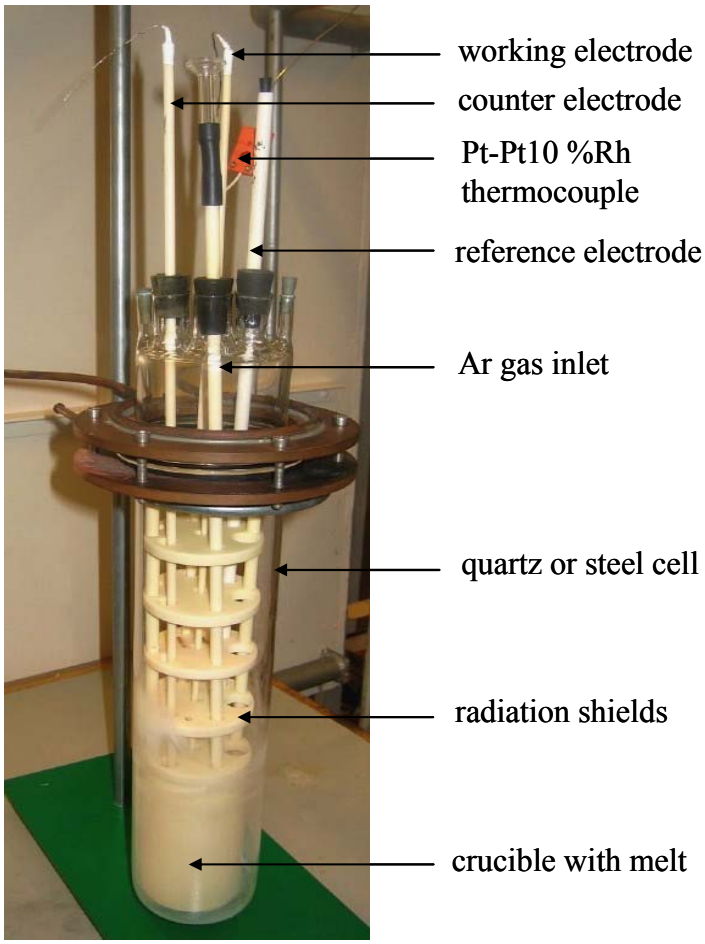

Figure 4.2 Experimental set-up with three electrode arrangement.

4.2 Chemicals

All chemicals and their specifications and treatment before they were used in the experiments are listed in Table 4.1.

Table 4.1 Chemicals used in the electrochemical experiments

Chemical	Producer	Quality	Treatment before use
Argon gas	Aga	(99.999 %)	Used as received
NaCl	Merck or Acros	for analysis	Heated to 750 ºC for 4 hours
$CaCl_2.2H_2O$	Merck	for analysis	Heated to 200 ºC for 4 hours, thereafter stored in glow box in Ar atmosphere
KCl	Merck	for analysis	Heated to 550 ºC for 4 hours, thereafter stored in glow box in Ar atmosphere
LiCl	Merck	for analysis	Heated to 550 ºC for 4 hours, thereafter stored in glow box in Ar atmosphere
Na_2SO_4	Merck	for analysis	Heated to 600 ºC for 4 hours, thereafter kept in a heating chamber at 200 ºC
K_2SO_4	Merck	for analysis	Heated to 600 ºC for 4 hours, thereafter kept in a heating chamber at 200 ºC
Na_2SO_3	Merck	for analysis	Heated to 200 ºC for 4 hours
K_2S	Merck	for analysis	Heated to 200 ºC for 4 hours
NaF	Merck	for analysis	Heated to 500 ºC for 4 hours, thereafter kept in a heating chamber at 200 ºC
AlF_3	Norzink	technical grade	Sublimated at 1090 ºC under vacuum for at least 12 hours, thereafter kept in a heating chamber at 200 ºC
γ-Al_2O_3	Merck	for analysis	Heated to 500 ºC for 4 hours, thereafter kept in a heating chamber at 200 ºC

4.3 Results and discussions. Electrochemical studies of sulphur species in molten chlorides

The electrochemical behaviour of sulphates was studied in a simple NaCl melt and in binary electrolytes of eutectic LiCl-KCl mixture and $CaCl_2$-NaCl (10-90 mol%) melt. Sulphur was also added in the form of sulphite and sulphide in the eutectic LiCl-KCl mixture and investigated at temperatures below 500 ºC. The potential range where electrochemical reactions of sulphur compounds can be monitored varies with the temperature and the decomposition potential of the supporting electrolyte. Standard decomposition potentials of selected chlorides used in the experiments calculated by FactSage software are given in Table 4.2. It follows from data in the table that the potential window broadens with decreasing temperature and that the single KCl melt is more stable than NaCl, LiCl or $CaCl_2$.

Table 4.2 Standard decomposition potentials for selected chlorides as a function of temperature.

E_d^θ [V] / T [K]	E_d^θ (NaCl)	E_d^θ ($CaCl_2$)	E_d^θ (LiCl)	E_d^θ (KCl)
1113	-3.21	-3.25	-3.35	-3.45
1013	-3.28	-3.32	-3.41	-3.52
733	-3.47	-3.51	-3.57	-3.72

The cathodic limit of the potential window is set by the reduction of the metallic element of the melt according to Equation 4.1 and oxidation of chloride to chlorine sets the limit for applying anodic potentials according to Equation 4.2.

$$M^{x+} + xe^- \rightleftharpoons M \qquad 4.1$$

$$yCl^- \rightleftharpoons y/2Cl_2 + ye^- \qquad 4.2$$

4.3.1 Electrode testing in chloride melts

The working electrode is an important part of the electrochemical set-up and must meet certain requirements, which are imposed on the material from which it is constructed. The requirements depend on the purpose of the studies as well as on the investigated system. Some of the essential demands are well-defined geometry in order to obtain even current and potential distributions and the chemical inertness of the electrode, which means that the material should not interact chemically with the components of the melt or the studied system. Especially in high temperature chemistry the selection of materials, which could withstand the temperature and corrosion attack of the bath, is limited. Thus for electrochemical studies in molten salts, solid electrodes such as platinum, gold and tungsten are usually used. Therefore the preliminary experiments were performed with a task to find the most inert and suitable material which would meet such criteria and from which the working electrode could be constructed and used for further experiments.

Due to the fact that carbon and some metals e.g. Al or Ni act as reducing agents for sulphur species [64, 79, 86], carbon crucibles and electrodes (glassy carbon as well) were preferably excluded from experiments. However, in a few preliminary investigations glassy carbon served as CE. Thus only metals (copper, molybdenum, tungsten and platinum) were chosen to be the working electrodes. Their stability and electrochemical behaviour were examined by means of cyclic voltammetry and Mo, W and Pt underwent a chemical stability test too. The CVs were performed in simple NaCl electrolyte at temperatures above 800 ºC with small quantities of sulphur added as Na_2SO_4. The characteristic cyclic voltammograms recorded on copper (see Figure 4.3), molybdenum (Figure 4.4), tungsten (Figure 4.5) and platinum (Figure 4.6) with detailed descriptions are presented below.

- *Copper electrode*

Typical cyclic voltammogram obtained on copper electrode with and without SO_4^{2-} anion present in NaCl melt is shown in Figure 4.3. Addition of sulphate increased the current response of the electrode and gave rise to a single reduction peak A associated with one oxidation peak A` in the reverse scan. During the experiment the Cu electrode was partially melted probably as a result of hot corrosion. Moreover according to the binary phase diagram of Cu-S formation of copper sulphides that is stable up to very high temperature is highly probable. Therefore the origin of the signal at potentials of peak A and A` could be the result of Cu-S interaction and cannot be assigned to sulphate reduction without ambiguity. Besides the potential window is limited by notable anodic oxidation of Cu which increases with the introduction of oxide ions as a component of sulphate anions. Due to the above mentioned reasons copper was excluded from further experiments.

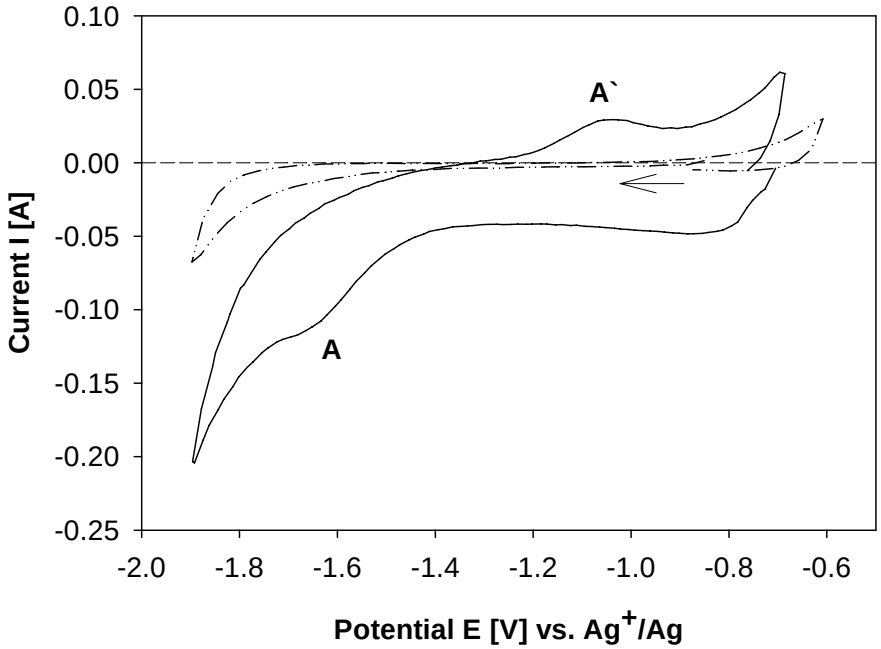

Figure 4.3 Cyclic voltammograms on a copper working electrode in molten NaCl before (dashed line) and after addition of $0.97 \cdot 10^{-5}$ mol.cm^{-3} Na_2SO_4 (solid line); CE = glassy carbon, v = 300 mV.s^{-1}, T = 850 ºC. The arrow indicates the scanning direction for both curves.

- *Molybdenum electrode*

CVs obtained on molybdenum electrode (Figure 4.4) show three main cathodic waves after sulphate ions were added to the electrolyte. In this experiment molybdenum also served as a quasi-reference electrode whose potential shifted with added Na_2SO_4 and caused the difference in potential windows. From the CVs a substantial difference is obvious between the 1st and 2nd scan of the sulphate reduction. As the number of the scans increased the current decreased indicating concentration changes of electroactive species or an additional process taking place on the surface of the electrode which would lead to a smaller active area of the electrode. Because the concentration of the sulphate ions could be considered constant a chemical interaction of sulphate with electrode which leads to blocking of the electrode surface remained as the only explanation. When the electrode was withdrawn from the melt, its surface was fully covered by a black deposit. According to the binary phase diagram of Mo-S this black layer can be attributed to molybdenum sulphides: MoS_2 or Mo_2S_3.

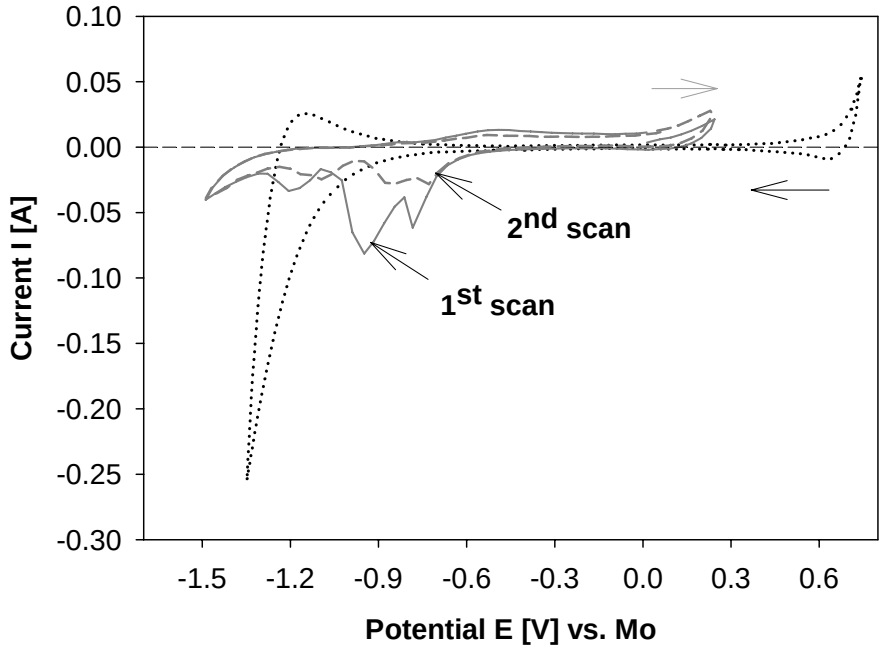

Figure 4.4 Cyclic voltammograms on a molybdenum working electrode in NaCl melt before (dotted black line) and after addition of $1.08 \cdot 10^{-5}$ mol.cm^{-3} Na_2SO_4 (grey lines); CE = Mo, v = 300 mV.s^{-1}, T = 850 ºC. The arrows indicate the scanning direction.

- *Tungsten electrode*

After the addition of Na_2SO_4 to NaCl, one sharp reduction peak A and a few anodic waves were observed in CVs obtained on tungsten (Figure 4.5). It is a well known fact from the binary phase diagram of W-O and from the studies of similar systems in molten salts that tungsten easily gets oxidized and a layer of stable tungsten oxide is formed on electrode. Moreover, the binary phase diagram of W-S says that tungsten forms with sulphur species sulphides with similar structure as MoS_2. During and after the experiment it was also observed that the tungsten electrode is not inert in the chloride-sulphate system and underwent surface changes. Due to these facts the peaks on the CVs could result from various redox processes and not only from sulphate reduction and reversed oxidation. During the experiment the electrode became thinner until the immersed part was finally dissolved completely in the melt. Thus tungsten cannot be used as electrode material.

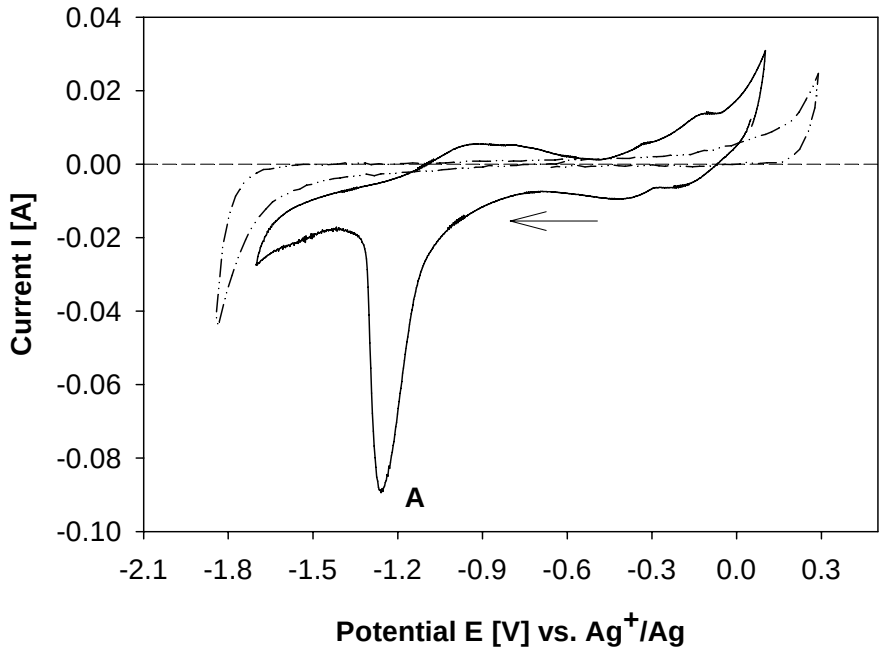

Figure 4.5 Cyclic voltammograms on a tungsten working electrode in NaCl melt before (dashed line) and after addition of $1.07 \cdot 10^{-4}$ mol.cm^{-3} Na_2SO_4 (solid line); CE = glassy carbon, v = 300 mV.s^{-1}, T = 845 ºC. The arrow indicates the scanning direction for both curves.

- *Platinum electrode*

A typical CV recorded on Pt in molten NaCl is shown in Figure 4.6. The potential window of Pt allows for monitoring electrochemical processes in range of approximately 2.5 V. However, the calculated theoretical standard decomposition potential of NaCl at 840 ºC is 3.2 V. This discrepancy can be explained by anodic dissolution and passivation of platinum in the presence of oxide or chloride ions. Such behaviour was observed by Burrows [68] and Sequeira[72]. and confirmed in the works of Inman [107] and Asakura [108] who studied the anodic behaviour of platinum in chloride systems. It was concluded that such passive layer could be built by sort of platinum oxides of Pt_nO_m type. Suggestion that complex of $PtCl_6^{2-}$ is responsible for the passivation was presented by Haan and Porter too [109]. Some anodic dissolution of platinum was also observed and suggested by Ambrová [86] in her work as well. This could lead to increased catalytic effect of platinum on the reduction of the sulphate species. The cathodic limit is set by sodium metal deposition that begins from about -1.7 V versus the Ag^+/Ag reference electrode. Because sodium deposition at low activity of Na is probable, this could also cause reduction of the potential window.

When sodium sulphate was added to the electrolyte of NaCl a reduction wave A close to metal deposition appeared connected with an oxidation reverse peak A`. Because the platinum electrode was not observed to be significantly attacked during the preliminary experiment Pt was found to be the most suitable material for investigating the cathodic processes such as sulphate reduction if the scanning in anodic direction is halted soon enough to avoid anodic polarization of Pt. Nevertheless it must be mentioned here that the binary phase diagram of Pt-S shows a phase of PtS stable up to 1240 ºC and reaction of Pt with a product or products of sulphate reduction was reported by Sequiera and Hocking [72] too. Ambrová [86] observed an attack of platinum crucible which served also as a counter electrode in her experiments but when she examined the Pt working electrode by microanalysis she did not detect any PtS on the surface. Similarly no sulphur layer on the surface of the working electrode was in fact detected after the experiments in the present work. Based on this, Pt is not inert material either but with some limitations it can be used as a working electrode.

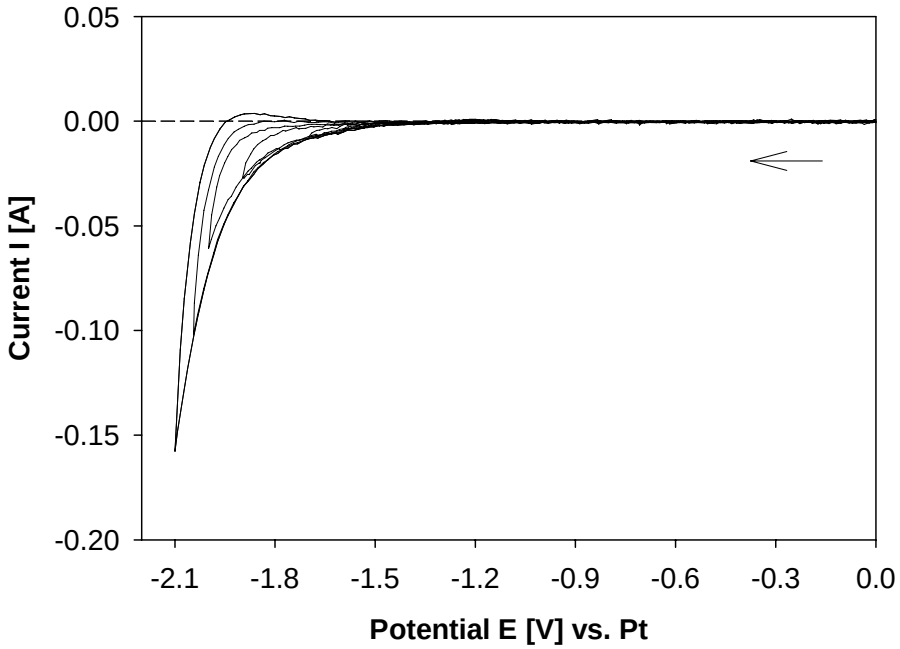

Figure 4.6 Cyclic voltammograms in NaCl with a platinum used as working, reference and counter electrode; v = 300 mV.s^{-1}, T = 835 ºC. Arrow shows the sweep direction.

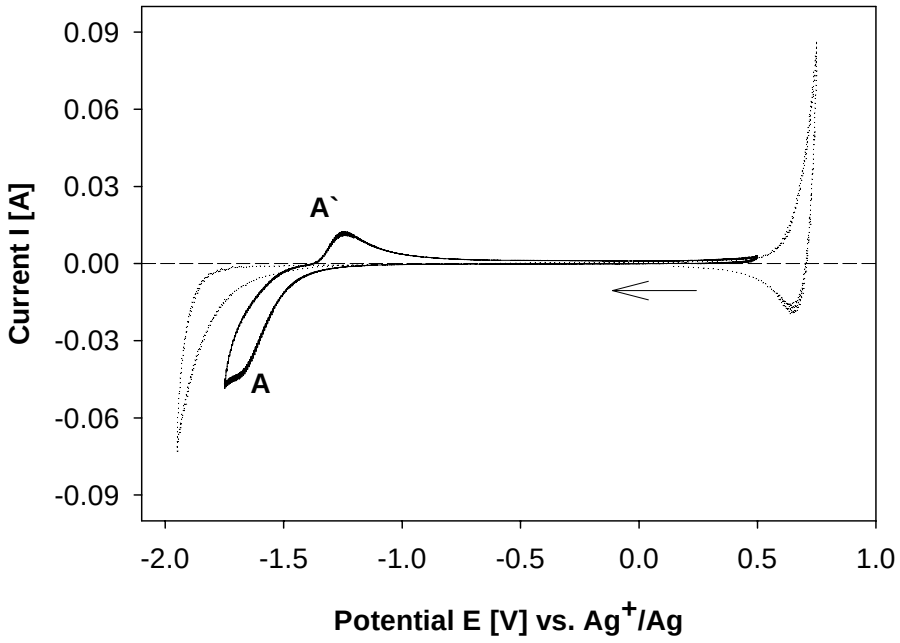

Figure 4.7 Cyclic voltammograms on a platinum working electrode in NaCl melt before (dotted line) and after addition of $1.08 \cdot 10^{-5}$ mol.cm^{-3} Na_2SO_4 (solid line). The arrow indicates the scanning direction for both curves. CE = Pt, v = 300 mV.s^{-1}, T = 840 ºC.

- *Chemical stability test*

Mo, W and Pt wires were subject of a so-called chemical stability test. They were immersed in the electrolyte consisting of NaCl with 5 wt% Na_2SO_4 and kept at 915 ºC without polarization. After 17 hours they were pulled out of the bath and the changes on their surface were examined visually. While platinum remained unchanged, remarkable modification of molybdenum and tungsten was visible. The Mo wire maintained the same diameter as it had before the experiment but was covered by a black deposit. On the other hand, the diameter of the tungsten wire was reduced to a very thin needle like shape without any adsorbed layer. These results only confirmed the previous observations and conclusions derived from cyclic voltammetry studies that Mo and W unlike Pt chemically react with sulphur species.

4.3.2 The NaCl-Na_2SO_4 system

Because the electrochemistry in high temperature molten salts is usually complicated and the high reactivity of sulphur compounds, a simple electrolyte with only one component such as NaCl was chosen for the primary studies of sulphate reduction. The NaCl-Na_2SO_4 system was investigated by means of CV and CA on a platinum working electrode versus a silver/silver chloride reference.

- *Cyclic voltammetry*

A typical cyclic voltammogram of sodium sulphate in NaCl at 840 ºC was given in Figure 4.7 and the more detailed picture with a region where the sulphate reduction takes place is shown in Figure 4.8. The dotted line represents the situation before sulphate was added and shows only sodium deposition (B) which also sets the cathodic limit of the melt. After addition of sulphate, a new cathodic peak (A) at -1.7 V vs. Ag^+/Ag appeared in the vicinity of the sodium deposition followed by a single reverse anodic peak (A`) at -1.3 V. The evolution of peak couple A/A` is evident from Figure 4.8 when changing the potential in cathodic direction from -1.5 V to -1.95 V. The shape of the A and A` peaks suggests a system involving soluble species (reactant as well as product).

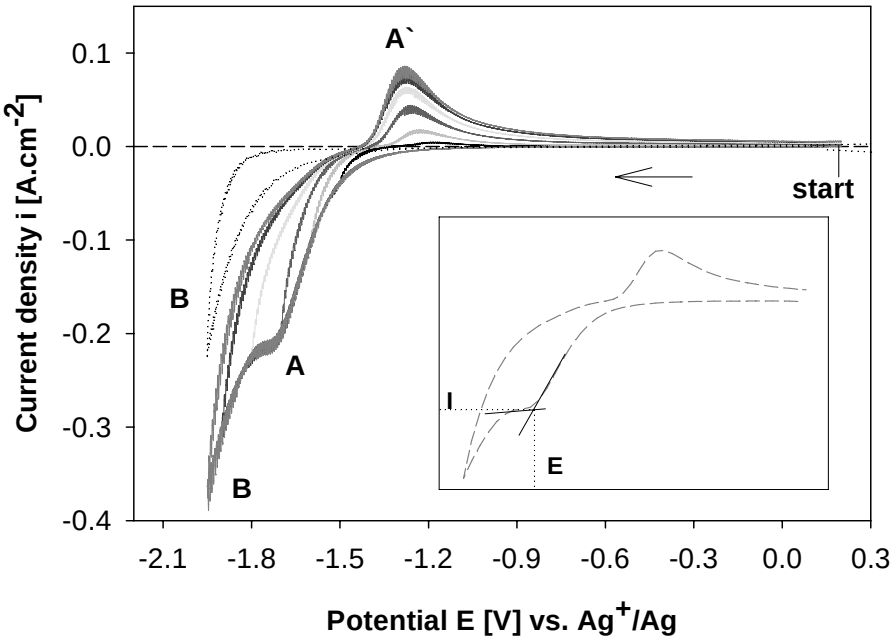

Figure 4.8 CVs recorded in sodium chloride melt before (dotted line) and after addition of $2.16 \cdot 10^{-5}$ mol.cm^{-3} Na_2SO_4 on a Pt electrode; T = 840 ºC, v = 300 mV.s^{-1}.

Due to the location of the cathodic peak A close to the sodium deposition the readability of the peak parameters is considerably influenced. Especially at sweep rates higher than 1.5 V.s^{-1} it was not possible to evaluate and obtain precise peak information because both reduction peaks A and B tend to merge and the current of sodium deposition becomes dominating. In the inset of Figure 4.8 it is shown how the peak parameters, i.e. peak current and peak potential, were determined.

The influence of sweep rate on current density of peak couple A/A` is shown in Figure 4.9. To check whether a plot of peak current is linearly proportional to the square root of the sweep rate is useful as the primary test of reversibility of the studied system. However, there are further diagnostic tests which should be satisfied by a reversible system. The plots for cathodic peak A resulting from sulphate reduction are given in Figure 4.10 for six various concentrations of sodium sulphate. To minimize the influence of current resulting from sodium deposition on the sulphate reduction (peak A), the response of pure sodium chloride melt was subtracted as a background current from the current of peak A. As it can be seen from Figure 4.10 a linear relationship between the peak current of peak A and the sweep rate has been obtained for sweep rates in range from 30 mV.s^{-1} up to 1200 mV.s^{-1}. Also a linear relationship between concentrations of reduced species and sweep rate was revealed.

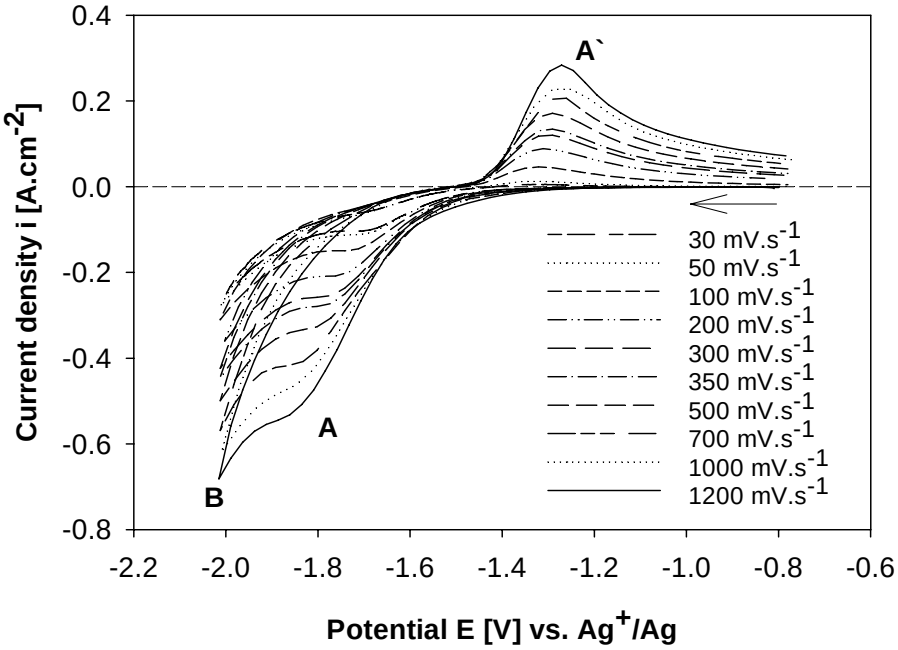

Figure 4.9 Voltammograms of the system A/A` with various sweep rates in NaCl melt at 830 ºC on a Pt electrode. Concentration of Na_2SO_4 : $3.28 \cdot 10^{-5}$ mol.cm^{-3}.

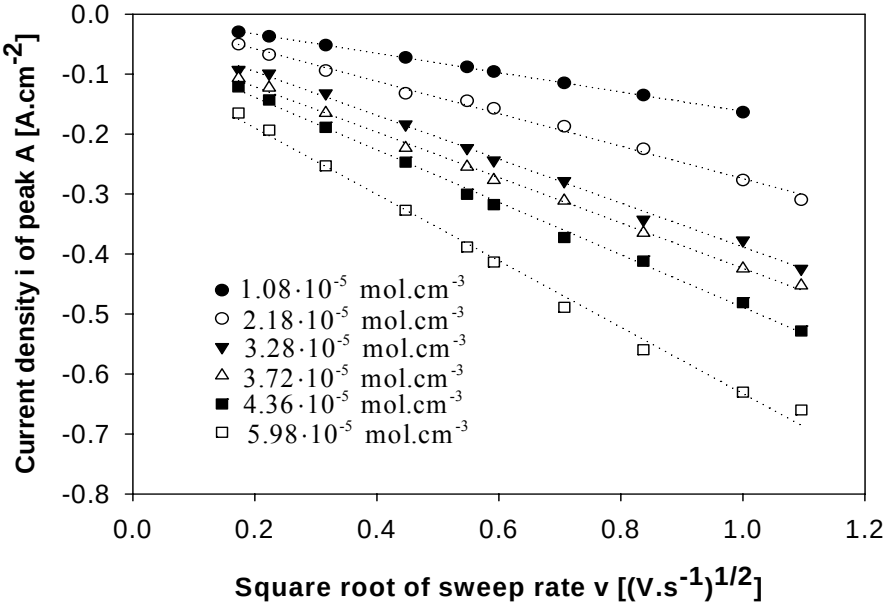

Figure 4.10 Plot of cathodic current densities of peak A versus the square root of the sweep rate with fitted regression lines for various concentrations of Na_2SO_4 in NaCl melt at 830 ºC. Sweep rate range: 30 mV.s^{-1} to 1200 mV.s^{-1}.

In an ideal case of a diffusion controlled system the regression lines should pass exactly through the origin. However, from Figure 4.10 a certain shift of the regression lines along the vertical axis is obvious increasing with the concentration of electroactive species. This shift might indicate that another process is taking place together with the diffusion, e.g. chemical reaction following charge transfer or it can be due to the influence of the sodium reduction. However, additional criteria which are stated in chapter 3.1.1 must be fulfilled for the system to be considered reversible.

For a system which is fully reversible, the peak potential should remain stable and the potential difference ΔE of anodic and cathodic peak defined as E_p^A-$E_p^{A`}$ should be a constant value independent on the sweep rate. It is noticeable from Figure 4.9 that the peak potential of peak A ($E^A$) shifts towards more negative potential values and the potential of peak A` ($E^{A`}$) shifts to more positive potentials as the sweep rate is increased. This is documented and more evident from Figure 4.11 where the potentials shift and peak separation ΔE are plotted as a function of the sweep rate. From sweep rates 750 mV/s and higher the potentials approaches a constant value and the influence of sweep rate is negligible. The observed shift of potentials might be an indication of a coupled chemical reaction taking place.

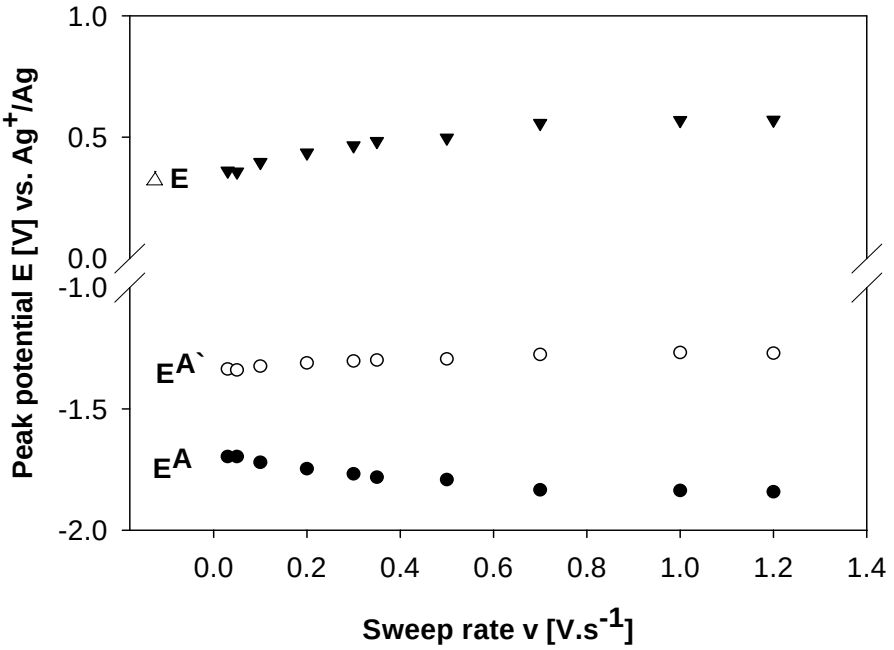

Figure 4.11 Potential values of A and A` plotted as function of sweep rate for $3.28 \cdot 10^{-5}$ mol.cm^{-3} Na_2SO_4 at 830 ºC. Sweep rate range: 30 mV.s^{-1} to 1200 mV.s^{-1}.

If a chemical reaction follows the charge transfer, the product of the reaction is removed from the electrode and the cyclic voltammograms then depend on the relative rates of these two steps. The peak current is proportional to $v^{1/2}$ as in the case of pure Nernstian diffusion [110, 111]. The cathodic peak potential is affected by the presence of the chemical reaction too. It shifts in the negative direction as the sweep rate increases till the moment when the influence of the chemical reaction reduces and the Nernstian diffusion begins to dominate. Thus the part of the plot where the peak potential is independent of sweep rate at fast scans corresponds to the diffusion controlled zone.

$$O + ne^- \rightleftharpoons R \qquad 4.3$$

$$R \rightarrow Y \qquad 4.4$$

If the charge transfer is reversible and the chemical reaction is irreversible and fast (according to "ec" scheme in Equations 4.3 and 4.4), at low sweep rates no reverse peak is observed and the electrode reaction is apparently totally irreversible. As the sweep rate is increased, the reverse peak becomes apparent and the current increases because the rate of the chemical reaction becomes smaller than the rate of the charge transfer. The ratio of the anodic and cathodic peak current continues to increase with the sweep rate until reversible behaviour is observed. Thus the absolute value of the current ratio of oxidation (I_p^{anodic}) and reduction ($I_p^{cathodic}$) peaks $\left|I_p^{anodic}/I_p^{cathodic}\right|$ is less than one but tends to approach unity with increasing sweep rate. For an ideal reversible diffusion controlled process the current ratio $\left|I_p^{anodic}/I_p^{cathodic}\right|$ should be equal to 1. Except that the cathodic peak potential shifts negatively as the sweep rate increases until reversible sweep rate independent behaviour starts to prevail, the ratio of cathodic peak current and the square root of the sweep rate ($I_p^{cathodic}/v^{1/2}$) is also influenced and decreases with increasing sweep rate. At slow scans when the cyclic voltammogram is completely irreversible the kinetics are controlled by a chemical reaction from which determination of the rate constant is possible. On the other hand the diffusion coefficients should be obtained only from high sweep rates.

From a closer look at Figure 4.9 it follows that the reverse anodic peak is almost invisible at 30-50 $mV.s^{-1}$ and its current rises with sweep rate but it is always smaller than the cathodic one. This fact is shown in Figure 4.12 where plots of current ratio of anodic peak A` and cathodic peak A as a function of sweep rate are shown. The increasing trend in Figure 4.12 and decreasing values of $I_p^A/v^{1/2}$ in Figure 4.13 are thus in agreement with the diagnostic tests for an irreversible chemical reaction following charge transfer. For the sulphate reduction in sodium chloride melt it follows that it proceeds via a quasi-reversible "ec" mechanism.

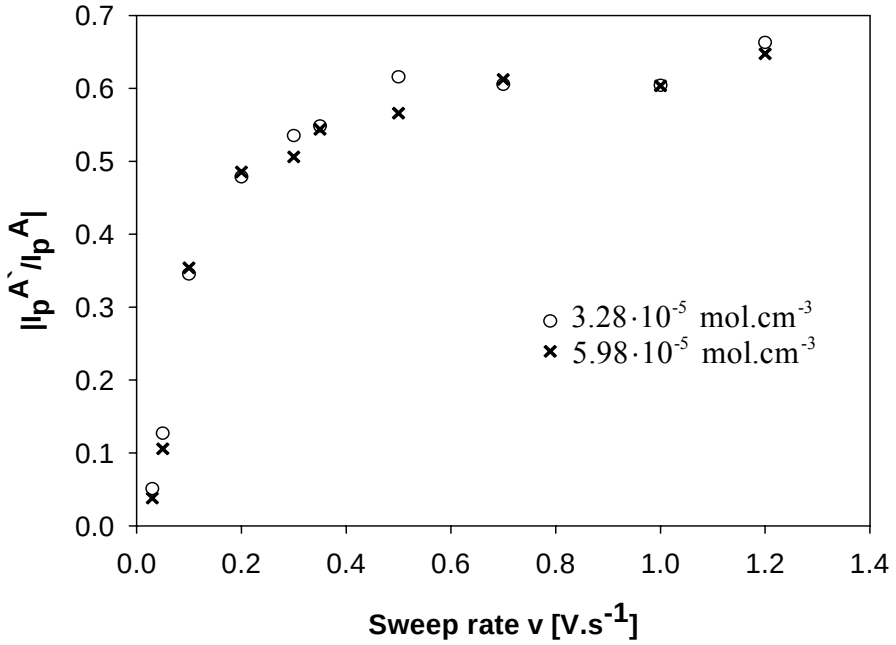

Figure 4.12 Plot of absolute values of current ratio of anodic peak A` and cathodic peak A versus sweep rate for two different Na_2SO_4 concentrations.

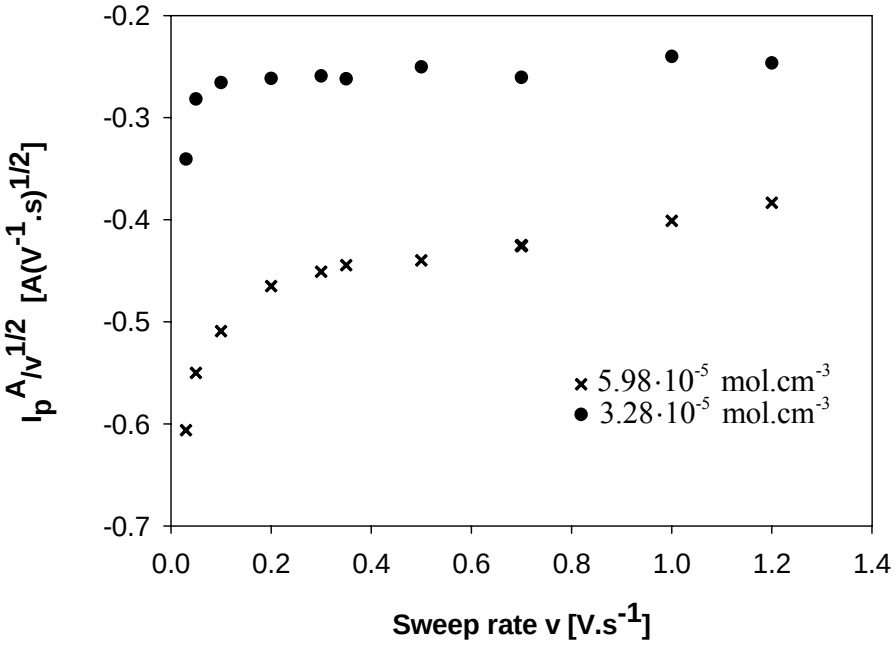

Figure 4.13 Current of reduction peak A divided by the square root of the sweep rate plotted versus sweep rate for two different Na_2SO_4 concentrations.

The number of electrons exchanged during sulphate reduction can be evaluated by applying Equation 3.18 The necessary data were obtained from voltammograms and are given in Table 4.2. Taking into account that the reduction proceeds via the "ec" mechanism only values at high sweep rates where the influence of chemical reaction is negligible should be considered in order to obtain reliable information about the charge transfer. The mean n value for electrons involved in the sulphate reduction is 1.6, calculated for the highest sweep rates in Table 4.3 where the effect of the chemical reaction on the voltammograms is not important.

Table 4.3 Data determined from CV for sulphate reduction peak A at various sweep rates at $3.28 \cdot 10^{-5}$ mol.cm^{-3} Na_2SO_4, T = 830 ºC.

Sweep rate [V.s^{-1}]	E_p^A [V]	$E_{p/2}^A$ [V]	Number of electrons
0.03	-1.697	-1.587	1.9
0.05	-1.697	-1.592	2.0
0.10	-1.721	-1.605	1.8
0.20	-1.747	-1.629	1.8
0.30	-1.768	-1.642	1.7
0.35	-1.782	-1.650	1.6
0.50	-1.792	-1.666	1.7
0.70	-1.834	-1.682	1.4
1.00	-1.837	-1.697	1.5
1.20	-1.842	-1.705	1.6

- *Chronoamperometry*

CA was performed using a platinum electrode in NaCl-Na_2SO_4. Typical current transients are shown in Figure 4.14. The potentials were applied with 20 mV steps from the open circuit potential (OCP) to -2 V where the sodium contribution on the recorded current is dominant. The signal of pure NaCl was subtracted from the sulphate current transient response which is shown in the inset of Figure 4.14. After each potential step a reverse oxidation scan was applied to re-establish equilibrium between the oxidized and reduced species.

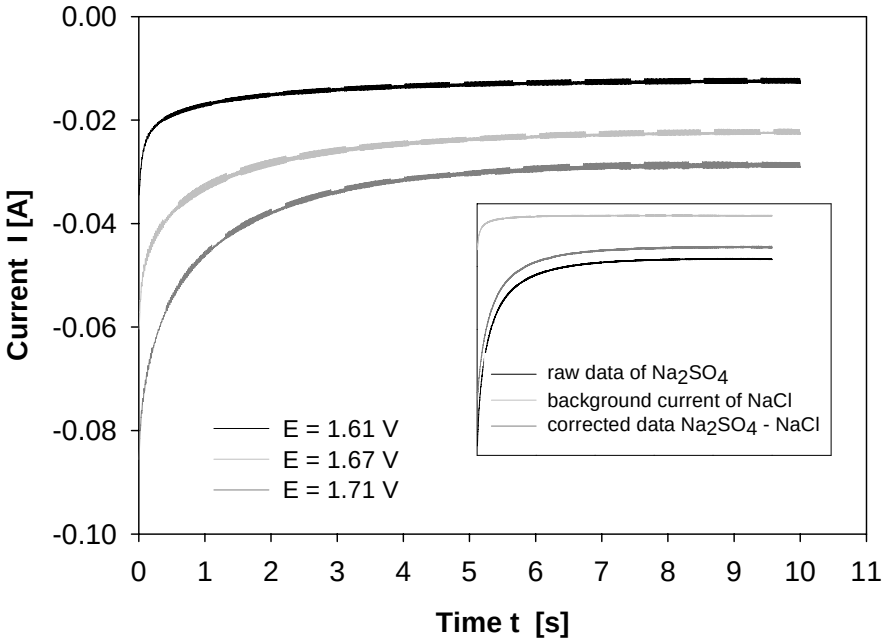

Figure 4.14 Current transients recorded in NaCl melt containing $3.24 \cdot 10^{-5}$ mol.cm^{-3} Na_2SO_4 and corrected for sodium background current. Applied potentials: -1.61, -1.67 and -1.71 V, T = 840 ºC**.** The procedure of the sodium background current correction is shown in the inset.

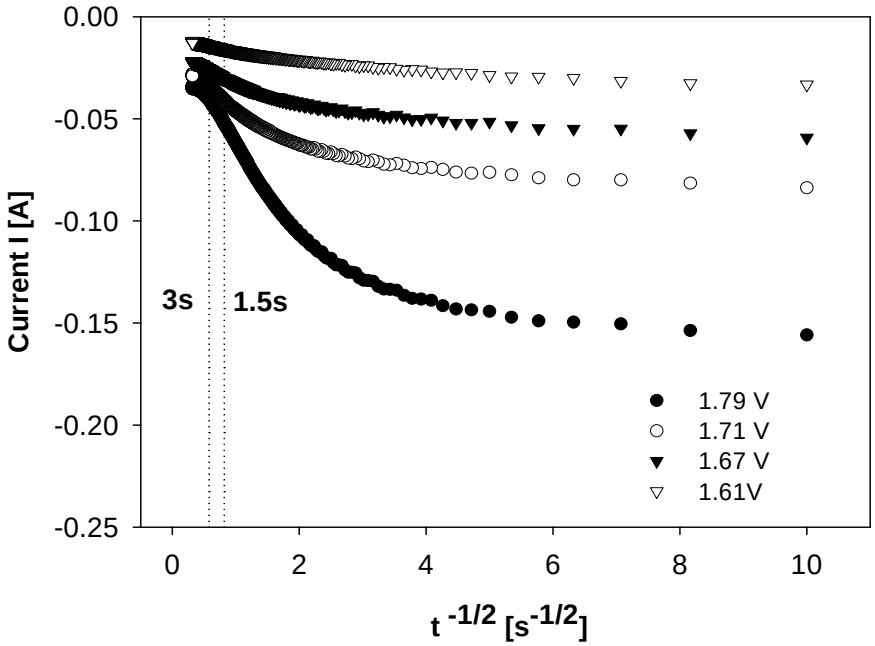

Figure 4.15 Current plotted as a function of $1/t^{1/2}$ for the data shown in Figure 4.14.

Then the chronoamperometric current is plotted as a function of $1/t^{1/2}$ and the zone controlled by diffusion can be determined. According to the Cottrel equation (Equation 3.21) current in such zone is linearly proportional to the inverted square root of time. The plots of current response as a function of $1/t^{1/2}$ at four various applied potentials are given in Figure 4.15. The diffusion controlled region of the sulphate reduction is marked between two vertical lines and corresponds to 1.5 s < t < 3 s. The current at shorter times is influenced by double layer charging while the longer times are determined by the effect of convection. However, in the one dimensional and semi-infinite diffusion controlled region the chronoamperograms obtained at various potentials should in a certain potential range merge together if enough time is passed to establish the diffusion layer. Figure 4.14 shows that the chronoamperograms do not approach to the same line which also suggests that the cathodic reduction of sulphate anions is not a simple electrochemical reaction.

Plots of current versus applied potential are shown in Figure 4.16. From such plots a limiting plateau can clearly be observed and the limiting current was thus easily determined as the point where the current reached its minimum within the limiting area. To be able to obtain the number of electrons involved in the sulphate reduction it was necessary to calculate the logarithm of the current which for soluble species can be written in the form $\ln[(I_{lim}-I)/(I_{lim}+I)]$. Then plots of potential versus the current function were constructed and are presented in Figure 4.17.

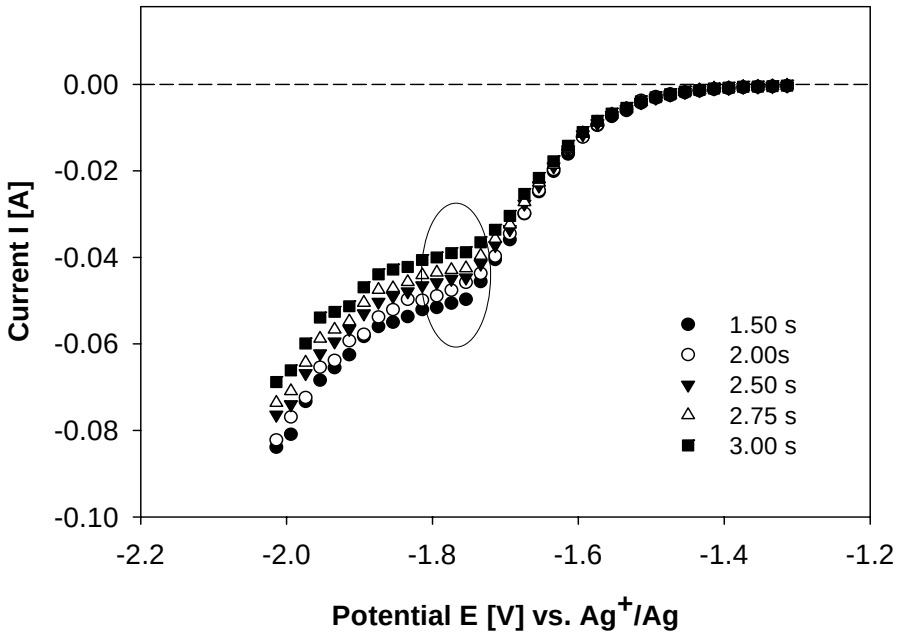

Figure 4.16 Current-potential curves of $3.24 \cdot 10^{-5}$ mol.cm^{-3} Na_2SO_4 in NaCl obtained by chronoamperometry at different times, T = 840 ºC.

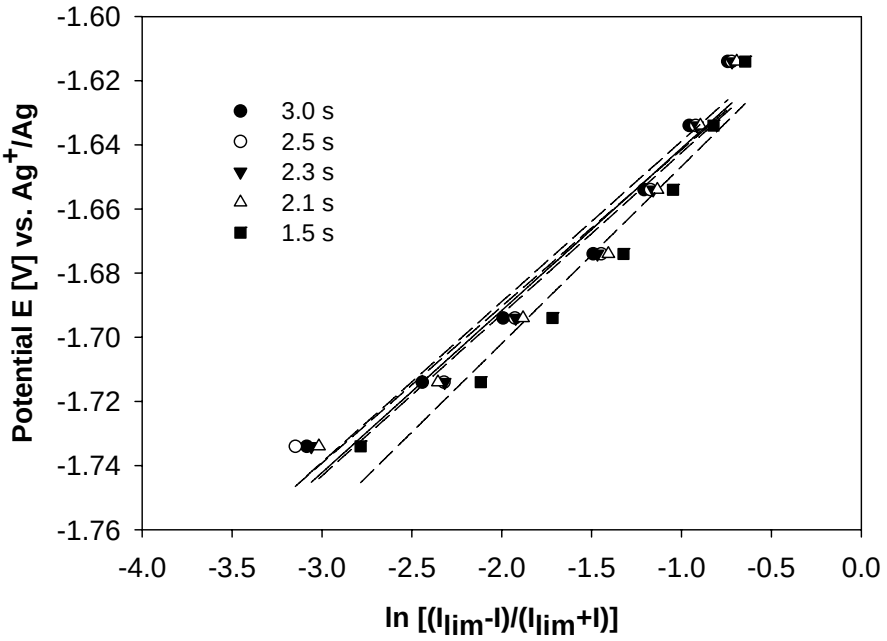

Figure 4.17 Plot of potential versus $\ln[(I_{lim}-I)/(I_{lim}+I)]$ with the regression lines for time interval from 1.5 s to 3 s.

According to the definition for an entirely diffusion controlled process the relationship between potential and current function should yield a linear and time independent behaviour. As can be seen from Figure 4.17, the linear fits do not fully pass through all the points on the figure. It means that the diffusion of sulphate anion is not the only process which occurs nearby the electrode. The influence from sodium is probable and could cause this effect which also follows from Figure 4.16 where the current continues to decrease after it reached the limiting value or it might be due to a following chemical reaction. However the value of exchanged electrons was evaluated according to Equation 3.23 from the slope of the curves shown in Figure 4.17. The values of n and the data of the limiting current together with the slopes of the regression lines within the time interval 1.5 s < t < 3 s are presented in Table 4.4. The average value for n is then equal to 1.9. From the chronoamperometric results thus follows that the sulphate reduction proceeds as a two electron exchange under the assumption that limiting conditions were met.

Table 4.4 Number of electrons determined by chronoamperometry. T = 840 ºC, $3.24 \cdot 10^{-5}$ mol.cm^{-3} Na_2SO_4.

Time [s]	Limiting current [A]	Slope	Number of electrons
3.00	-0.040	0.0501	1.9
2.67	-0.042	0.0503	1.9
2.50	-0.043	0.0489	2.0
2.40	-0.043	0.0518	1.9
2.30	-0.044	0.0506	1.9
2.20	-0.044	0.0499	1.9
2.10	-0.045	0.0504	1.9
2.00	-0.046	0.0509	1.9
1.75	-0.049	0.0529	1.8
1.50	-0.052	0.0552	1.7

Because similar numbers for the n value were obtained from CV and CA methods, two-electron transfer could be considered and sulphate reduction in NaCl can in simplicity be written as in Equation 4.5 and followed by a chemical reaction.

$$S^{6+} + 2e^- \rightleftharpoons S^{4+} \qquad 4.5$$

If the sulphur species in oxidation state +IV is in the form of sodium sulphite Na_2SO_3 this is not stable and due to the temperature effect it might be transformed to sulphate and sulphide according to the following reaction:

$$4Na_2SO_3 = 3Na_2SO_4 + Na_2S \qquad 4.6$$

However when titrimetric analysis by iodine was performed on the solidified samples of the electrolyte no sulphides were detected in the melt. This might be due to the fact that a low concentration of added sulphate might result in even lower content of the transformed form which could be below the detection limit of the titrimetric method. Besides, part of the sulphite could have left the furnace in the form of SO_3 or SO_2, even though no decrease in sulphate concentration was observed during the time of the experiments. Anyway, low concentrations of SO_2 (eventually SO_3 but this would decompose to SO_2 at the experimental temperature) was detected when the off-gases were bubbled through a 3 % solution of hydrogen peroxide and oxidized to H_2SO_4. This was then titrated by NaOH and transformed to Na_2SO_4, which presence was detected by using phenolphthalein indicator.

4.3.3 The $CaCl_2$-NaCl-Na_2SO_4 system

According to Table 4.2 the standard decomposition potentials for NaCl and $CaCl_2$ are almost equal. Therefore it is likely that reduction of both metals; Na and Ca can be expected to occur simultaneously and should theoretically give a similar potential window as in pure NaCl. Figure 4.18 shows the cathodic side of a typical CV of $CaCl_2$-NaCl (10-90 mol%) recorded on platinum electrode with Ag^+/Ag reference.

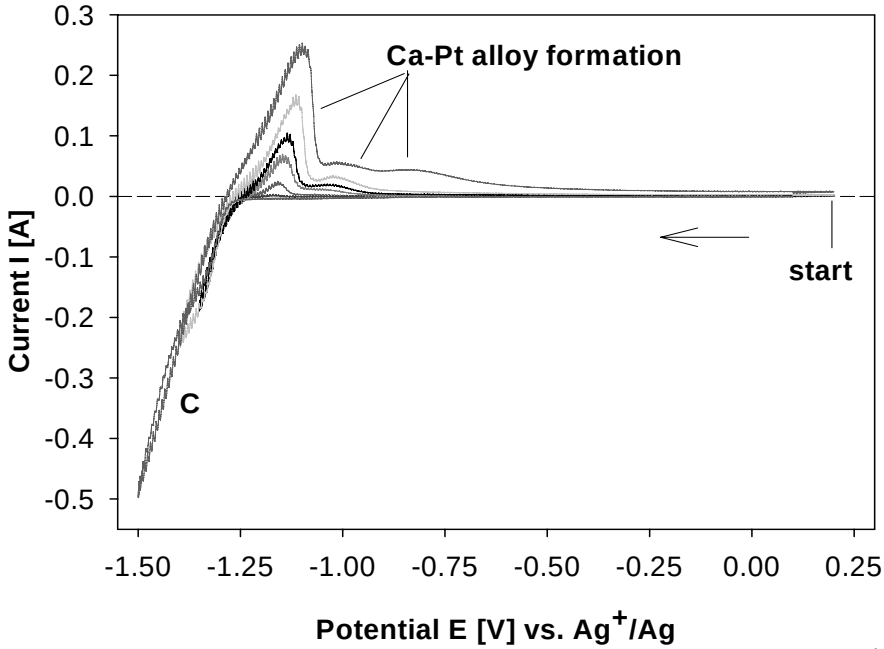

Figure 4.18 Cyclic voltammograms of $CaCl_2$-NaCl (10-90 mol%) at 350 $mV.s^{-1}$. Applied second vertex potentials from -1.1 V to -1.5 V, T = 840 ºC.

When comparing Figure 4.18 with 4.6, the potential from which the metallic cations begin to be reduced in the melts containing $CaCl_2$ is less negative than in the simple NaCl melt at similar experimental conditions. It is due to co-deposition of calcium metal that forms an alloy with the platinum substrate which limits the potential window in the cathodic region (peak C) and depending on the potential stepped to more negative values, more peaks corresponding to reoxidation of Ca-Pt alloy are increasing in the reversed scan (see Figure 4.18).

- *Cyclic voltammetry*

When the $CaCl_2$-NaCl (10-90 mol%) mixture was used as base electrolyte, a different behaviour of the sulphate anion from that in pure NaCl was observed (Figure 4.19). After sulphate addition three major signals appeared on the cyclic voltammograms: a cathodic peak A, associated with the anodic peaks A` and A``, the last one visible only as a wave at sweep rates higher than 100 $mV.s^{-1}$, and an anodic peak B. Peak C is resulting from the Ca-Pt alloy formation and its reoxidation as mentioned earlier.

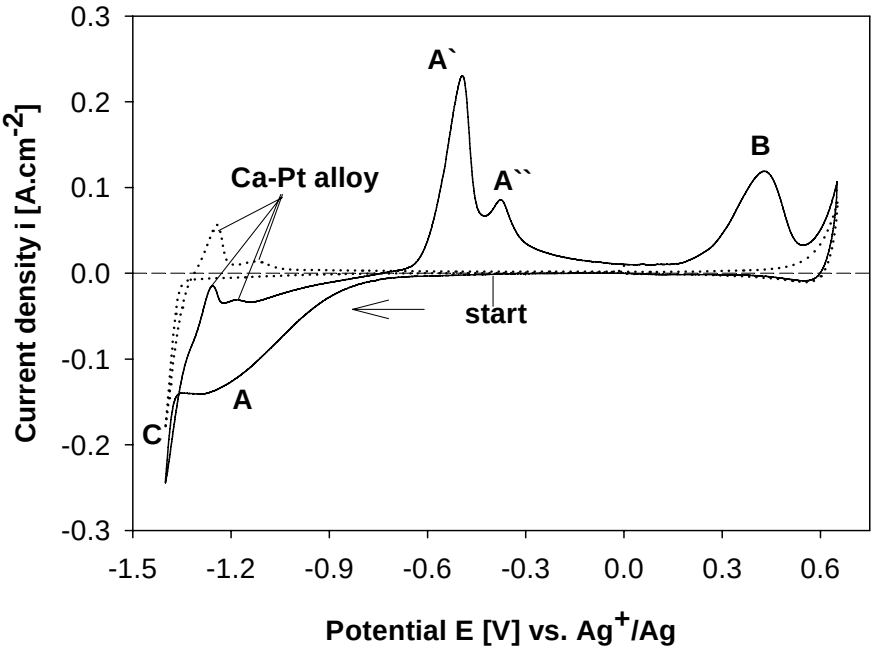

Figure 4.19 CVs recorded in the mixture of $CaCl_2$-NaCl (10-90 mol%) before (dotted line) and after addition (solid line) of $3.38 \cdot 10^{-5}$ $mol.cm^{-3}$ Na_2SO_4, T = 840 ºC, Pt working electrode, v = 300 $mV.s^{-1}$.

When recording the CVs at different cathodic potentials, the increase of current of peaks A`, A`` and B can be observed in Figure 4.20 in connection with the evolution of peak A. When the CVs are recorded starting in the anodic direction, peaks A`, A` and B do not appear in the first scan until the sweep is reversed and the reduction of sulphate at potential of peak A proceeds. Only then the oxidation peaks are observed in the second anodic scan, shown in Figure 4.21. From the observation described above it follows that all oxidation peaks A`, A`` and B seem to be the products of the reduction reaction.

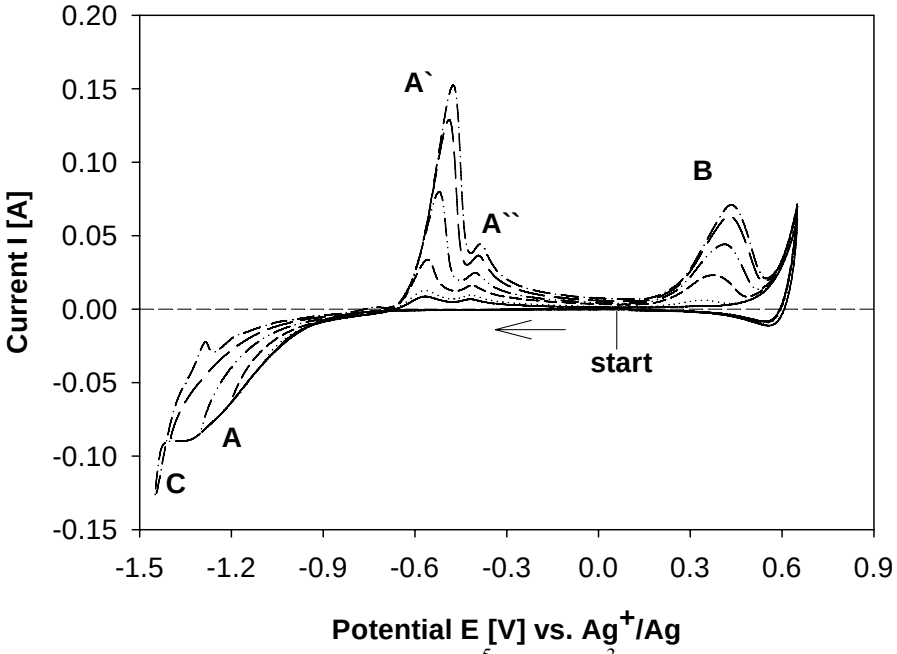

Figure 4.20 Cyclic voltammograms of $4.56 \cdot 10^{-5}$ mol.cm^{-3} Na_2SO_4 in $CaCl_2$-NaCl (10-90 mol%), v = 300 mV.s^{-1}, T = 840 ºC.

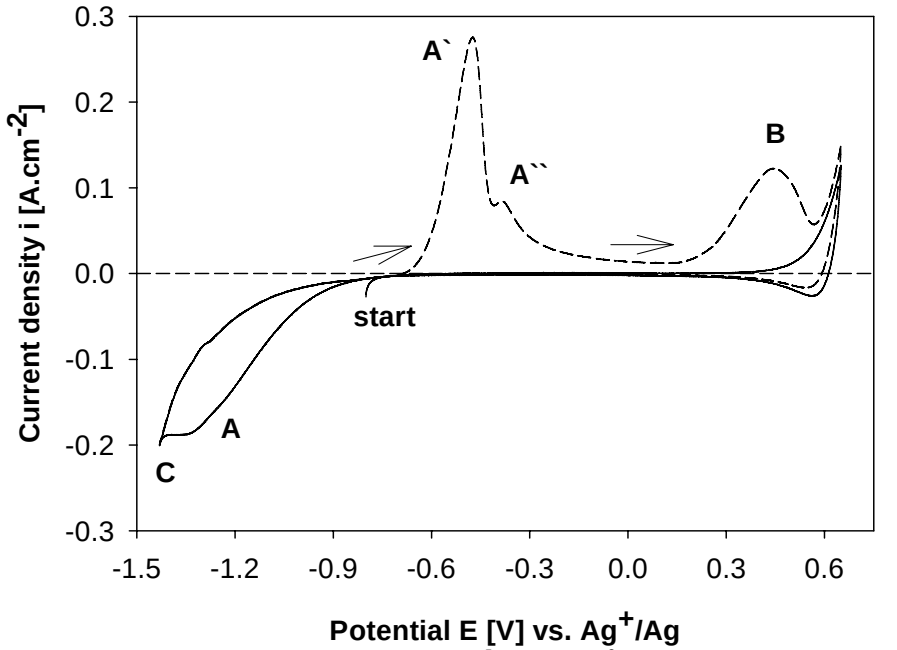

Figure 4.21 Cyclic voltammograms of $4.56 \cdot 10^{-5}$ mol.cm^{-3} Na_2SO_4 in $CaCl_2$-NaCl (10-90 mol%) with two scans recorded first in the anodic direction (solid line - 1st scan, dashed line - 2nd scan), v = 300 mV.s^{-1}, T = 840 ºC.

Moreover, from the sharpness and symmetrical shape of peaks A` and A`` one could consider the formation of insoluble products or an adsorption phenomenon. In the case of adsorption the peak current of wave A (I_p^A) should be proportional to the sweep rate v but not to its square root. As it can be observed from Figure 4.22 this is not the case. The relationship between the cathodic current density of peak A and the square root of the sweep rate shows linear dependence for two various concentrations of the sulphate anion.

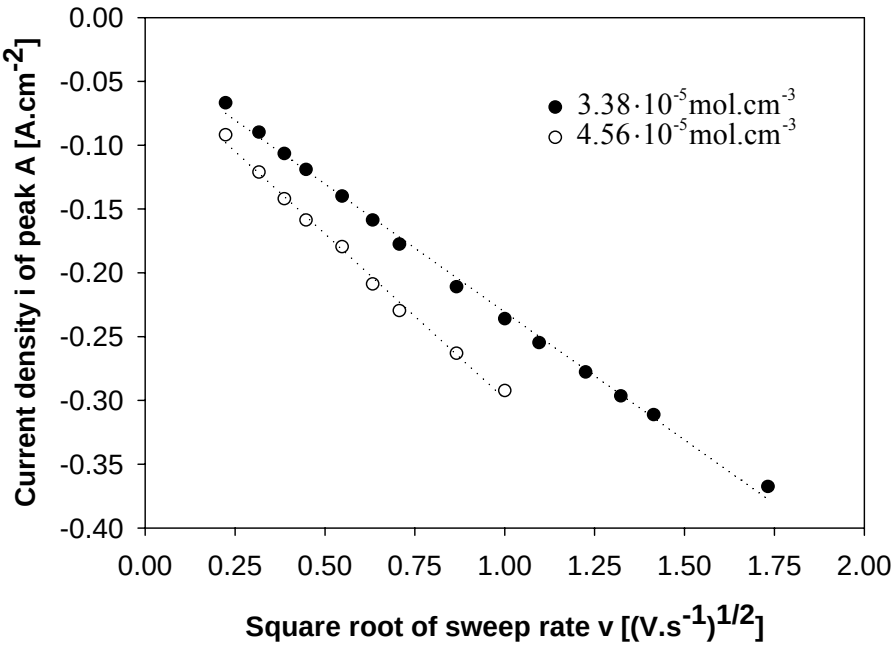

Figure 4.22 Variation of the current density of peak A as a function of the square root of the sweep rate for two concentrations of Na_2SO_4 in $CaCl_2$-NaCl (10-90 mol%), v = 300 $mV.s^{-1}$, T = 840 ºC.

Additionally, the significantly enhanced reverse peak A` could be a positive sign of a weak product adsorption but in such situation the potential of the reduction peak A would have shifted to more positive values with increasing sweep rate, which it does not (see Figure 4.23).

Like in simple NaCl the ratio of the current of the cathodic and anodic peak is not equal to 1. From Figure 4.24 it clearly follows that the current value of peak A`` is increasing with increasing sweep rate but it is always smaller than the current of the reduction peak. On the other hand the current of peak A` increases until it reaches the maximum at 0.4 $V.s^{-1}$ and then it starts to decrease with increasing square root of the sweep rate.

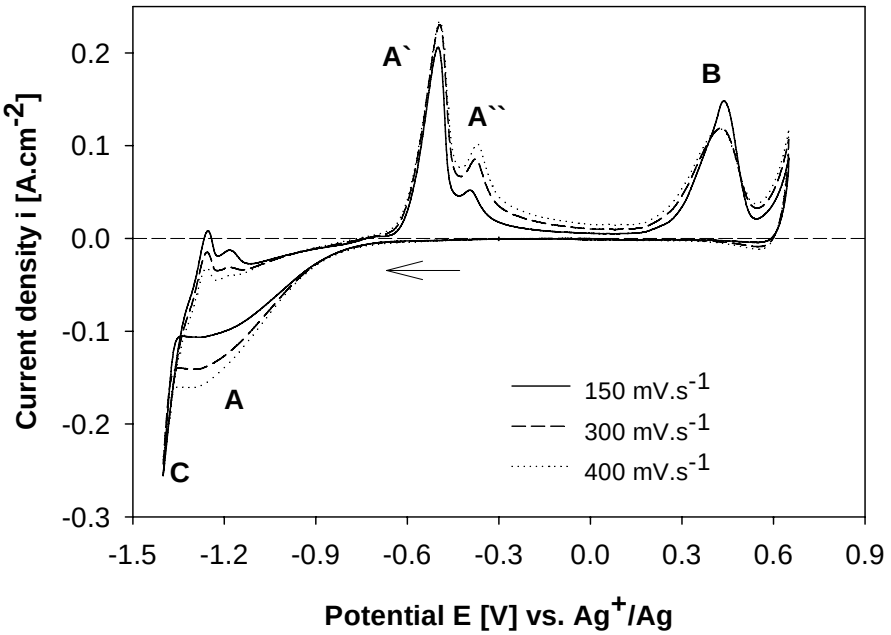

Figure 4.23 Cyclic voltammograms of $3.38 \cdot 10^{-5}$ mol.cm^{-3} Na_2SO_4 in $CaCl_2$-NaCl (10-90 mol%) obtained at different sweep rates, T = 840 ºC.

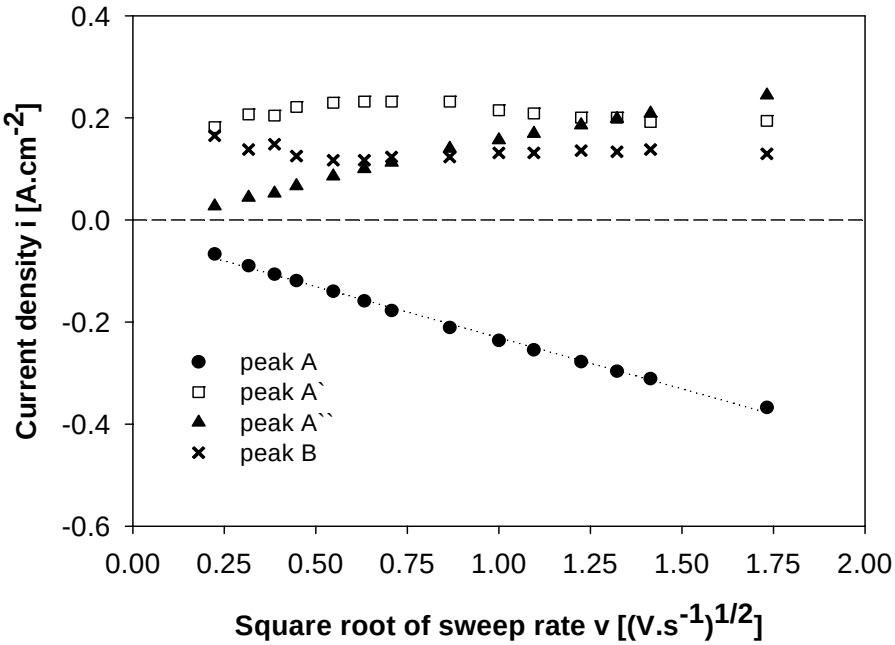

Figure 4.24 Plots of current densities of peaks A, A`, A`` and B as a function of the square root of the sweep rate for $3.38 \cdot 10^{-5}$ mol.cm^{-3} Na_2SO_4 in $CaCl_2$-NaCl (10-90 mol%), T = 840 ºC.

The variation of the current behaviour of the peaks with sweep rate is more obvious from Figures 4.25 and 4.26 where the ratios of anodic signal A` (respectively A``) and the cathodic peak current A $\left|I_p^{A`}/I_p^{A}\right|$ respectively $\left|I_p^{A``}/I_p^{A}\right|$ are plotted. Peak B is almost independent on the sweep rate except for slightly higher values at slow sweep rates.

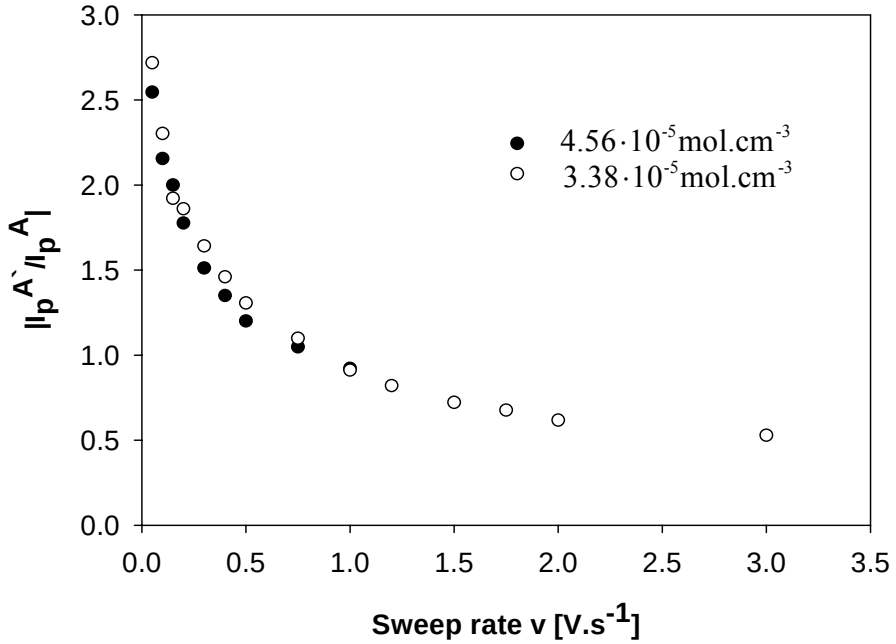

Figure 4.25 Plot of absolute values of the current ratio of anodic peak A` and cathodic peak A versus sweep rate for two various Na_2SO_4 concentrations in $CaCl_2$-NaCl (10-90 mol%), T = 840 ºC.

The increasing trend in Figure 4.26 and decreasing values of cathodic peak A plotted as $I_p^A/v^{1/2}$ versus sweep rate in Figure 4.27 are in agreement with the diagnostic tests for a following chemical reaction. Thus from the observations described above it follows that the sulphate reduction in NaCl melt containing 10 mol% $CaCl_2$ probably also proceeds via an "ec" mechanism but the number and shape of the electrochemical signals showed in the voltammograms suggest that the sulphate reduction involves different products than in the simple NaCl melt.

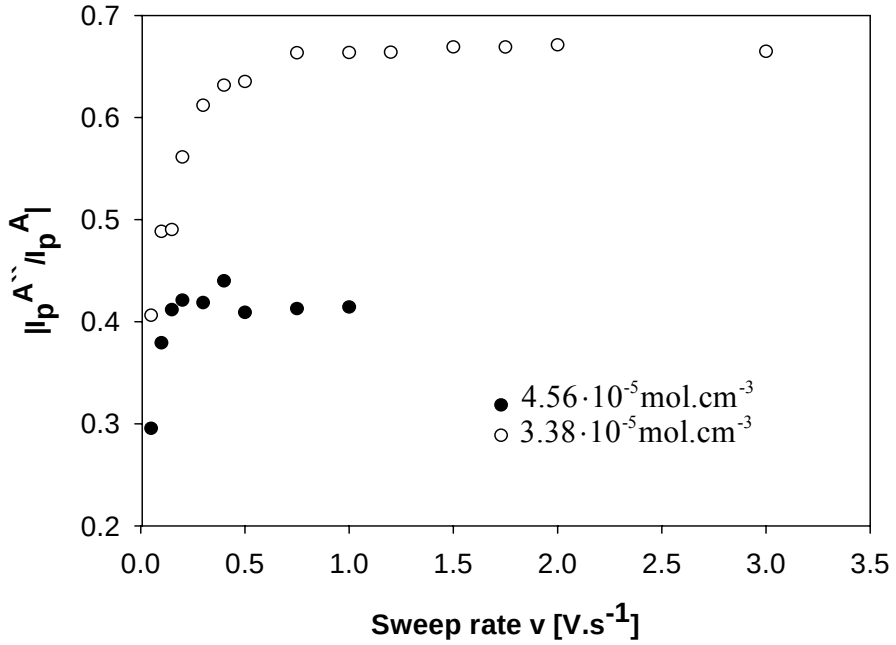

Figure 4.26 Plot of absolute values of current ratio of anodic peak A`` and cathodic peak A versus sweep rate for two Na_2SO_4 concentrations in $CaCl_2$-NaCl (10-90 mol%), T = 840 ºC.

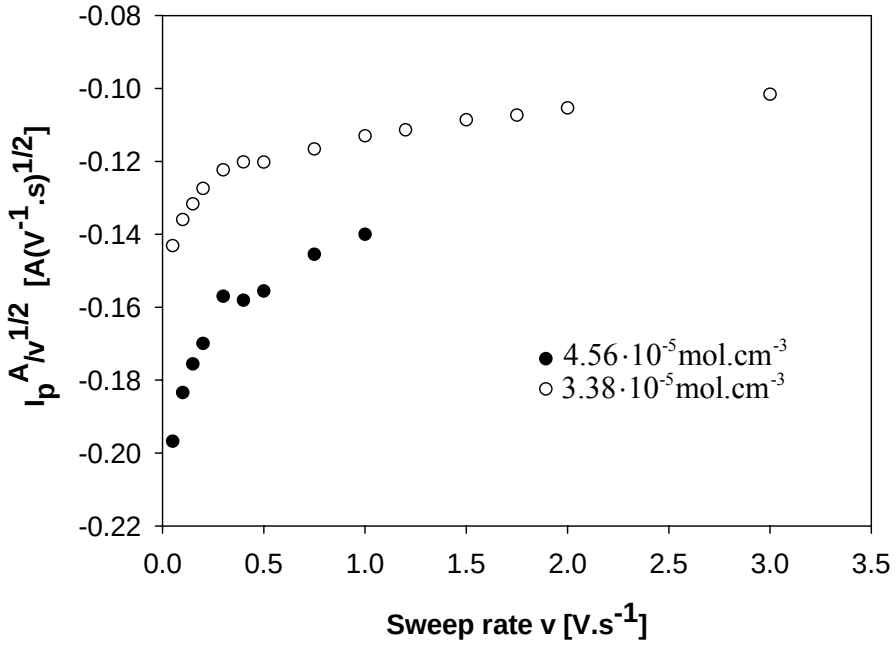

Figure 4.27 Cathodic current of peak A divided by the square root of the sweep rate plotted versus sweep rate for two Na_2SO_4 concentrations.

- *Chronoamperometry*

The number of electrons exchanged in the sulphate reduction step in this system was determined by chronoamperometry in a similar manner than for the NaCl melt. The potentials were applied with respect to the open circuit potential from -0.7 V to -1.4 V in 10 mV steps and after each measured curve a reverse scan was recorded. Chronoamperometric curves measured in $CaCl_2$-NaCl (10-90 mol%), containing $3.38 \cdot 10^{-5}$ mol.cm^{-3} Na_2SO_4 are shown in Figure 4.28. The background current of the carrying electrolyte was subtracted from the data of sodium sulphate response like for the simple NaCl melt.

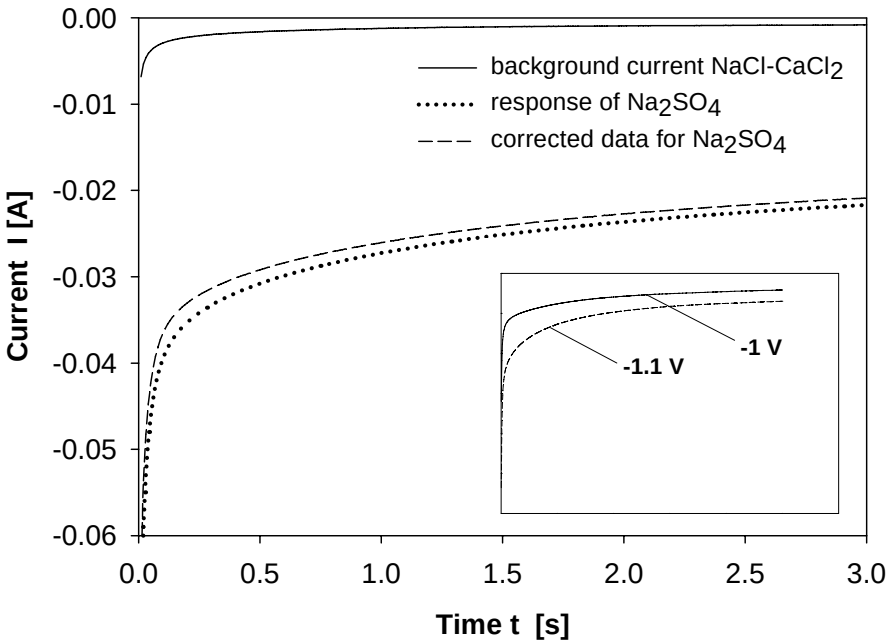

Figure 4.28 Potentiostatic current transients of $3.38 \cdot 10^{-5}$ mol.cm^{-3} Na_2SO_4 in $CaCl_2$-NaCl (10-90 mol%), for applied potentials -1 and -1.1 V and corrected for the background current, T = 840 ºC, Pt electrode.

Figure 4.29 shows the current response as function of time $1/t^{1/2}$ where part of the plot between horizontal lines corresponding to time values from the interval 1.8 s < t < 4 s where the Cottrell equation is valid. When the current was replotted as a function of potential for times from 1.8 s to 4 s given in Figure 4.30, V-shaped curves were obtained. From such plots only one limiting plateau can be observed between -1.06 V and -1.15 V. The current at -1.1 V was thus taken for each time to be the limiting value.

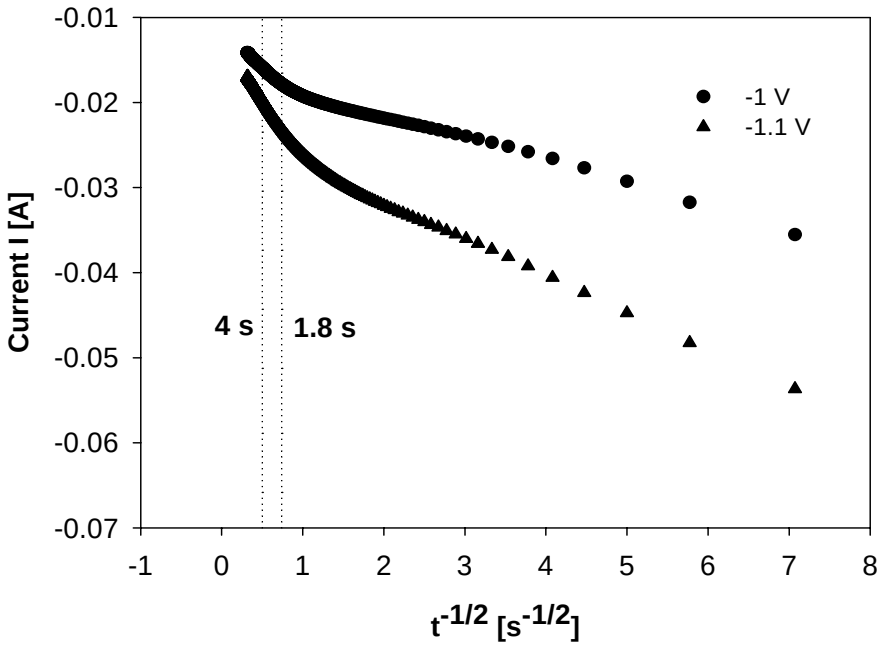

Figure 4.29 Current plotted as a function of $1/t^{1/2}$. Applied potentials: -1 and -1.1 V, for $3.38 \cdot 10^{-5}$ mol.cm^{-3} Na_2SO_4, T = 840 ºC.

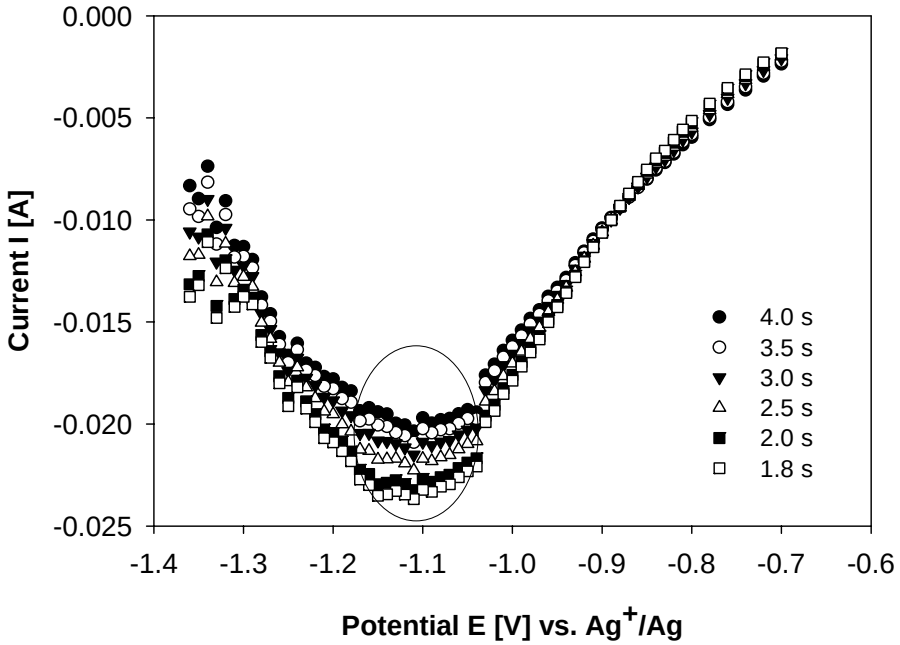

Figure 4.30 Current-potential curves of $3.38 \cdot 10^{-5}$ mol.cm^{-3} Na_2SO_4 obtained by chronoamperometry at different times, T = 840 ºC.

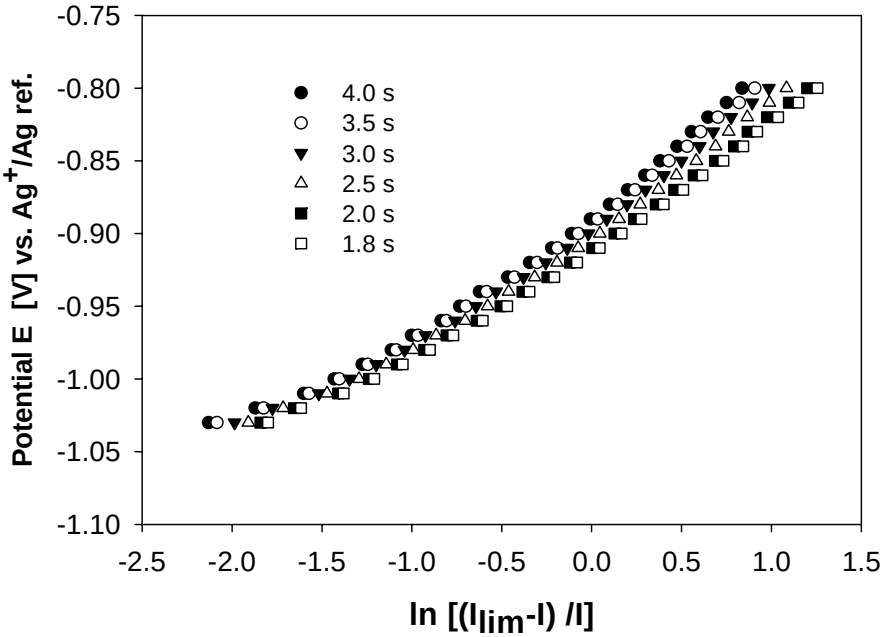

Figure 4.31 Relation between the potential and ln[(I_{lim}-I)/I] constructed from current-potential chronoamperometric curves at various times.

Because insoluble products are probably involved in this system, Equation 3.22 must be applied and the relationship of the potential versus ln[(I_{lim}-I)/I] must be plotted in order to determine the number of electrons exchanged. Such plots are presented in Figure 4.31 and the obtained values are gathered in Table 4.5. Based on the results in Table 4.5 a one electron reduction step seems to take place in NaCl melt containing 10 mol% $CaCl_2$.

Table 4.5 Number of electrons determined by chronoamperometry, $3.38 \cdot 10^{-5}$ mol.cm^{-3} Na_2SO_4, T = 840 ºC.

Time [s]	Limiting current [A]	Slope	Number of electrons
4.0	-0.020	0.081	1.2
3.5	-0.020	0.080	1.2
3.0	-0.021	0.080	1.2
2.5	-0.022	0.079	1.2
2.0	-0.023	0.078	1.2
1.8	-0.023	0.077	1.2

From the cyclic voltammetry it is clear that the sulphate anions behave differently in simple NaCl electrolyte as they do in $CaCl_2$-NaCl mixture. This aspect was related to the difference in oxoacidity of the carrying electrolytes [112]. A similar explanation was previously given by Wrench and Inman when studying the sulphate behaviour in molten NaCl-KCl [67]. In the presence of an acidic medium such as $CaCl_2$ the sulphate anion decomposes according to

reaction 4.7 and dissolved SO_3 then probably becomes the electroactive species.

$$SO_4^{2-} = SO_3 + O^{2-} \qquad 4.7$$

Based on the results obtained from the electrochemical measurements the cathodic peak A could be the reduction of SO_3 to SO_2 and O^{2-} anions according to the following reactions:

$$SO_3 + e^- \rightarrow SO_3^- \qquad 4.8$$

$$SO_3^- + e^- \rightarrow SO_3^{2-} \qquad 4.9$$

$$SO_3^{2-} \rightarrow SO_2 + O^{2-} \qquad 4.10$$

According to Wrench [67] a chemical combination of two SO_3^- anions as given in Equation 4.11 is more probable than further reduction according to Equation 4.9. Because only one cathodic signal A is observed in the voltammograms this could support that assumption.

$$SO_3^- + SO_3^- \rightarrow S_2O_6^{2-} \qquad 4.11$$

The anodic peak B was ascribed to the oxidation of O^{2-} to O_2 and peak A` to the oxidation of SO_2 according to the reaction:

$$SO_2 + O^{2-} \rightleftharpoons SO_3 + 2e^- \qquad 4.12$$

Once SO_3 is present in the electrolyte at that temperature it can thermally decompose to SO_2 or it could combine with the sulphate anion according the Equation 4.13 and subsequently be reduced as in Equation 4.14.

$$SO_3 + SO_4^{2-} \rightarrow S_2O_7^{2-} \qquad 4.13$$

$$S_2O_7^{2-} + 1e^- \rightarrow SO_4^{2-} + SO_3^- \qquad 4.14$$

Slightly higher concentration of sulphur oxides: SO_2 resp. SO_3 was detected in the off gases after their oxidation followed by subsequent determination as previously described. Similarly no sulphides in the solidified samples of the electrolyte were detected by iodimetric titration.

4.3.4 The LiCl-KCl-K_2SO_4 system

The behaviour of the sulphate anions was also studied in the eutectic LiCl-KCl mixture. The intention of this experiment was to examine the sulphate reduction in an electrolyte which could be operated at temperature below 800 ºC. Thus the effect of temperature on the behaviour of the sulphur species could be monitored and compared in a melt with a stable composition where the temperature would be the only variable. Therefore the LiCl-KCl mixture with eutectic composition (40 mol% KCl – 60 mol% LiCl) was chosen as the supporting electrolyte and the working temperatures were ranging from 450 ºC to 840 ºC.

Figure 4.32 represents the voltammograms obtained on a Pt electrode without sulphate addition. According to the calculations summarized in Table 4.2 theoretical possibility to study sulphate behaviour in this electrolyte should be allowed in a range of approximately 3.5 V. As can be observed from Figure 4.32 the real potential window is about 1 V less. The cathodic limit is set by peak B which is associated with B`. They are probably related to Pt-Li alloy formation and its further oxidation.

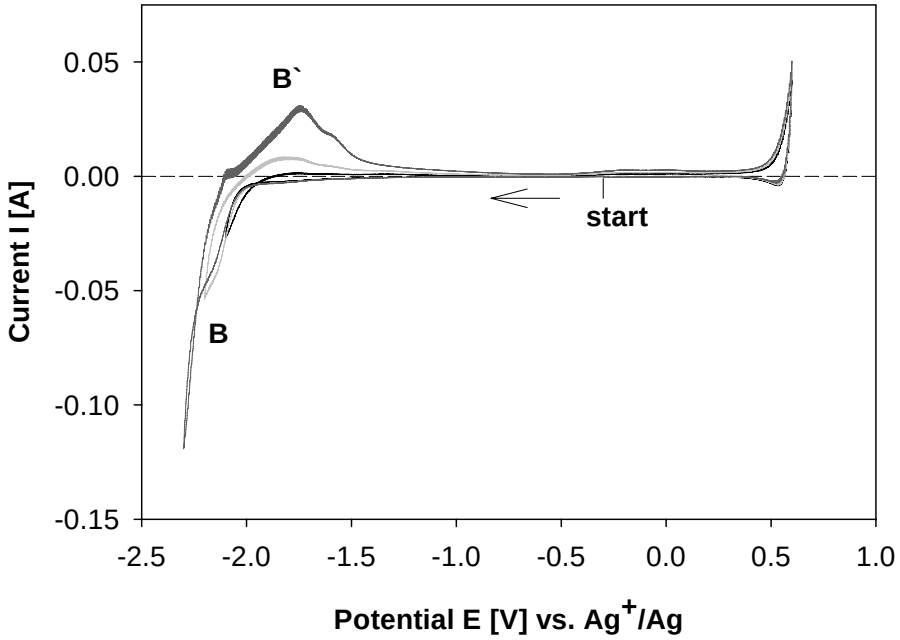

Figure 4.32 Cyclic voltammograms of the LiCl-KCl eutectic before additions of sulphate ions; T = 450 ºC, v = 300 $mV.s^{-1}$.

When sulphate ions were added to the bath at 460 ºC, no additional peaks were observed. As the temperature of the electrolyte was increased to 740 ºC a single cathodic wave A resulting from the reduction of sulphate added as K_2SO_4 appears coupled by one oxidation peak A` in the reversed scan. With increasing

temperature up to 840 ºC peaks A and A` became more pronounced (see Figure 4.33). It has been concluded that probably a rapid decrease of the sulphate solubility at lower temperatures more likely than the slower reduction kinetic caused the problems to investigate the system at temperatures lower than 700 ºC.

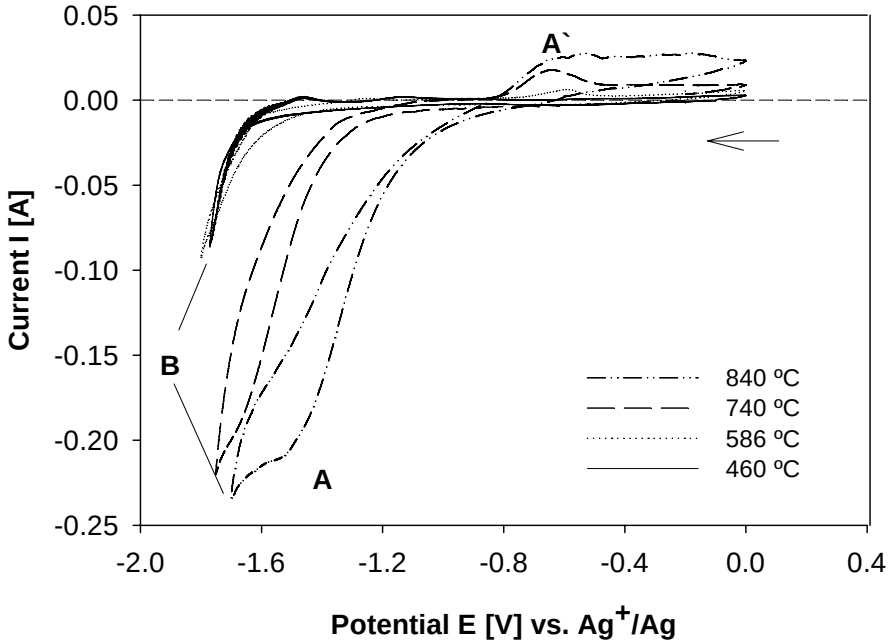

Figure 4.33 Effect of the temperature on sulphate solubility. The CVs are recorded in the eutectic LiCl-KCl containing $5.71 \cdot 10^{-5}$ mol.cm^{-3} K_2SO_4 at 50 mV.s^{-1}.

When comparing the shape of the peaks in the voltammograms in Figure 4.34 the behaviour of K_2SO_4 in the eutectic LiCl-KCl seems to be similar to the reduction of Na_2SO_4 in the pure NaCl. The reaction probably involves soluble product and soluble reactant in both cases. This similar behaviour of the sulphate anion in NaCl and the mixture of LiCl-KCl could be related to the similar oxoacidity of both these electrolytes. However in the LiCl-KCl melt the separation of the cathodic and reverse anodic peaks A/A` is bigger than in the NaCl melt indicating irreversibility of the system or the presence of a chemical reaction which could play a key role and influence the high of the reverse peak A`.

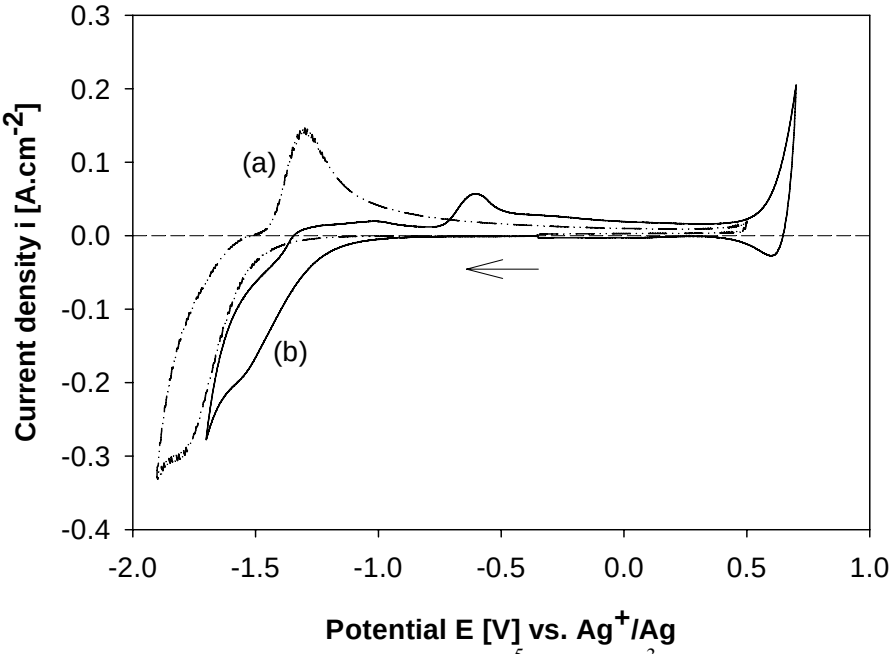

Figure 4.34 Cyclic voltammograms of $2.71 \cdot 10^{-5}$ mol.cm^{-3} Na_2SO_4 in NaCl (a) and $1.83 \cdot 10^{-5}$ mol.cm^{-3} K_2SO_4 in the LiCl-KCl eutectic (b); T = 840 ºC, v = 500 mV.s^{-1}.

The analysis of the relation between the current density of peak A and the square root of the sweep rate showed a linear dependency at various concentrations as in the NaCl melt (Figure 4.35).

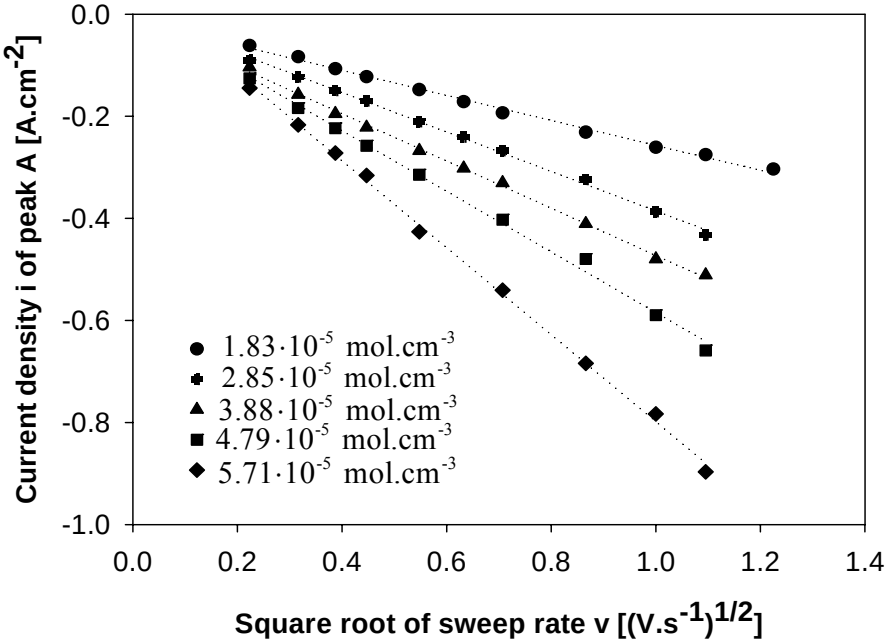

Figure 4.35 Variation of the current density of peak A and the square root of the sweep rate as a function of the K_2SO_4 content in LiCl-KCl eutectic at 840 ºC.

From Figure 4.36 one can see the influence of increasing sweep rate on the peak current. Also in this melt the evolution of peak A` is considerably behind the current increase of signal A at the same sweep rates. But as the sweep rate increases, A` becomes more and more apparent. Figure 4.37 shows this feature as an increasing trend of the current ratio of A and A`. Figure 4.38 shows the potential shifts of peaks A and A` with sweep rate. This becomes stagnant from about 500 $mV.s^{-1}$ from which the value of potential of peak A` can be considered to be more or less constant. All these facts point to the existence of a chemical reaction after the sulphate reduction takes place, as it was for the simple NaCl system.

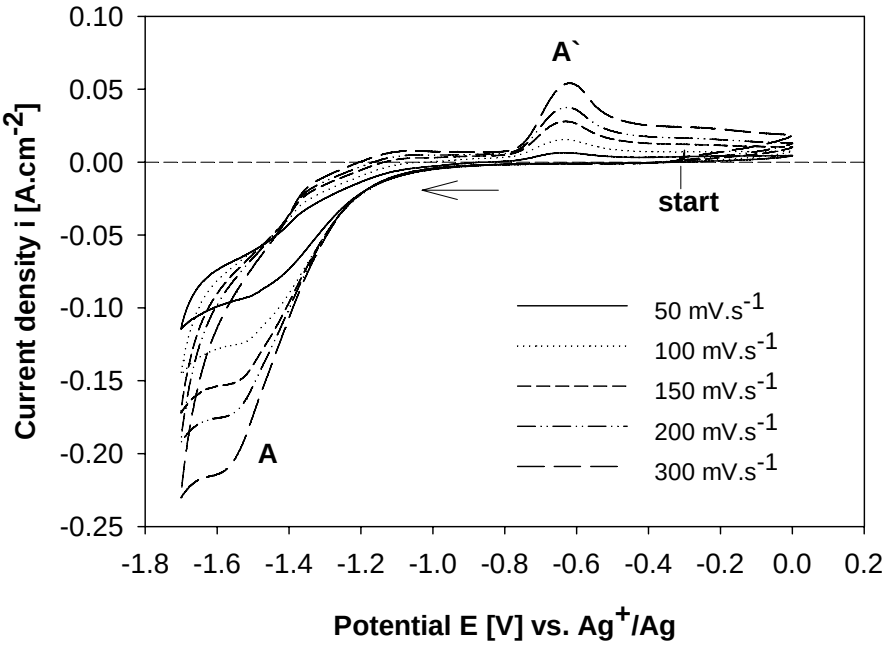

Figure 4.36 Effect of sweep rate on cyclic voltammograms containing $2.85 \cdot 10^{-5}$ mol cm^{-3} K_2SO_4 in eutectic LiCl-KCl mixture, 840 ºC.

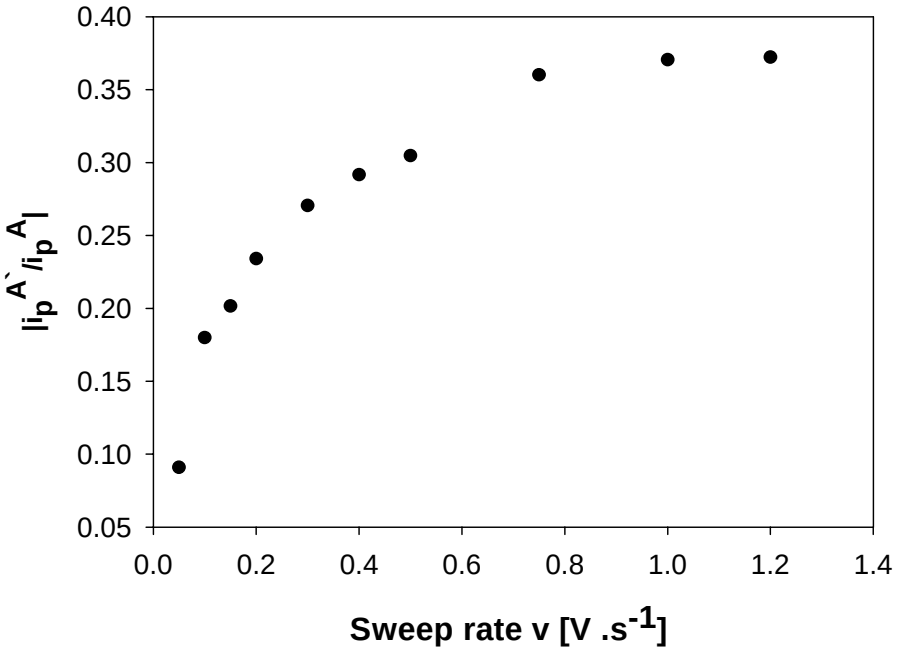

Figure 4.37 Plot of absolute values of current ratio of anodic peak A` and cathodic peak A versus sweep rate for $3.88 \cdot 10^{-5}$ mol cm^{-3} K_2SO_4.

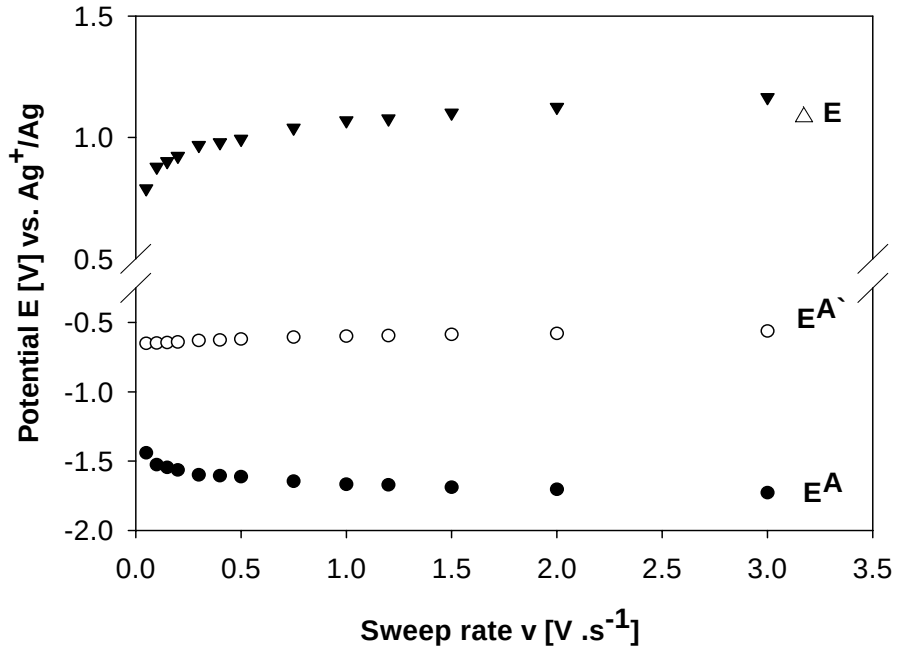

Figure 4.38 Potential values of peaks A and A` plotted as a function of the sweep rate for $3.88 \cdot 10^{-5}$ mol.cm^{-3} K_2SO_4, 840 ºC.

Samples of the electrolyte after sulphate anion reduction were analyzed by iodometric titration to check if sulphides could be the reaction product. Similarly as in the NaCl electrolyte no traces of S^{2-} were found in LiCl-KCl. An assumption that sulphate anions are reduced in a similar way than in the simple NaCl melt as well as in the LiCl-KCl eutectic was made based on the observations from cyclic voltammograms described above. According to Picard [112] an explanation for the corresponding mechanism of the sulphate behaviour in the mentioned electrolytes could be their similar oxoacidic character. This shows the importance of considering the influence of the character of the electrolyte on the electrochemistry of sulphur species at high temperature experiments.

4.3.5 The LiCl-KCl-Na_2SO_3 and LiCl-KCl- K_2S systems

- *Behaviour of Na_2SO_3*

Figure 4.39 shows a CV obtained on a Pt electrode in the eutectic LiCl-KCl mixture at 460 ºC before and after Na_2SO_3 addition. As it was shown above, the presence of sulphate electroactive species cannot be observed electrochemically at temperatures below 700 ºC. In this system three reduction (A, B and C) and two oxidation (A` and B`) peaks appeared when adding sulphite ions to the melt.

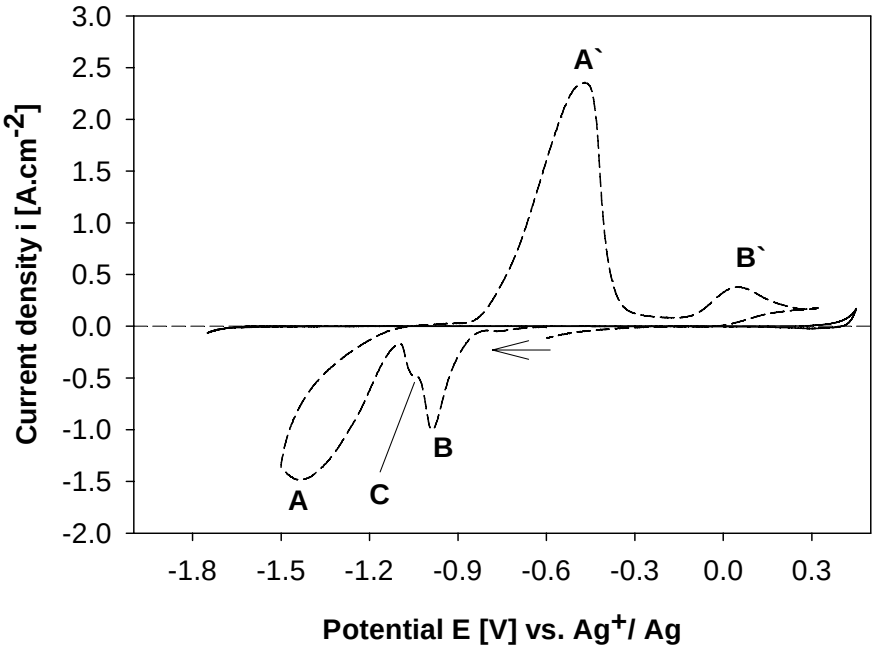

Figure 4.39 CV recorded before (solid line) and after (dashed line) addition of Na_2SO_3 to the eutectic LiCl-KCl at 460 ºC on a Pt electrode. Sweep rate 500 $mV.s^{-1}$.

As shown in Figure 4.40 reduction waves B and C do not appear in the 1st voltammogram scan until an oxidation at 0.04 V proceeds. Peaks B and C are therefore signals resulting from the reduction of the product of the reaction at the potential of peak B`. The species obtained in B, C and A` are probably insoluble and block the electrode surface which leads to a current decrease in the following scan (pseudo-passivation). On the other hand, the shape of A has a character of the soluble species.

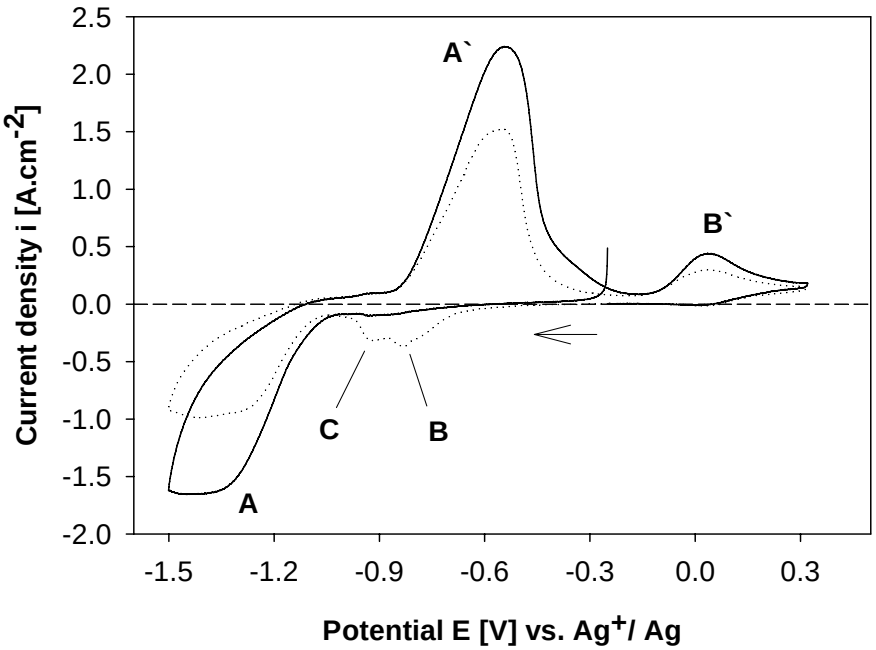

Figure 4.40 Cyclic voltammograms of Na_2SO_3 in the eutectic LiCl-KCl mixture (solid line – 1st scan, dotted line -2nd scan) on a Pt electrode, T = 460 ºC, v = 500 mV.s^{-1}.

Figures 4.41 and 4.42 show the effect of the sweep rate on the current of peaks A and A`. The relationship between the current of peak A and the square root of the sweep rate is linear from 50 to 750mV.s^{-1}. At higher speed the parameters of the cathodic signal A in the voltammograms became unreadable. Also in this system the potentials of the peaks shift with increasing sweep rate; to more negative values in the case of A and to more positive values for A` which can be seen in Figure 4.41.

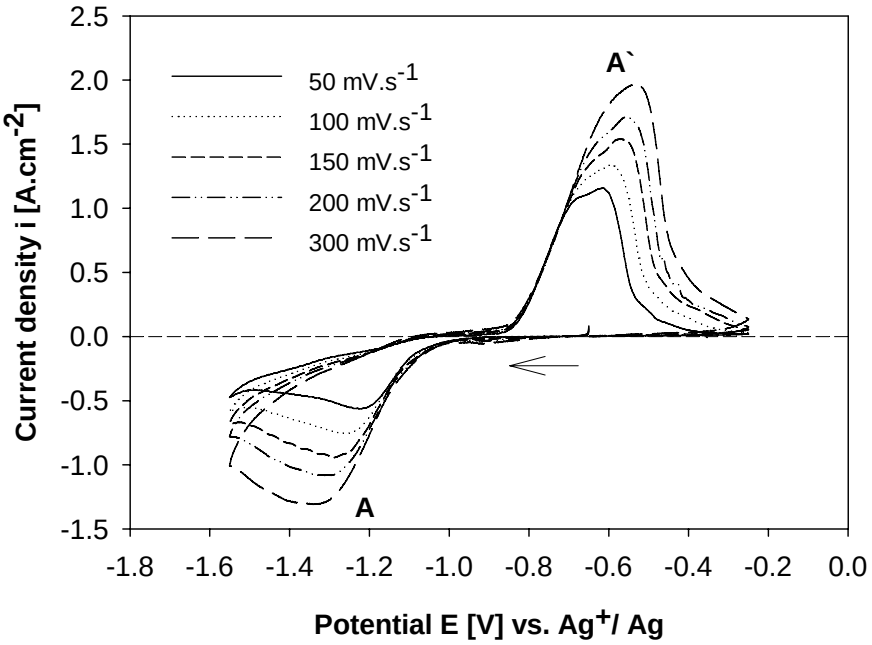

Figure 4.41 Evolution of the peaks A and A` originating from Na_2SO_3. Otherwise the same conditions as in Figure 4.40.

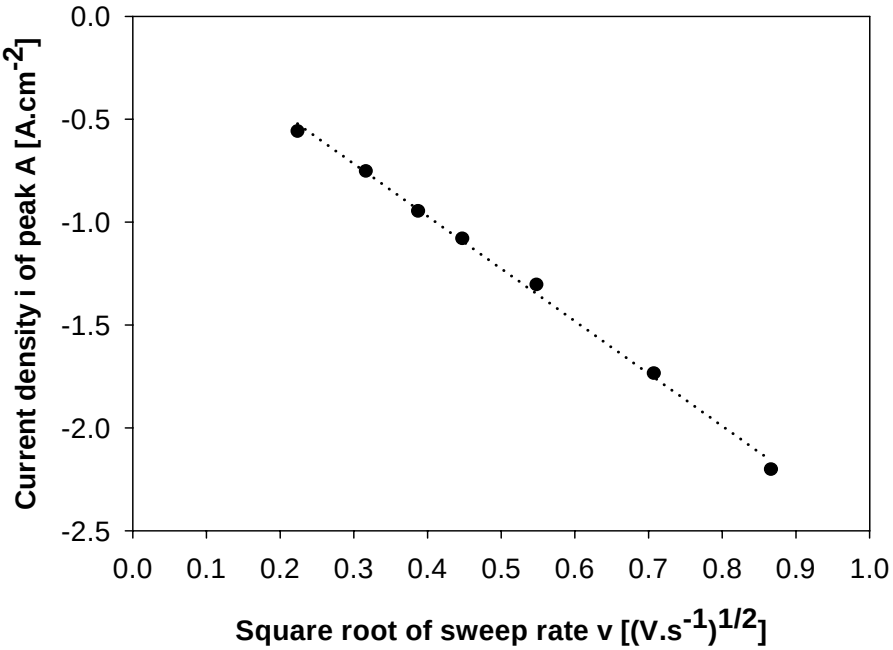

Figure 4.42 Relationship between current density of peak A and the square root of the sweep rate from data in Figure 4.41.

Although this time the current ratio $\left|I_p^{A`}/I_p^{A}\right|$ decreases (see Figure 4.43) with higher values of sweep rate, but is always greater than 1. This is an important difference which excludes the possibility that the sulphite reduction takes place through the "ec" mechanism in the LiCl-KCl eutectic.

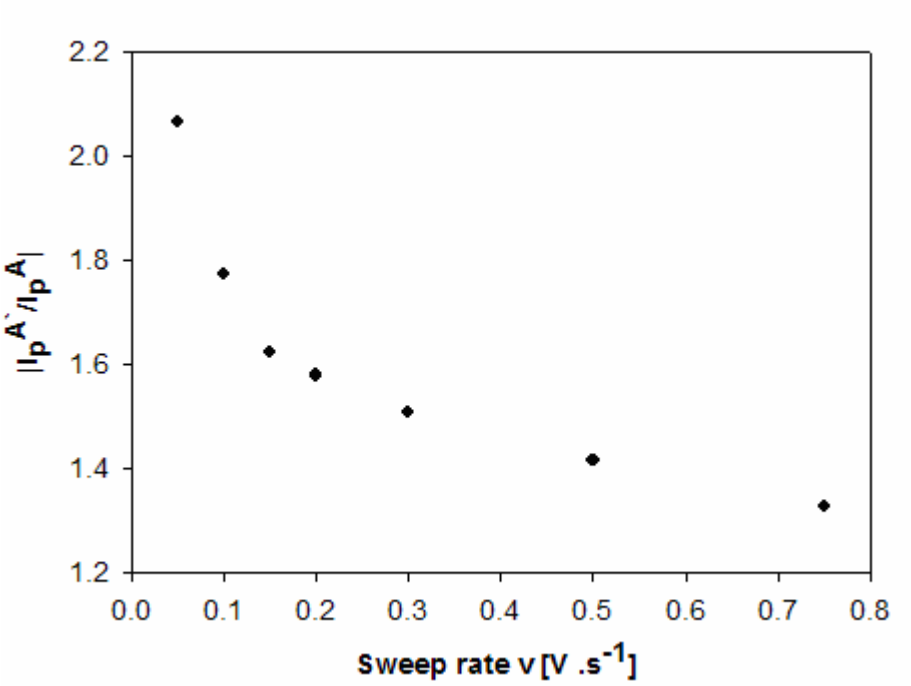

Figure 4.43 Plot of current ratio of A` and A peaks versus the sweep rate from data in Figure 4.41.

- *Behaviour of K_2S-$S_2O_3^{2-}$ mixture*

Voltammetric study of the sulphide behaviour was carried out with the aim to compare the location and response of the signal belonging to sulphide with the signals of the electroactive species where sulphur exists in different oxidation states from -II, e.g. SO_4^{2-} or SO_3^{2-}. Unfortunately sulphides such as sodium or potassium sulphides get readily oxidized in air to the corresponding thiosulphates: $S_2O_3^{2-}$. Even though K_2S was carefully dried before the experiment and the contact with air was minimized, the compound contained about 20 % of thiosulphate as a part of its composition. Thus, when referring further in the text to sulphide addition it is necessary to be aware of that it refers to the approximate concentration of K_2S from which about 20 % is in the form of $S_2O_3^{2-}$.

The electrochemical behaviour of S^{2-} plus $S_2O_3^{2-}$ species in the eutectic LiCl-KCl mixture could not be studied on a Pt substrate because Pt in the presence of sulphide is covered by a thin PtS film which passivates the surface of the

electrode. Then glassy carbon was used as the working electrode due to its higher chemical resistance against sulphide. But when using carbon in the experiments it is necessary to keep in mind that any kind of carbon has a capacity to act as a reducing agent, as it was explained in chapter 4.3.1, and thus influences the kinetics of the processes taking place on its surface. Therefore an evaluation of the kinetic parameters from the voltammetric curves is not possible. Only qualitative information can be extracted. A characteristic CV of this system is shown in Figure 4.44. Addition of K_2S gives rise to an anodic signal A` at about 0.8 V associated with to two cathodic waves: A and B.

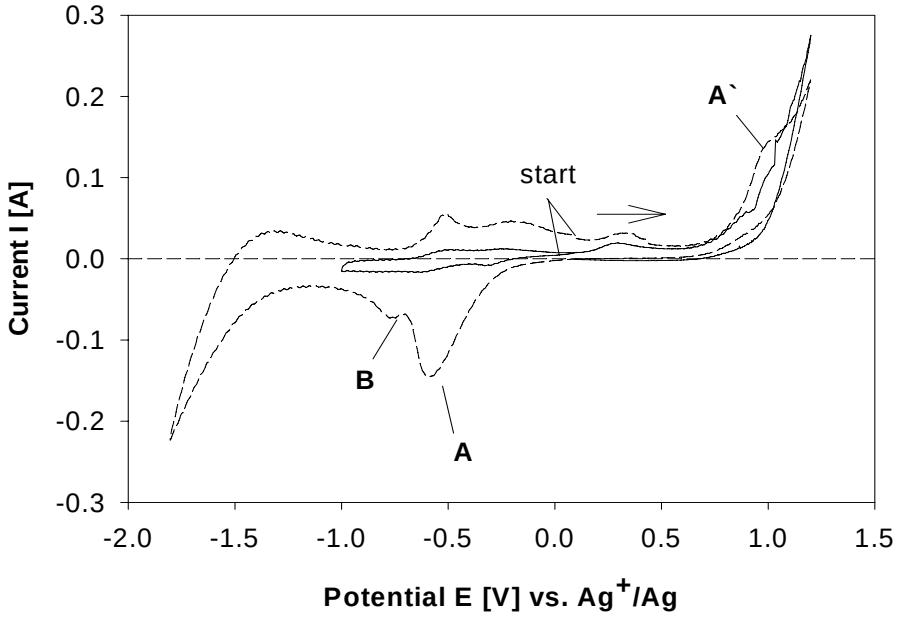

Figure 4.44 CVs obtained in the eutectic LiCl-KCl mixture on a glassy carbon electrode at 453 ºC after addition of K_2S recorded in the anodic (dashed line) and the cathodic (solid line) directions. Sweep rate 1500 $mV.s^{-1}$.

When increasing the content of K_2S, the anodic wave A` was shifted towards more positive potentials and the cathodic peaks A and B merged together in a single electrochemical wave. The same behaviour was observed when starting the scan in the anodic direction (Figure 4.45).

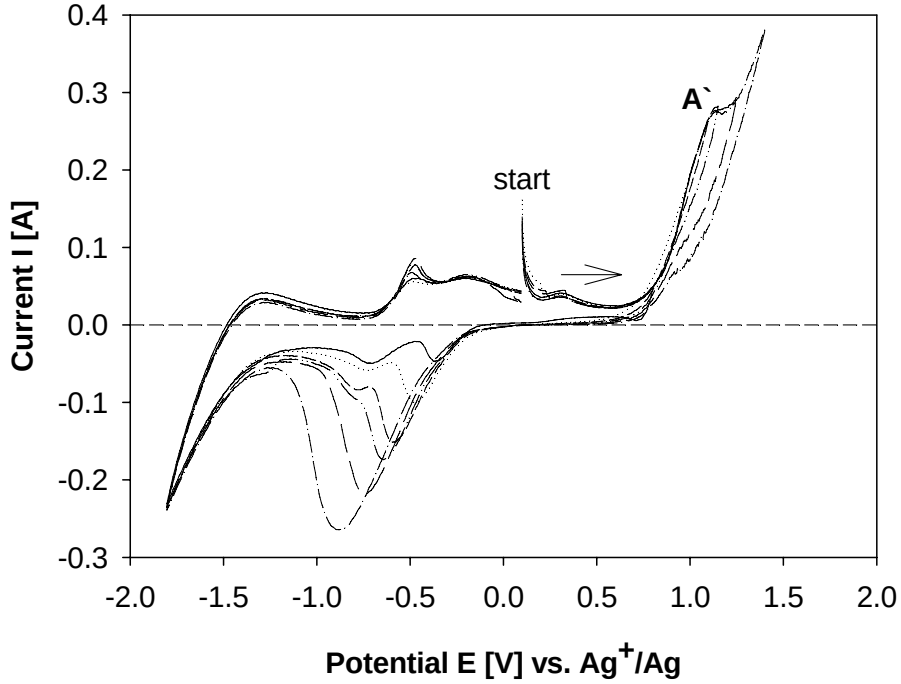

Figure 4.45 Cyclic voltammograms of K_2S in LiCl-KCl eutectic on a glassy carbon at 453 ºC; 1500 $mV.s^{-1}$ recorded in the anodic direction at different anodic vertex potentials.

More information about other peaks visible in the voltammograms from the K_2S containing melt cannot be given without doubts about their origin when taking into account also the presence of thiosulphate as the electroactive species. In addition and as mentioned earlier, carbon helps to reduce sulphur compounds and thus the carbon electrode was with high probability not totally inert in this experiment.

Analysis of the variation of the current density of peak A` was found to be proportional to the square root of the sweep rate within the interval from approximately 50 to 1000 $mV.s^{-1}$ indicating a diffusion controlled oxidation of S^{2-} species. This is shown in Figure 4.46.

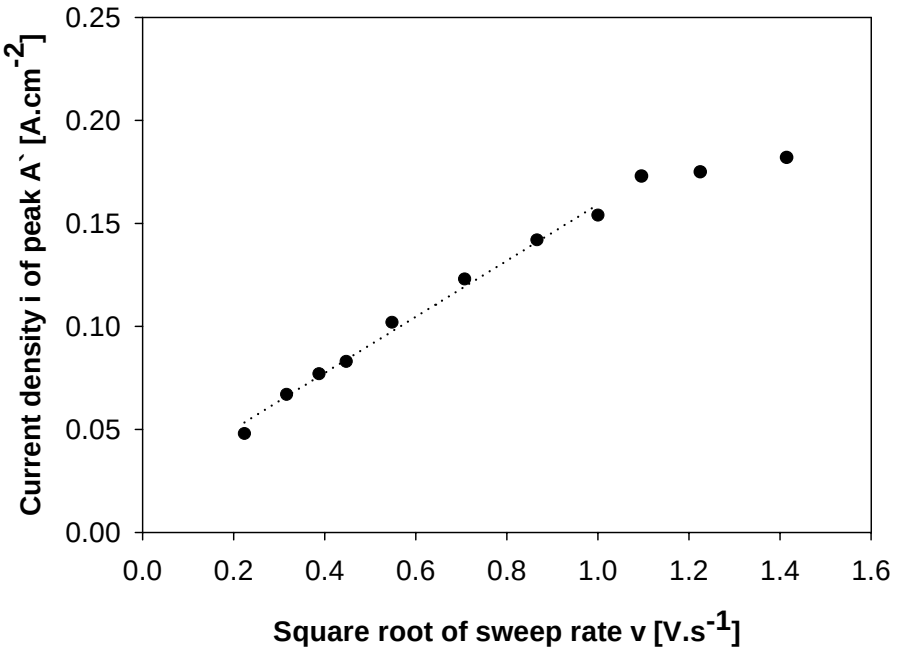

Figure 4.46 Influence of the sweep rate on the current density of 0.4 wt% K_2S in the LiCl-KCl eutectic. T = 453 ºC.

4.3.6 Conclusions

The electrochemical behaviour of sulphate, sulphite and sulphide was studied in various chloride melts at different temperatures. When sulphate was introduced to the simple NaCl melt, cyclic voltammetry showed a single cathodic peak at a potential very close to that of the alkali metal deposition associated to a single reverse anodic peak. The chronoamperometric experiments revealed that the sulphate anion undergoes two electrons exchange reduction from S (+VI) to S (+IV). If the sulphur species in the oxidation state +IV is Na_2SO_3 this will not be stable at the experimental temperature and could then decompose into other sulphur compounds, more likely to sulphur oxides than sulphides because the presence of those were not detected by titrimetric analysis. Analysis of the cyclic voltammograms obtained in the simple NaCl electrolyte indicated that the sulphate species are probably reduced via an "ec" mechanism, i.e. a chemical reaction following the charge transfer. A similar electrochemical behaviour of the sulphate anions was observed in the eutectic LiCl-KCl melt with comparable oxoacidity but the peak separation was considerably bigger as in the pure NaCl.

In the CaCl-$NaCl_2$ mixture (10:90 mol %), a different behaviour in the reduction of the sulphate anions was revealed with the formation of insoluble product. This was related to the difference in oxoacidity of the $CaCl_2$-based melts compared to

that of the pure NaCl melt or the eutectic LiCl-KCl mixture. Moreover, the chronoamperometric measurements revealed only a one-electron reduction step but probably coupled also by a chemical reaction. The electrochemical reduction of sulphate in the three above mentioned systems is probably diffusion controlled at the sweep rates where the effect of chemical reaction is negligible regardless of the supporting electrolyte. But, the transformation of the sulphate anions to lower oxidation forms might be dependent on the composition and character of the supporting electrolyte.

From the analysis of the electrolyte samples taken after the experiments and the off-gases investigations it follows that it is not likely that sulphate anions can be reduced directly to sulphur species in low oxidation states such as S (0) or S (-II) without the presence of an agent which would otherwise catalyze the cathodic reduction of sulphate to lower oxidation states such as S (0) or the whole way to (-II).

4.4 Results and discussions. Electrochemical studies of sulphur species in molten fluorides

The electrochemical behaviour of sulphur-containing species added in the form of Na_2SO_4 was studied in molten cryolite-based electrolyte (Na_3AlF_6) saturated by alumina (Al_2O_3) and variable content of AlF_3. The temperature of the bath varied depending on the supporting electrolytes that were kept in alumina crucibles. The choice of the working electrode material was the first step of the work in fluoride melts. Electrodes made of W, Pt and Au were examined. In all experiments a counter electrode was constructed from a coiled Pt wire prepared in the same way as in chloride melts. An aluminium electrode was used as a reference electrode.

4.4.1 Electrode testing in fluoride melts

- *Platinum electrode*

First the possibilities for finding a suitable working electrode material were examined in alumina saturated cryolite melt without an excess of AlF_3. Despite the fact that Pt was a good option as a material of a working electrode during experiments in the chloride melts, it was found not to be suitable for studies of sulphate reduction in molten fluorides. A typical voltammogram obtained on a Pt electrode in synthetic cryolite is shown in Figure 4.47.

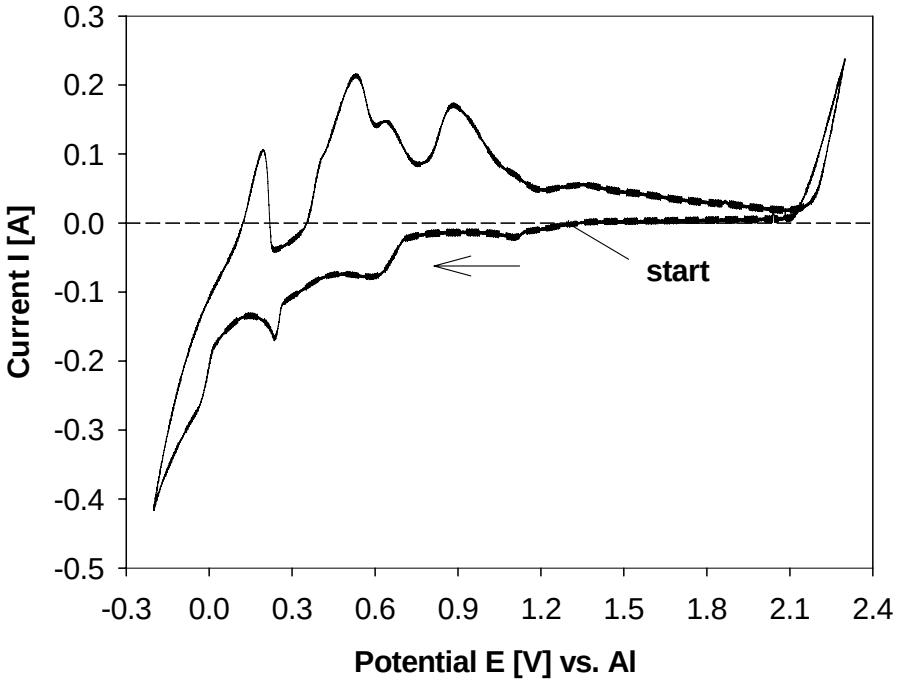

Figure 4.47 CV obtained on a Pt electrode in synthetic cryolite saturated by alumina without sulphate addition, T = 1006 ºC, v = 100 $mV.s^{-1}$.

The shape of the CV reveals extensive alloy formation between the deposited metal and platinum as well as the potential dependent formation of intermetallic compounds between aluminium and platinum which was also reported by Duruz et al. [113]. Due to this fact the limitations for using Pt in cryolite are obvious. Thus, only anodic processes taking place at very positive potentials in a range approximately from 1.1 V to 2.1 V could be studied on a Pt substrate.

- *Tungsten electrode*

The voltammograms obtained on a W electrode (shown in Figure 4.48) were recorded with various cathodic potentials halted at 0.1, 0, -0.1 and -0.2 V. The cathodic limit corresponds to the reduction of aluminium ions starting as a sharp peak from 0 V versus the aluminium reference connected with an anodic stripping peak in the reverse scan. When using a tungsten electrode it was not possible to sweep to more anodic potentials than to the open circuit potential without the risk of oxidation of the electrode material resulting in the formation of tungsten oxides on the electrode surface. This is in agreement with observations and voltammograms recorded by Thisted [12].

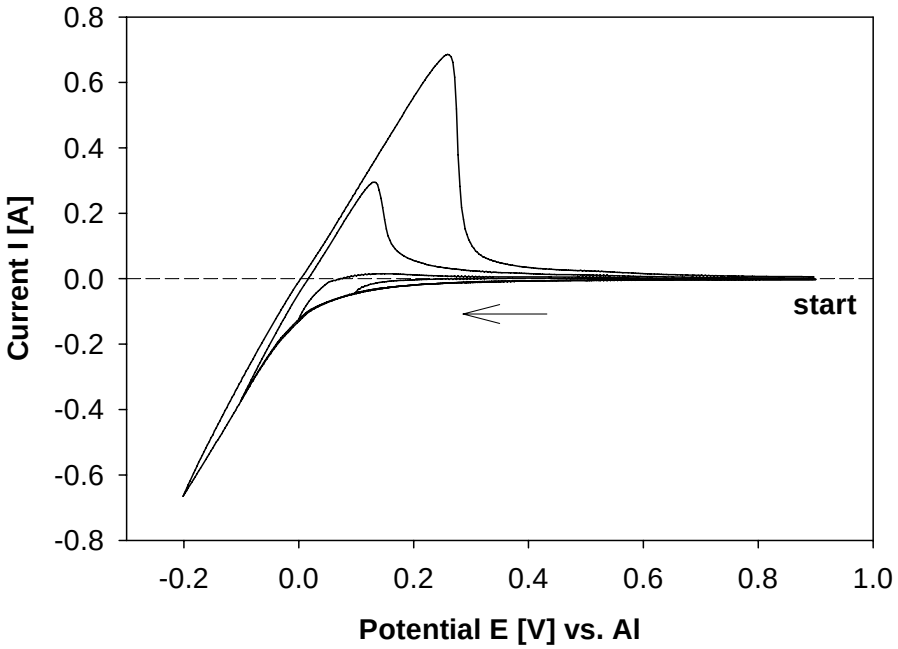

Figure 4.48 CV obtained on a tungsten electrode in synthetic cryolite-saturated by alumina without sulphate addition, T = 1000 ºC, v = 300 $mV.s^{-1}$. The arrow indicates the scanning direction.

After addition of Na_2SO_4 to the melt the same behaviour of tungsten electrode was noticed as that described in the chlorides melts. When the electrode was pulled out from the electrolyte its diameter was reduced along the part of the electrode which was not protected by an Alsint tube (see Figure 4.50).

- *Gold electrode*

When a gold electrode was used a CV presented in Figure 4.49 was obtained. During the cathodic scan at potentials more negative than 0.5 V, the electrode started to deteriorate rapidly by melting. This was explained by Duruz [113] to be due to both sodium and aluminium metal deposition and subsequent formation of alloys with the gold substrate (see Figure 4.51). Because such Na-Au or Na-Al-Au alloys have low melting point this leads to dissolution of gold during polarization in the cryolite bath. However, the observed potential region on a gold electrode in which current is essentially zero is large (~1.7 V). Moreover the addition of sulphate did not chemically affect the electrode properties. When scanning in a potential range where no deposition of Na or Al occurs, gold wire is well suited as a working electrode for electrochemical experiments with sulphate ions in molten cryolite melts.

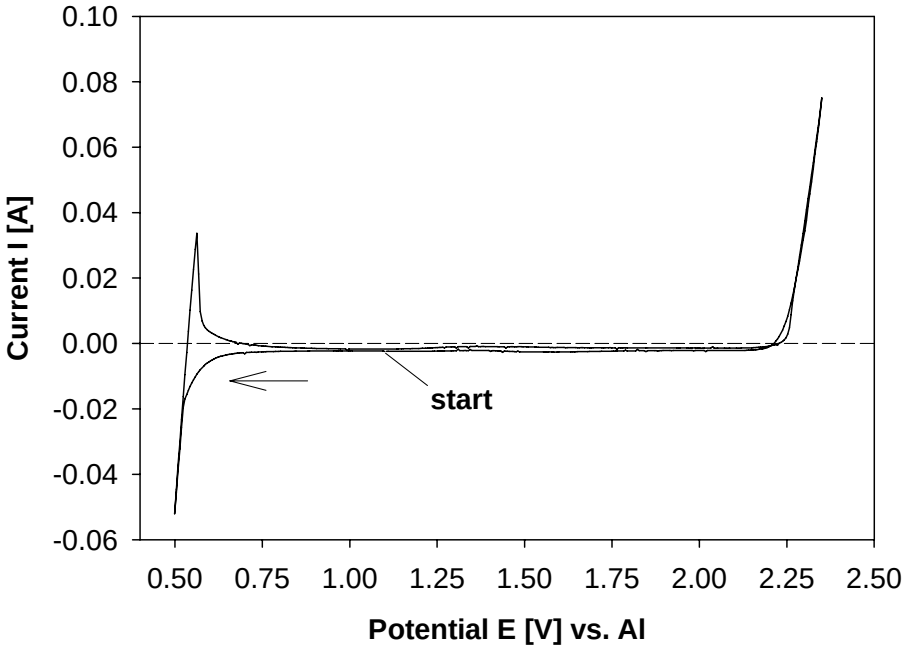

Figure 4.49 CV obtained on a gold electrode in synthetic cryolite-saturated by alumina without sulphate addition, T = 1000 ºC, v = 50 $mV.s^{-1}$. The arrow indicates the scanning direction.

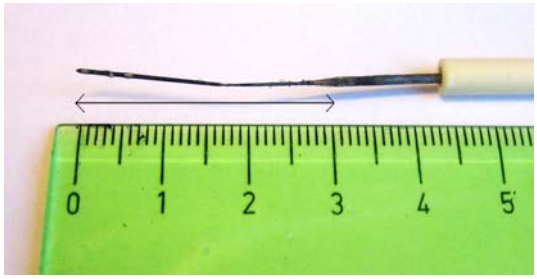

Figure 4.50 Tungsten working electrode after removal from electrolyte consisting of synthetic cryolite saturated by alumina. The arrow indicates the part of wire not protected by the alumina tube.

Figure 4.51 Al-Au-Na alloy deposited at 0.6 V on a gold electrode during four hours in the alumina saturated synthetic cryolite.

4.4.2 Molten Na_2SO_4-NaF-AlF_3 with CR = 3 saturated by Al_2O_3

For the first sets of experiments the composition of the mixture of NaF and AlF_3 was chosen to correspond to the cryolite ratio = 3 $\left(CR = \frac{\text{mol\% NaF}}{\text{mol\% AlF}_3}\right)$ which is in fact identical to cryolite with the formula Na_3AlF_6. The phase diagram of NaF-AlF_3 is given in Figure 4.52 and the composition of the basic electrolyte corresponding to CR = 3 (75 mol% NaF- 25 mol% AlF_3) is indicated by an arrow in the horizontal axis. Alumina (Al_2O_3) was mixed with the fluorides to saturate the melt with oxides in order to decrease the temperature of the electrolyte to 1000 ºC and prevent dissolution of the Alsint crucible.

- *Cyclic voltammetry*

When Na_2SO_4 was added to the electrolyte the voltammogram shown in Figure 4.53 was obtained when using Au as the working electrode. It revealed two cathodic signals A and B at potentials about 1.3 V and 0.7 V versus Al reference, both associated with a single anodic peak A` at 1.5 V. Peak B is located very close to the potential where Al-Au and Au-Na alloy formation start. From the shape of the peaks the assumption of a soluble-soluble system can be considered.

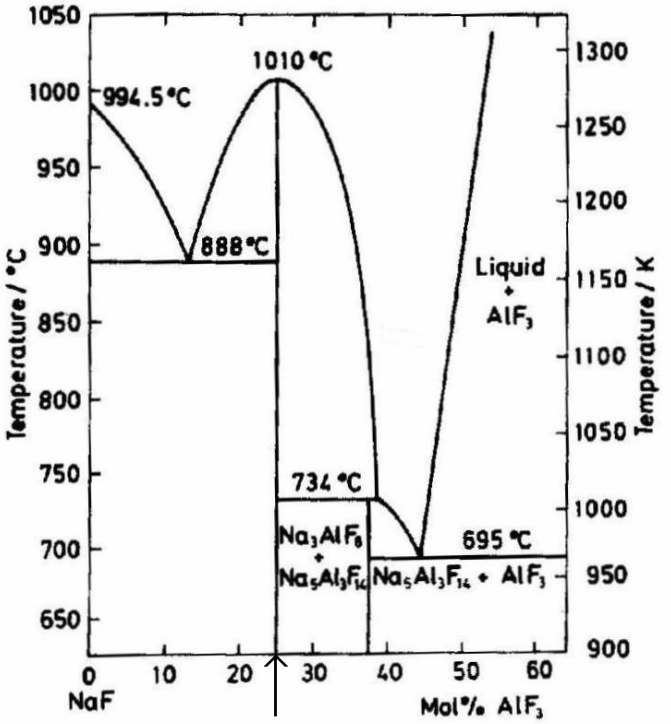

Figure 4.52 The binary phase diagram of $NaF\text{-}AlF_3$ [114]. The arrow indicates the composition of cryolite.

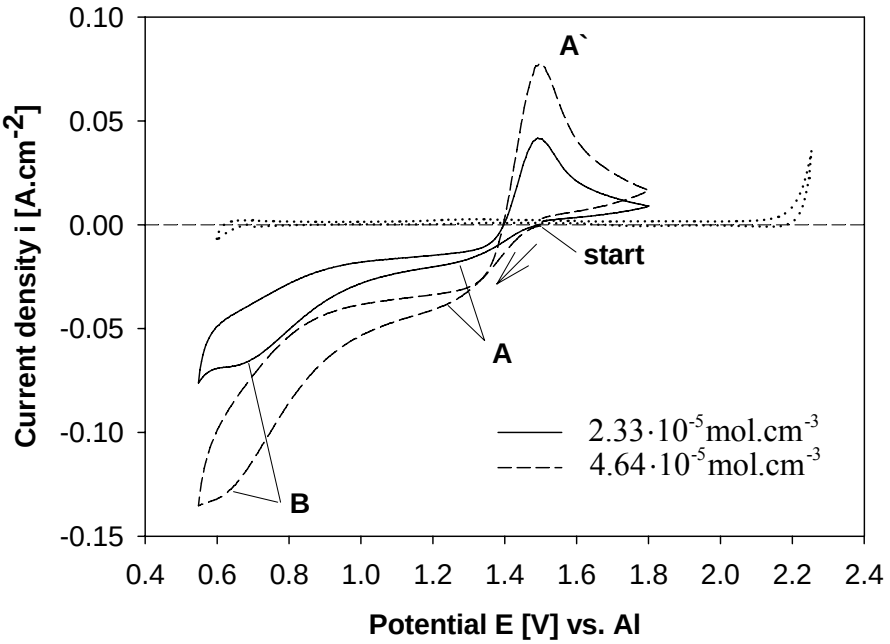

Figure 4.53 Cyclic voltammograms of Na_2SO_4 in an alumina-saturated Na_3AlF_6 melt at 1000 ºC and 300 $mV.s^{-1}$. The dotted line corresponds to the voltammogram of the supporting electrolyte.

Figure 4.54 shows a set of voltammograms recorded by changing the second vertex potential in the cathodic direction from 1.3 V to 0.55 V. It seems that the anodic peak A` can be primary attributed to the cathodic process at the potential of peak A since peak A` started to appear in the reverse scan after potential of 1.3 V was reached in the forward sweep.

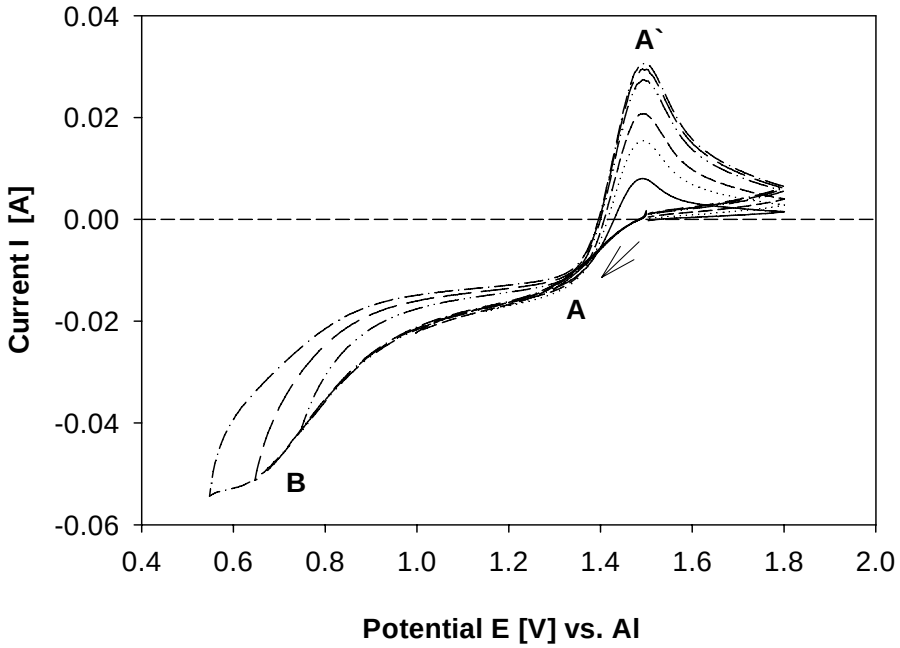

Figure 4.54 Cyclic voltammograms of $4.64 \cdot 10^{-5}$ mol.cm^{-3} Na_2SO_4 in synthetic cryolite saturated by alumina with various vertex potentials; T = 1000 ºC and v = 300 mV.s^{-1}.

Figure 4.55 shows the dependence of the peak couple A-A` on the sweep rate. It appears that the cathodic current density corresponding to peak A is increasing linearly with the square root of the sweep rate only for values lower than 30 mV.s^{-1}, but the plots shown in Figure 4.56 do not go through the origin. This might indicate the presence of a chemical reaction. On the other hand the reverse peak A` increases and is linearly proportional to the square root of the sweep rate in a broad range from 5 to 3000 mV.s^{-1}.

The same shape and behaviour of the A-A` system was also observed on a Pt electrode. The CVs on the Pt and Au working electrodes are shown for comparison in Figure 4.57.

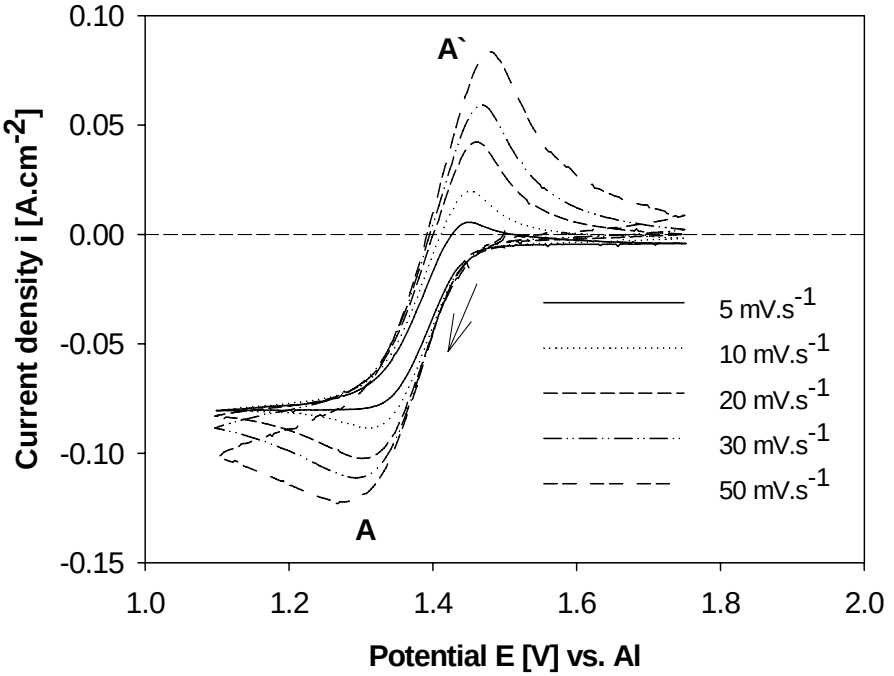

Figure 4.55 Cyclic voltammograms of $9.28 \cdot 10^{-5}$ mol.cm^{-3} Na_2SO_4 in synthetic cryolite saturated by alumina obtained for various sweep rates; T = 1000 ºC.

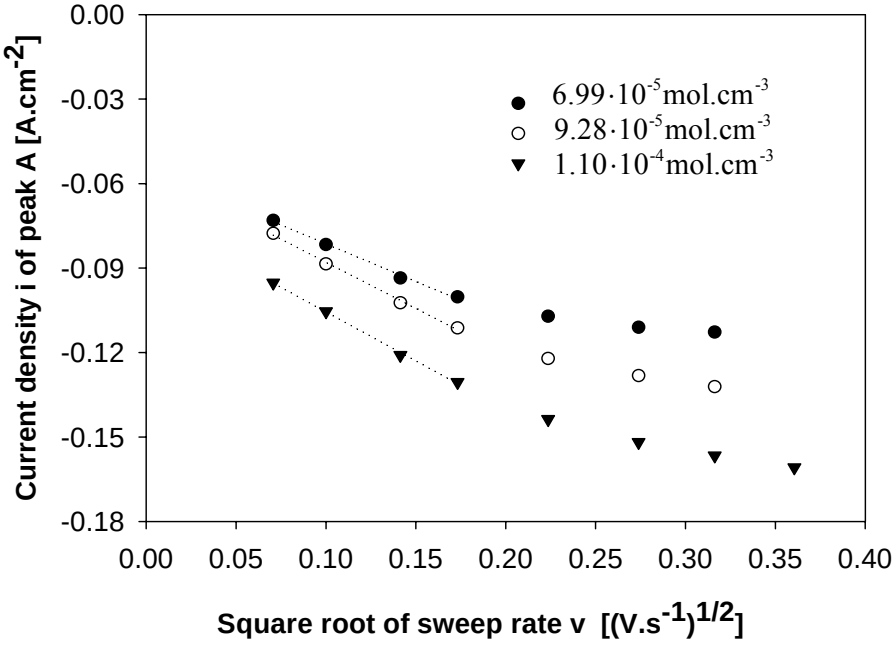

Figure 4.56 Current density of peak A as a function of the square root of the sweep rate for three concentrations of Na_2SO_4 in molten synthetic cryolite saturated by alumina at T = 1000 ºC.

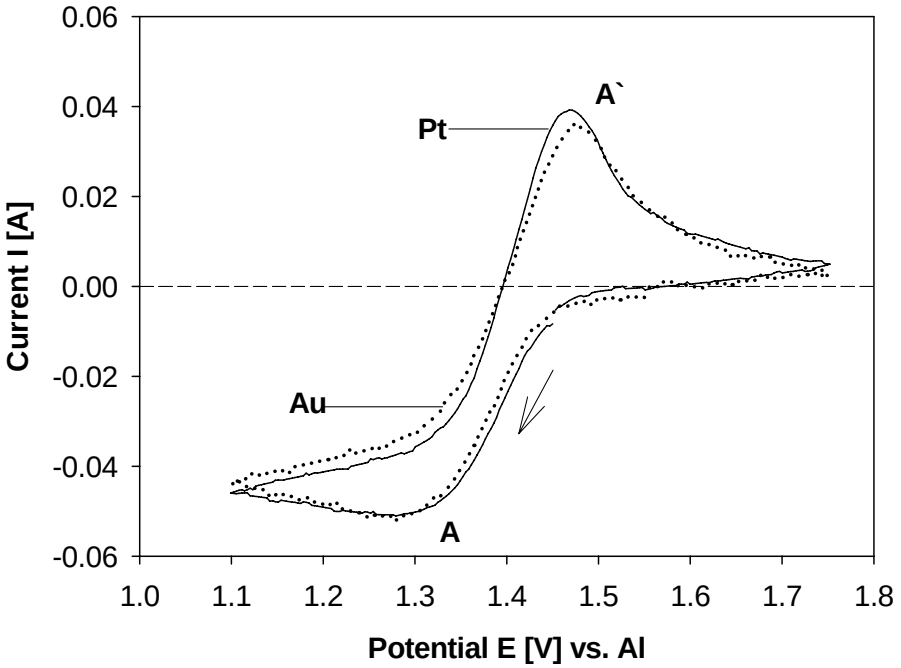

Figure 4.57 Comparison of the voltammograms of $6.99 \cdot 10^{-5}$ mol.cm^{-3} Na_2SO_4 in synthetic cryolite saturated by alumina recorded on gold and platinum. Electroactive area of both electrodes: 0.479 cm^2, T = 1000 ºC, v = 50 mV.s^{-1}.

It was observed that the current signal of peak A` was always bigger than the cathodic peak A. Modified current density of the cathodic peak A ($i_p^A/v^{1/2}$) and the ratio of the anodic A` and the cathodic A signals ($I_p^{A`}/I_p^A$) were plotted as a function of the sweep rate and are shown in Figures 4.58 and 4.59. Both, the decreasing trend of the data in the Figure 4.58 and the increasing value of the current ratio (which is always bigger than one) are in agreement with the diagnostic tests for a "ce" reaction mechanism, i.e. the electrochemical reduction proceeds after a chemical modification of the sulphate anions. This can be in simplicity written as the following reaction sequence:

$$Y \underset{\overleftarrow{k}}{\overset{\overrightarrow{k}}{\rightleftharpoons}} O \qquad 4.15$$

$$O + ne^- \rightleftharpoons R \qquad 4.16$$

If the chemical reaction is very fast then at low sweep rates the electrochemical process could be considered to be corresponding to a simple diffusion controlled electron transfer because the effect of the chemical reaction on the charge transfer will be negligible. As the sweep rate increases the influence of the chemical reaction becomes more significant and then the surface concentration of the reduced entities, and hence the current, will be partially controlled by the kinetics of the reaction 4.15.

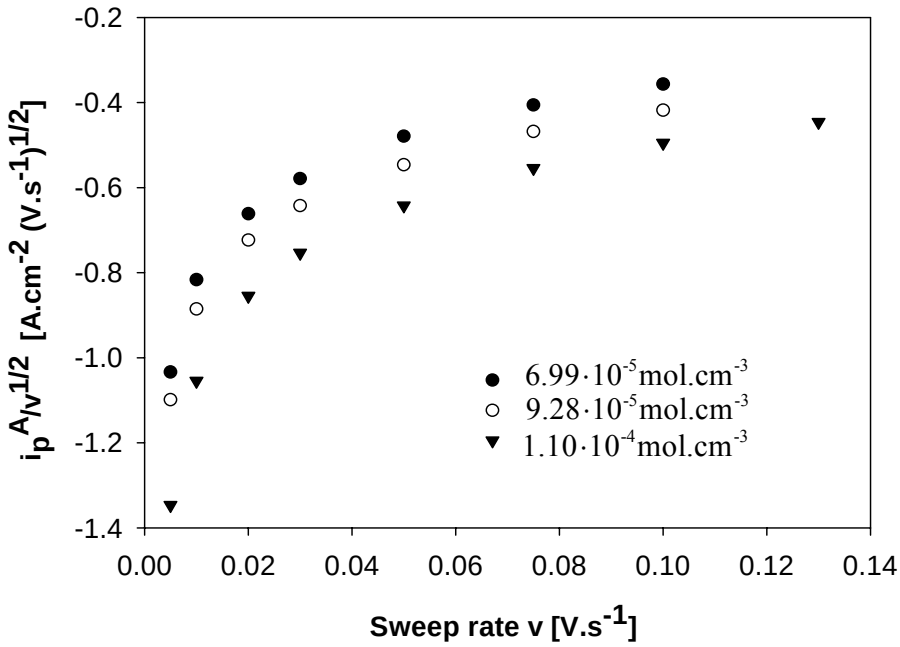

Figure 4.58 Plot reflecting the relationship between $i_p^A/v^{1/2}$ of peak A and the sweep rate plotted for three concentrations of Na_2SO_4, T = 1000 ºC.

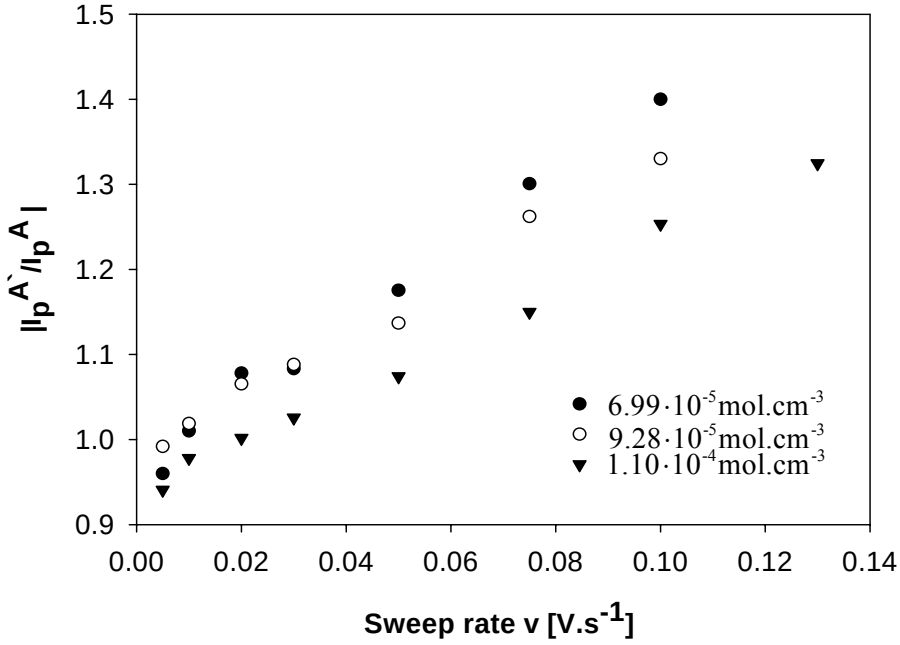

Figure 4.59 Plots of the absolute values of the current ratio of oxidation A` and reduction A peaks with concentration of Na_2SO_4 as variable, T = 1000 ºC.

Thus assuming reversible behaviour of reduced species at low sweep rates the number of electrons involved in reduction taking place at the potential of signal A was calculated from Equation 3.18. Table 4.6 contains the values of peak and half peak potentials from which the n values were determined at different sweep rates. Because Figure 4.56 showed that the reversibility criteria were fulfilled only from 5-30 $mV.s^{-1}$, then the number of exchanged electrons was defined as the mean value of n restricted to the above mentioned interval of the sweep rates. The mean value thus revealed that the first reduction step involves three electrons.

Table 4.6 Data of peak and half peak potentials determined from CV and calculated n values corresponding to sulphate reduction peak A at a concentration of $6.99 \cdot 10^{-5}$ $mol.cm^{-3}$ Na_2SO_4 in synthetic cryolite saturated by alumina, T = 1000 ºC.

Sweep rate [$V.s^{-1}$]	E_p^A [V]	$E_{p/2}^A$ [V]	Number of electrons
0.005	1.333	0.068	3.6
0.010	1.321	0.078	3.1
0.020	1.313	0.083	2.9
0.030	1.305	0.088	2.8
0.050	1.284	0.105	2.3
0.075	1.272	0.110	2.2
0.100	1.260	0.120	2.0

From the slope of the regression lines in Figure 4.56 constructed from data obtained at sweep rates from 5-30 $mV.s^{-1}$, the diffusion coefficient for the sulphate species could be calculated according to the Randles-Sevčik equation (Equation 3.17). The obtained diffusion coefficients of the sulphate anions for three different concentrations of SO_4^{2-} are summarised in Table 4.7 assuming three electrons exchange. Because the data were obtained from measurements on an electrode made from a wire, at such low sweep rates the influence of a spherical effect must be taken into account.

Table 4.7 Diffusion coefficients of the sulphate anion in a synthetic cryolite saturated by alumina at 1000 ºC.

Concentration of Na_2SO_4 [$mol.cm^{-3}$]	Diffusion coefficient [$cm^2.s^{-1}$]
$6.99 \cdot 10^{-5}$	$3.2 \cdot 10^{-5}$
$9.28 \cdot 10^{-5}$	$2.7 \cdot 10^{-5}$
$11.0 \cdot 10^{-5}$	$2.2 \cdot 10^{-5}$

According to Figure 4.60 the current of peak B increases with the increasing sweep rate. At sweep rates higher than 500 $mV.s^{-1}$ the wave is not well defined and thus not readable.

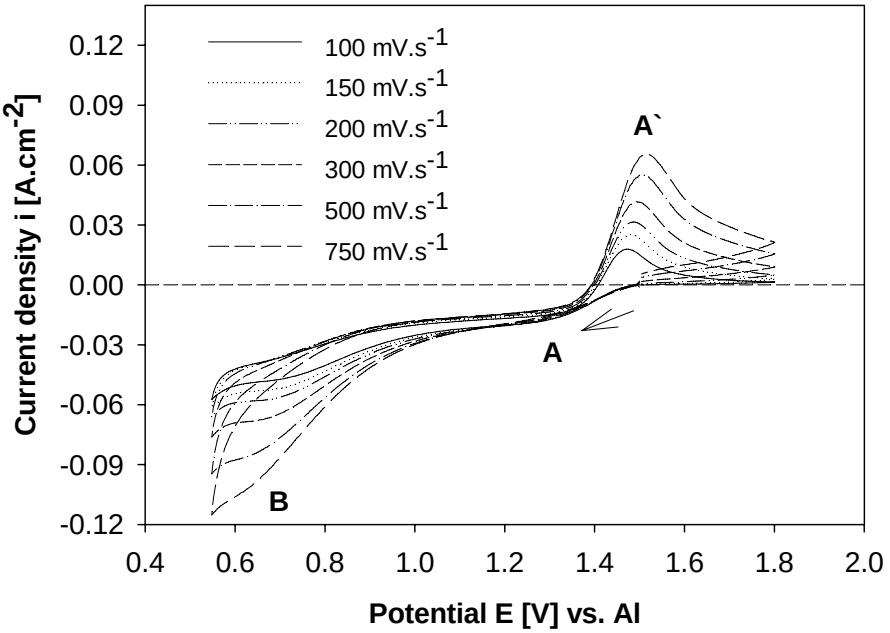

Figure 4.60 Voltammograms of $2.33 \cdot 10^{-5}$ $mol.cm^{-3}$ Na_2SO_4 in synthetic cryolite saturated by alumina recorded on a gold at different sweep rates; T = 1000 ºC.

The current of peak B plotted as a function of the square root of the sweep rate in the interval of sweep rates from 50 to 500 $mV.s^{-1}$ is shown in Figure 4.61. The plot revealed that the current is proportional to the square root of the sweep rate only at the sweep rates lower than 200 $mV.s^{-1}$. At the sweep rates higher than that deviation from the linearity was found, which might indicate a transition of from reversible to irreversible behaviour. In addition one should note that the plots do not pass through the origin. Due to the proximity of the cathodic limit of the melt on a gold electrode, the extraction of the data of peak B was not easy and could be affected by the Al-Na-Au alloy formation.

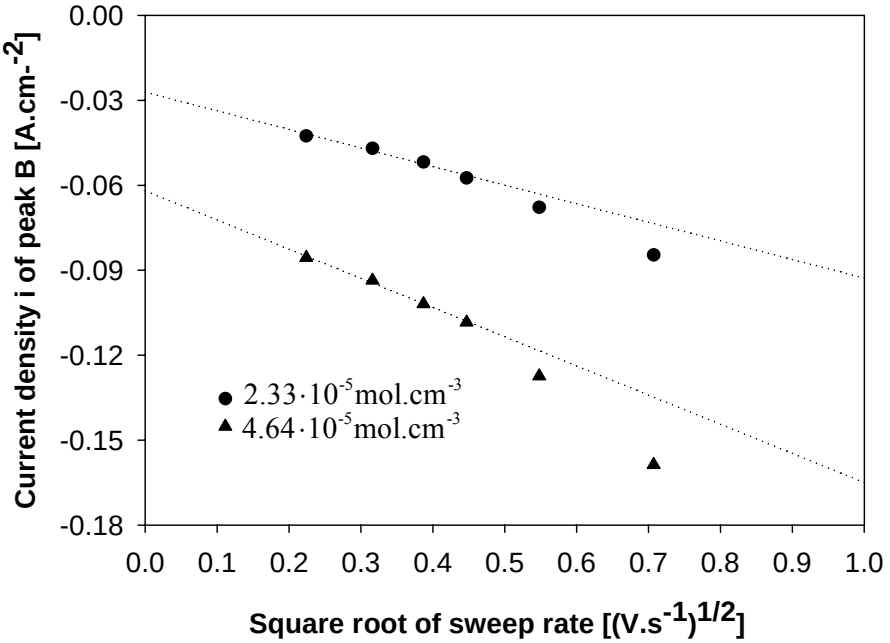

Figure 4.61 Relationship between the current densities of peak B and the square root of the sweep rate at two concentrations of Na_2SO_4 in synthetic cryolite saturated by alumina; T = 1000 ºC, sweep rate range: 50-500 $mV.s^{-1}$.

- *Chronoamperometry*

A chronoamperometric investigation of Na_2SO_4 in synthetic cryolite saturated by alumina was also carried out. The CA curves were analysed in the same manner as described previously (see chapters 4.3.2 and 4.3.3).

Typical current transients of sulphate anions in a melt consisting of synthetic cryolite and alumina are shown in Figure 4.62

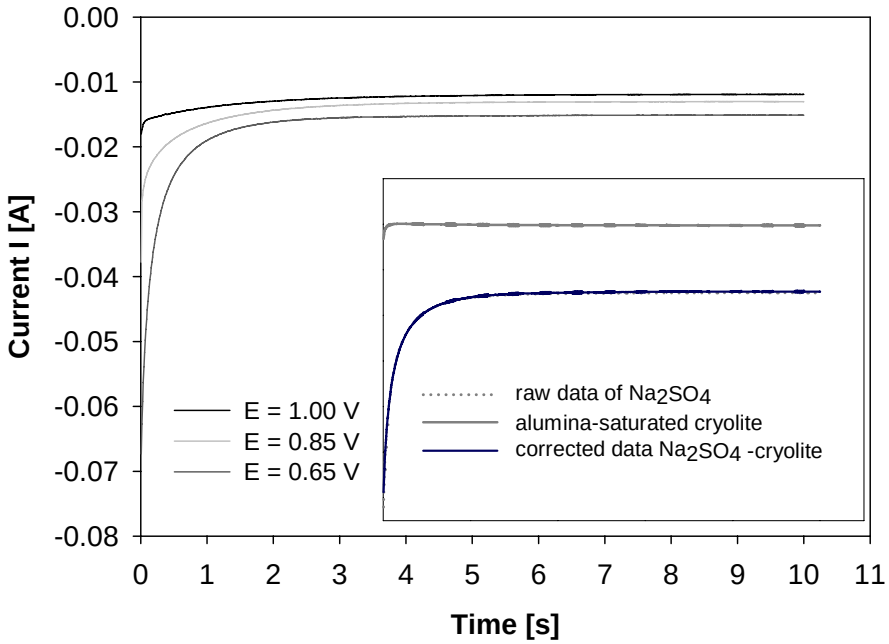

Figure 4.62 I-t curves obtained for $4.64 \cdot 10^{-5}$ mol.cm^{-3} Na_2SO_4 in alumina-saturated synthetic cryolite T = 1000 ºC, Au electrode. Potentials applied with respect to OCP are shown in the figure. The curves were also corrected for the background current.

When the obtained current values were analysed according to the Cottrell equation a linear part in the time interval from 0.17-1.4 s was revealed. Within this time interval it can be assumed that the process is diffusion controlled. I-E curves constructed with the time as a variable showed two regions where the current was passing through minimum. The first limiting current was determined at approximately 1.26 V and the second one at 0.68 V which correspond to the potentials belonging to the cathodic signals A and B respectively. The number of electrons exchanged in the first (A) and second (B) reduction process was derived from the slopes of the plots showing dependence of potential upon $\ln[(I_{lim}-I)/(I_{lim}+I)]$ following from Equation 3.23. Such plots are presented in Figures 4.63 for the first reduction step, A, and in Figure 4.64 for the second cathodic process, B, respectively. In the ideal diffusion controlled case the slope of the regression lines are independent of time. Apparently this is not totally fulfilled (especially in Figure 4.64). This means that the second cathodic step, B, is not properly diffusion controlled and an assumption of a certain influence of charge transfer must be considered. Therefore, the accuracy of the chronoamperometric results regarding the second reduction step can be questionable.

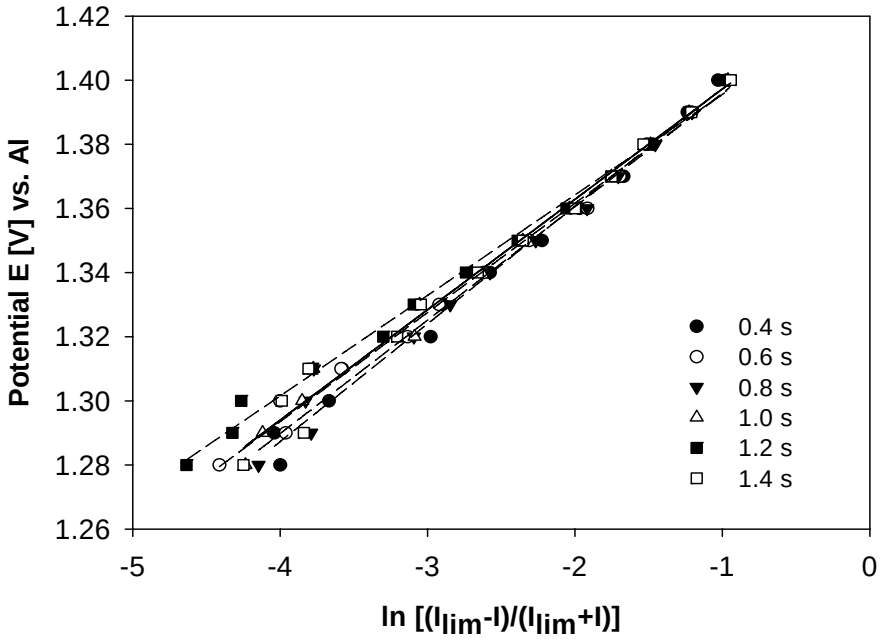

Figure 4.63 Plots of E versus ln[(I_{lim}-I)/(I_{lim}+I)] corresponding to the A reduction wave. I_{lim} reached at 1.26 V. Sulphate concentration $4.64 \cdot 10^{-5}$ mol.cm^{-3}.

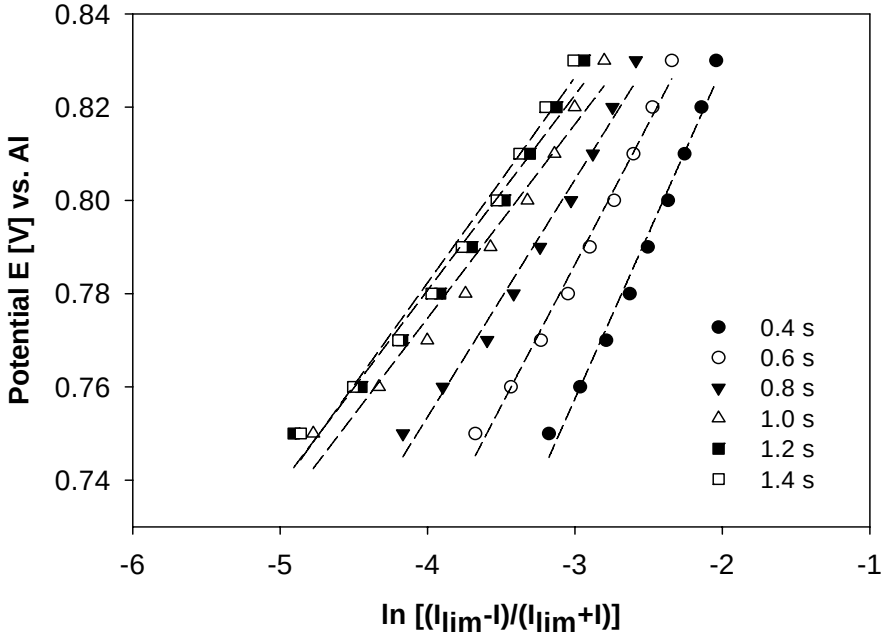

Figure 4.64 Plot of E versus ln[(I_{lim}-I)/(I_{lim}+I)] corresponding to the B reduction wave. I_{lim} reached at 0.68 V. Sulphate concentration $4.64 \cdot 10^{-5}$ mol.cm^{-3}.

Tables 4.8 and 4.9 gather the data of limiting current, slope and calculated electrons for both A and B cathodic steps respectively. The average value of exchanged electrons for the first reduction process was found to be equal to 3. This is in good agreement with the n value determined from the cyclic voltammetry. The second cathodic step at the potential of peak B seems to involve only 2 electrons.

Table 4.8 Number of electrons determined from the values obtained by chronoamperometry and corresponding to the first reduction step A. I_{lim} reached at 1.26 V. T = 1000 ºC, $4.64 \cdot 10^{-5}$ mol.cm^{-3} Na_2SO_4.

Time [s]	Limiting current [A]	Slope	Number of electrons
0.4	-0.0109	0.0367	3.0
0.6	-0.0112	0.0341	3.2
0.8	-0.0115	0.0354	3.1
1.0	-0.0114	0.0344	3.2
1.2	-0.0115	0.0313	3.5
1.4	-0.0116	0.0345	3.2

Table 4.9 Number of electrons determined from the values obtained by chronoamperometry and corresponding to the second reduction step B. I_{lim} reached at 1.26 V. T = 1000 ºC, $4.64 \cdot 10^{-5}$ mol.cm^{-3} Na_2SO_4.

Time [s]	Limiting current [A]	Slope	Number of electrons
0.4	-0.0267	0.0710	1.5
0.6	-0.0229	0.0606	1.8
0.8	-0.0206	0.0509	2.2
1.0	-0.0191	0.0416	2.6
1.2	-0.0181	0.0419	2.6
1.4	-0.0174	0.0441	2.5

According to Castro [89] Na_2SO_4 becomes partly thermally unstable at temperatures above 900 ºC. Sulphate is then converted to another S-species while Na vaporises as Na_2O. Then a scheme of thermal stability of sulphate and S-species presented in Figure 4.65 can be suggested with the final products Na_2O and SO_3. At temperatures above 500 ºC SO_3 also decomposes to the gaseous compounds SO_2 and O_2. If Na_2SO_4 is partially transformed due to the temperature effect to a lower oxidation state species such as sodium sulphite, Na_2SO_3, this is also thermally unstable and decomposes to Na_2SO_4 and Na_2S. However, at the temperature maintained in the experiments with the melt composition used, sodium sulphate probably does not decompose totally but an equilibrium between Na_2SO_4 and Na_2SO_3 might be possible.

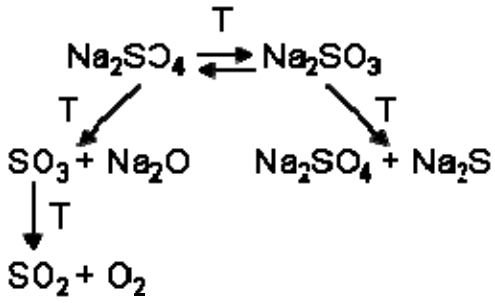

Figure 4.65 Scheme of the temperature effect on the S-species.

If the reduced entity in this system is sulphur (+VI) in the form of sulphate and the number of exchanged electrons calculated from the previous described electrochemical measurements is taken into account, the following reduction mechanism could be proposed:

$$2SO_4^{2-} + 3e^- \rightarrow S_2O_4^{2-} + 4O^{2-} \qquad 4.17$$

$$S_2O_4^{2-} + 2e^- \rightarrow S_2O + 3O^{2-} \qquad 4.18$$

It is known that S_2O cannot be stable and could only exist as a reaction intermediate. At higher temperatures it polymerizes but above 150 ºC the polymer decomposes to SO_2 and S^0. It is difficult to say whether sulphur was one of the final products in the melt or not since no yellow coloration of the melt, typical for the presence of S^0, was observed. Titrimetric analysis of the samples did not confirm any S^{2-} either.

4.4.3 Molten Na_2SO_4-NaF-AlF_3 with CR = 2 saturated by Al_2O_3

The Composition of the industrial electrolyte typically contains from 6 - 13 wt% AlF_3 in addition to aluminium fluoride which is a part of cryolite. For this set of experiments the mixture of fluorides with the composition of 67 mol% NaF and 33 mol% AlF_3 (equal to 10 wt% in addition to AlF_3 in cryolite) was chosen which corresponds to CR = 2. Since the experiments were performed in Alsint crucibles the melt was also saturated by alumina. The phase diagram of NaF-AlF_3 is given in Figure 4.66 and the composition of the basic electrolyte is indicated by an arrow in the horizontal axis. The higher AlF_3 contents allowed decreasing the temperature of the melt to 960 ºC. The measurements were performed with a gold working electrode, aluminium as reference and platinum as counter electrodes. The electroactive species were added as Na_2SO_4 powder.

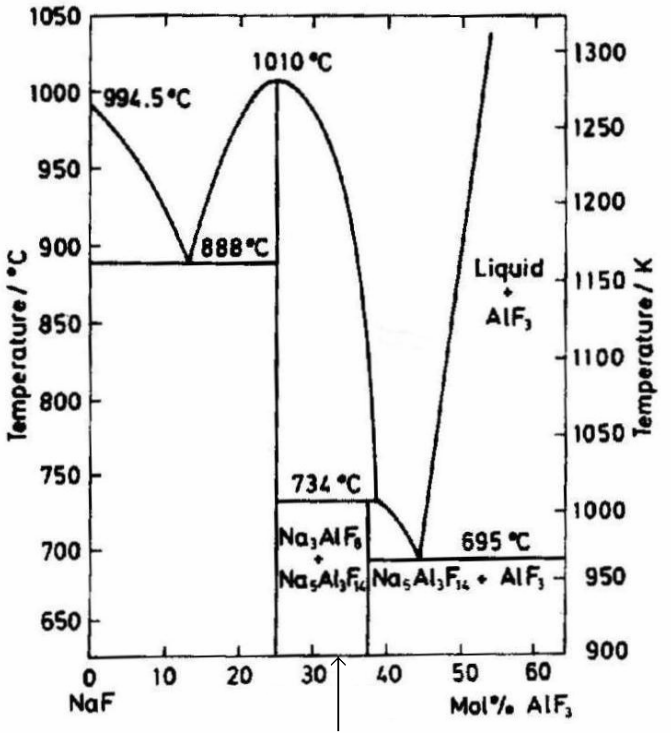

Figure 4.66 The binary phase diagram of NaF-AlF_3 [114]. The arrow indicates the melt composition of CR = 2.

- *Cyclic voltammetry*

A typical cyclic voltammogram recorded on a gold electrode before and after addition of sulphate ions to the mixture of NaF-33 mol% AlF_3 saturated by alumina are presented in Figure 4.67. The voltammograms of the supporting electrolyte showed the same features as the one obtained in the alumina-saturated synthetic cryolite melt. Addition of sodium sulphate revealed a single reduction peak A at a potential around 1.35 V associated with one oxidation wave A` at ~ 1.55 V. Unlike the previous system, a second cathodic peak B obtained at a lower potential was not observed in this melt.

A series of cyclic voltammograms was acquired for the melt containing sulphate anions as a function of the sweep rate and the sulphate concentration (Figure 4.67). Unfortunately, a dramatic decrease of sulphate concentration from the electrolyte was observed shortly after the third addition of the SO_4^{2-} anion which precluded the studied system from further investigation. However, the data gained from the CV for the first two sulphate concentrations were analysed.

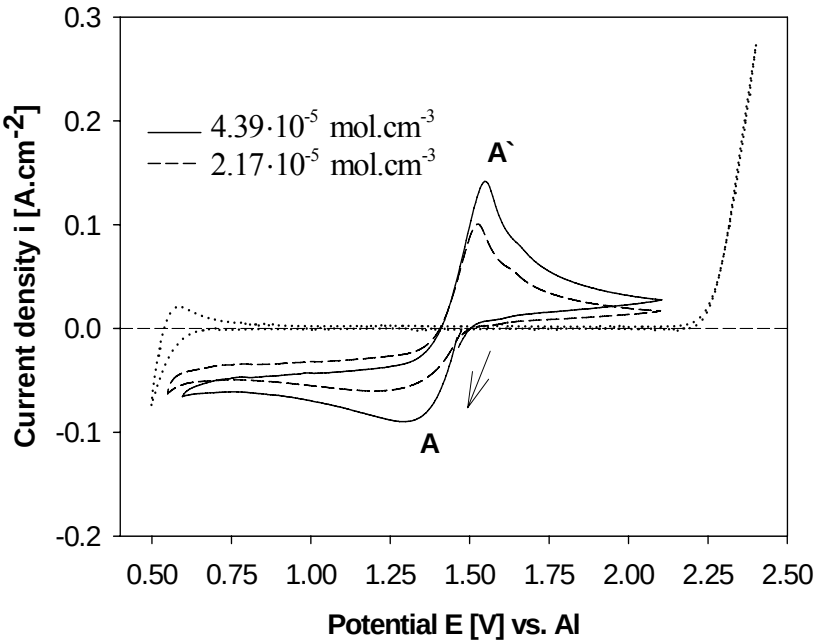

Figure 4.67 CVs in an alumina-saturated mixture of NaF–33 mol% AlF_3 melt before (dotted line) and after addition of two concentrations of Na_2SO_4 (solid and dashed lines). T = 960 ºC, v = 500 $mV.s^{-1}$. The arrow indicates the scanning direction.

The formation of an insoluble product on the Au working electrode was checked before the data of the peak parameters were evaluated. A constant potential was applied at 1.35 V and subsequently a reverse anodic scan to 2.1 V was performed. The same procedure was repeated for three various periods of time of applied potential and the result is shown in Figure 4.68. If the insoluble species formation occurs, doubling the time of applied potential should be reflected in the reverse scan as current response twice as high as for the undoubled time due to the twice amount of the product formed on the electrode surface. As it can be observed from Figure 4.68 doubling of the time did not lead to higher current of the oxidation peak but gave the same values independently of time. This fact confirmed that the species reduced at the electrode could be considered being soluble.

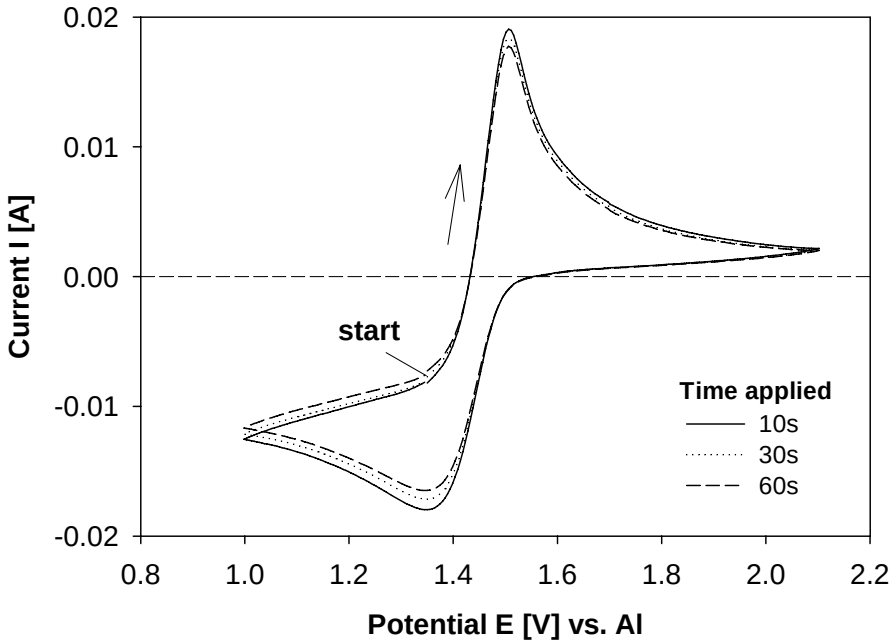

Figure 4.68 CVs recorded on Au electrode at 100 $mV.s^{-1}$ after applying a potential of 1.35 V for various period of time, T = 960 ºC.

The current response of the peak couple A-A` increased with increasing sweep rate up to 750 $mV.s^{-1}$ (see Figure 4.69). At higher sweep rates the current approached a limiting value.

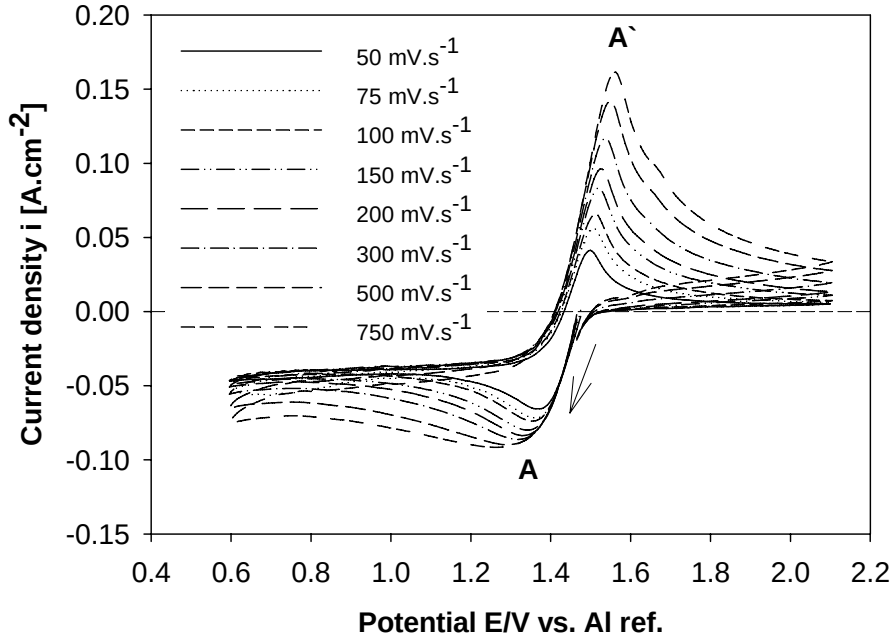

Figure 4.69 Voltammograms of $4.39 \cdot 10^{-5}$ $mol.cm^{-3}$ Na_2SO_4 in NaF – 33 mol% AlF_3 mixture saturated by alumina at different sweep rates; T = 960 ºC.

A plot of the cathodic current density versus the square root of the sweep rate is shown in Figure 4.70.

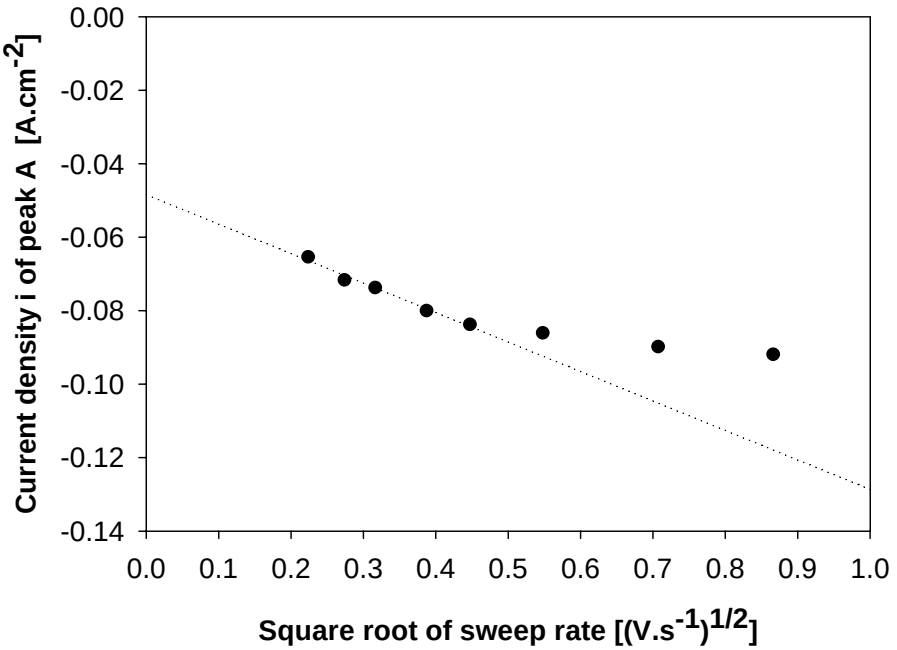

Figure 4.70 Relationship between the current density of peak A of $4.39 \cdot 10^{-5}$ mol.cm^{-3} Na_2SO_4 added to NaF – 33 mol% AlF_3 mixture saturated by alumina and the square root of the sweep rate at 960 ºC.

The figure demonstrates that the peak current can be considered to be proportional to the square root of the sweep rate only at low sweep rates (in the range from 50-200 mV.s^{-1}). The plot of this relationship does not pass through the origin, which might indicate a coupled chemical reaction. The sweep rates from which the peak current becomes non-proportional to the square root of sweep rate are approximately four times higher than in the system described in chapter 4.2.2. The peak separation A-A` is also much smaller than in the previous case.

A linear current increase with the square root of the sweep rate in the whole range of applied sweep rates was found to be characteristic for the behaviour of the anodic peak A`. It was also observed that the signal of A` was always larger than the cathodic peak current and increased with the sweep rates. This is presented in Figure 4.71 as a proportion of current values coming from the A`-A system and in Figure 4.72 plotted as a function $\frac{i_{(A)}}{v^{1/2}}$ versus the sweep rate. The first mentioned relationship shows increasing trend with the current ratio and is always greater than one while in Figure 4.72 the current function gets decreasing trend as the sweep rate increases.

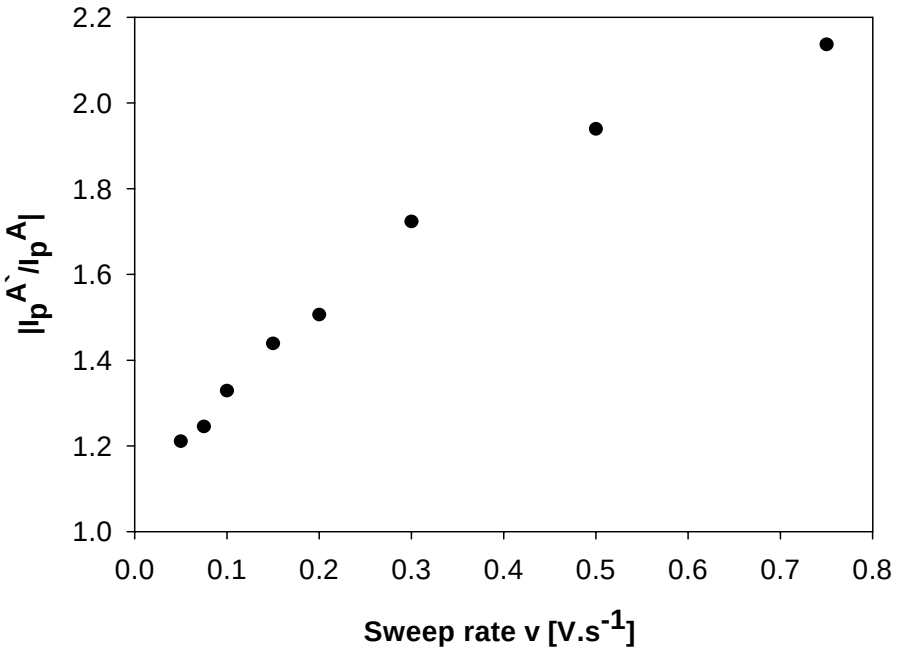

Figure 4.71 Dependence of the current ratio of oxidation A` and reduction A signals upon the sweep rate for $4.39 \cdot 10^{-5}$ mol.cm^{-3} of Na_2SO_4 in alumina-saturated NaF – 33 mol% AlF_3 mixture. T = 960 ºC.

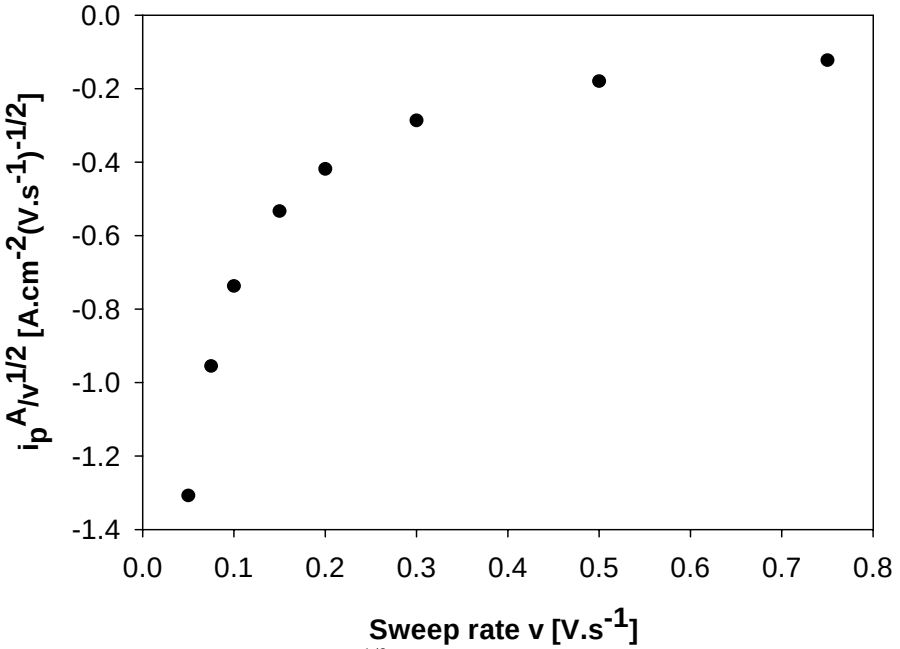

Figure 4.72 Relationship between ($i/v^{1/2}$) function of the cathodic peak A and the sweep rate. The data were obtained in the same melt and at the same experimental conditions as in Figure 4.70.

The above results are in agreement with the diagnostic tests for a "ce" reaction mechanism. Moreover, the reduction mechanism for the A-A` system seems to be similar in both the synthetic cryolite melt saturated by alumina (described in chapter 4.4.2) and this melt.

The n value in the A-A` system was derived from the difference between the peak potential and the half peak potential of peak A (Equation 3.18). The potential values of peak A are presented in Table 4.10 for corresponding sweep rates in the range from 50-200 $mV.s^{-1}$ where the studied system was assumed to be in a diffusion controlled region. The calculated number of exchanged electrons is also included in Table 4.10 and their mean value gave three electrons exchanged in the cathodic step.

Table 4.10 Data of the peak and the half peak potentials determined from CV and calculated n values corresponding to the sulphate reduction peak A at concentration $4.39 \cdot 10^{-5}$ $mol.cm^{-3}$ Na_2SO_4 in the alumina-saturated NaF – 33 mol% AlF_3 mixture, T = 960 ºC.

Sweep rate [$V.s^{-1}$]	E_p^A [V]	$E_{p/2}^A$ [V]	Number of electrons
0.050	1.372	1.443	3.3
0.075	1.366	1.439	3.2
0.100	1.357	1.433	3.1
0.150	1.344	1.427	2.8
0.200	1.335	1.430	2.5

The diffusion coefficient for SO_4^{2-} anion was then calculated from the slope of the dependence shown in Figure 4.70 and Equation 3.17 was applied assuming reversible system involving soluble species. Neither in this case the sweep rates are high enough to neglect the effect and contribution of spherical diffusion.

Table 4.11 The diffusion coefficient of the sulphate anion determined from the slope in Figure 4.70, n = 3, T = 960 ºC.

Concentration of Na_2SO_4 [$mol.cm^{-3}$]	Diffusion coefficient [$cm^2.s^{-1}$]
$4.39 \cdot 10^{-5}$	$0.71 \cdot 10^{-5}$

The solidified samples of the electrolyte were subject of titrimetric analysis but iodimetry did not confirm the presence of sulphide ions.

It is known that fluorides stabilize higher oxidation states, at least in the case of metal ions. Thus the question can be asked if a similar effect could be expected on sulphur compounds and how a higher content of AlF_3 contributes to stabilization of sulphur species in the higher oxidation states. In the next paragraph a few ideas are presented on how the sulphur entities might interact

with the supporting electrolyte. It must be emphasised here that the below described chemical mechanism could be considered only as a theoretical as long as no experimental or analytical evidence is given in this work.

In inorganic chemistry species such as fluorosulfonic acid, FSO_2OH or sulfuryl fluoride, SO_2F_2 are known. Fluorosulfonic acid forms a large number of stable salts, fluorosulfates, which can be prepared by the reaction of SO_3 with fluorides, e.g Cs, Ca. If a reaction of AlF_3 with SO_3 is considered, one can get:

$$AlF_3 + 3SO_3 \rightarrow Al(SO_3F)_3 \qquad 4.19$$

When such a salt of fluorosulfuric acid is heated, sulfuryl fluoride could be formed (as it is formed from $Ba(SO_3F)_2$) thus aluminium fluorosulfuric salt could react according to the reaction below:

$$2Al(SO_3F)_3 \rightarrow Al_2(SO_4)_3 + 3SO_2F_2 \qquad 4.20$$

If one of the oxide atoms is replaced by two fluoride ions, sulphur tetrafluoride oxide is formed, SOF_4 which can react with a strong Lewis acid such as AlF_3 and form a complex: $SOF_3^+AlF_4^-$.

4.4.4 Molten Na_2SO_4-NaF-AlF_3 with CR = 1.5 saturated by Al_2O_3

Since the beginning of the history of aluminium industry the idea of inert anodes has been alive. Introduction of such anodes will be closely connected with the modifications of the electrolyte which is used nowadays. One of the approach proposes to use an electrolyte with low CR (high mol % of AlF_3) [115]. A cell with such a low CR could be kept at a lower temperature and a lower rate of chemical attack of the cell components would become a benefit. On the other hand, it will decrease the solubility of alumina in such a bath. However, because such a melt has been considered and seems to be interesting in the future, same part of the experimental work in molten fluorides was focused on the investigation of sulphate ions in a melt with CR lower than 2.

The arrow in Figure 4.73 shows the composition of the supporting electrolyte containing alumina saturated mixture of NaF-40 mol% AlF_3 with CR = 1.5 in which the electrochemical behaviour of the sulphate anions added, again as Na_2SO_4, was investigated, and the results are shown in this chapter. The temperature of the melt was kept at 850 ºC but the electrodes were made of the same material as in the previous two chapters (gold working electrode and platinum counter electrode) and the potential was monitored versus the aluminium reference electrode.

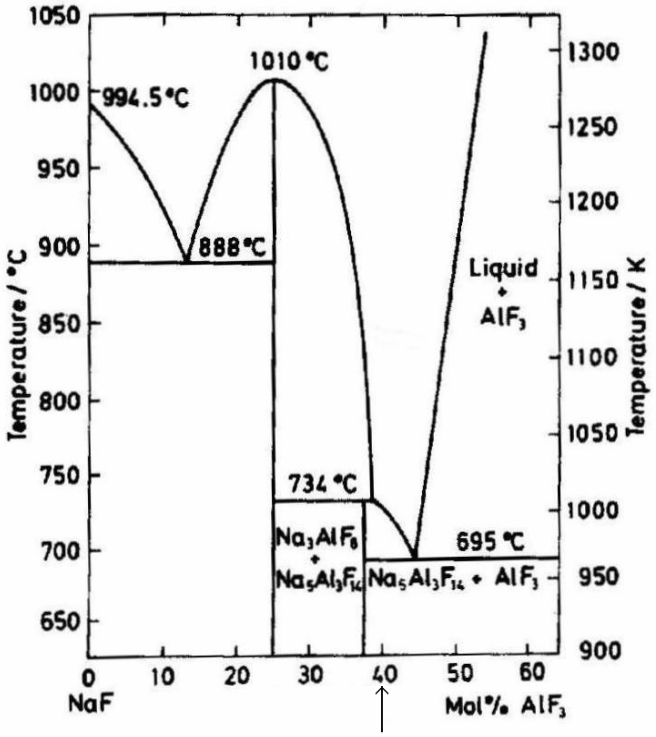

Figure 4.73 The binary phase diagram of NaF-AlF_3 [114]. The arrow indicates the melt composition of CR = 1.5.

- *Cyclic voltammetry*

Figure 4.74 shows the CVs of the electrolyte before and after addition of sodium sulphate. The voltammograms of the melt without sulphate are similar to the voltammograms of the supporting electrolyte in the previous two chapters. When sulphate was added two reduction waves A (~ 1.43V) and B (~ 1.22V) appeared associated with two oxidation peaks A` (~ 1.55V) and B` (~ 1.35V) in the subsequent anodic scan. Additionally, unlike the above described systems sulphate additions in this melt gave rise to a couple of small, sharp, anodic signals starting from about 1.6 V up to 2.1 V. Such signals usually indicate gas formation. In this case it means that the sulphur species formed during reduction and oxidized in the following scan are evolved in the form of gases. The evolution of the different waves with the potential is visible in Figure 4.75. The first scan halted at 1.4 V already showed small signals between 1.7-1.9 V caused by gas evolution and their intensity was increasing while the potential was stepped further to more cathodic values up to 1.2 V. Then the current of the gas peak formation reached a constant current and remained independent of the stepped potential.

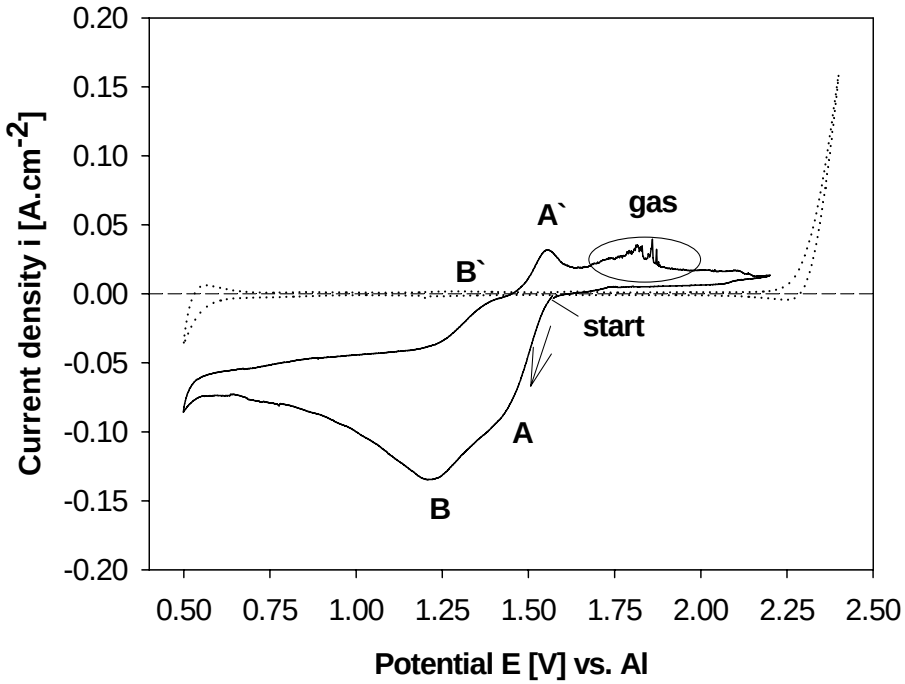

Figure 4.74 CVs recorded in the mixture of NaF-40 mol% AlF_3 saturated by Al_2O_3 before (dotted line) and after addition of $4.58 \cdot 10^{-5}$ mol.cm^{-3} Na_2SO_4 (added concentration) on Au working electrode; T = 850 ºC, v = 300 mV.s^{1}.

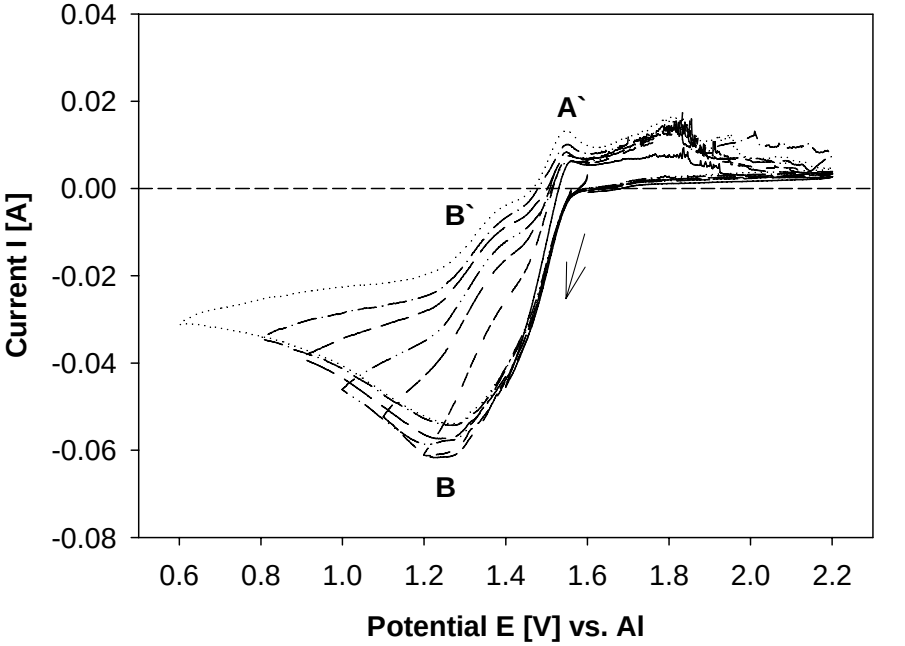

Figure 4.75 Voltammograms of the NaF-40 mol% AlF_3 melt saturated by Al_2O_3 with addition of 7.52 10^{-5} mol.cm^{-3} Na_2SO_4 (added concentration) obtained at 300 mV.s^{-1} and at different cathodic vertex potentials, T = 850 ºC.

It must be mentioned that a few complications accompanied the investigation of this system. One of them is connected with the unstable nature of sodium sulphate at the working conditions. Figure 4.76 shows the unpredictable decrease of the current for the second sulphate addition (dotted line) instead of an expected increase. This caused a problem to estimate the concentration of sulphate accurately. Therefore the amount of sulphate in the melt must be considered only as approximate. Because the surface of the working electrode was not attacked and no deposition was observed on its surface it is believed that sulphur was escaping from the furnace with the gas or trapped as sulphate on small particles of the electrolyte or as volatile sulphurous species formed during the experiment. The second explanation appears to be more likely when taking into account that such behaviour was not observed at higher temperatures in molten fluorides and at similar temperatures in the simple NaCl melt. Moreover, voltammograms in this system repeatedly showed signals corresponding to gas evolution.

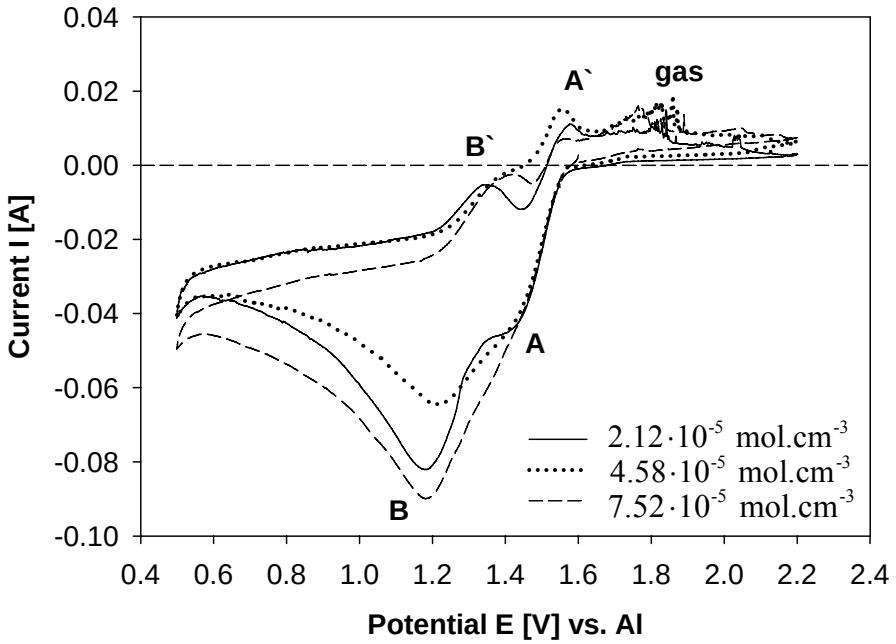

Figure 4.76 Voltammograms recorded in cathodic direction for different concentrations of sulphate added to alumina-saturated mixture of NaF-40 mol% AlF_3. T = 850 ºC, v = 300 $mV.s^{1}$.

Figure 4.77 offers an overview of the signals when the sweep rate varied from 150-1000 $mV.s^{-1}$. It can be observed that the cathodic peak A is visible only at low sweep rates (< 400 mV/s) while at higher sweep rates it tends to merge with the wave B which increases with the sweep rate.

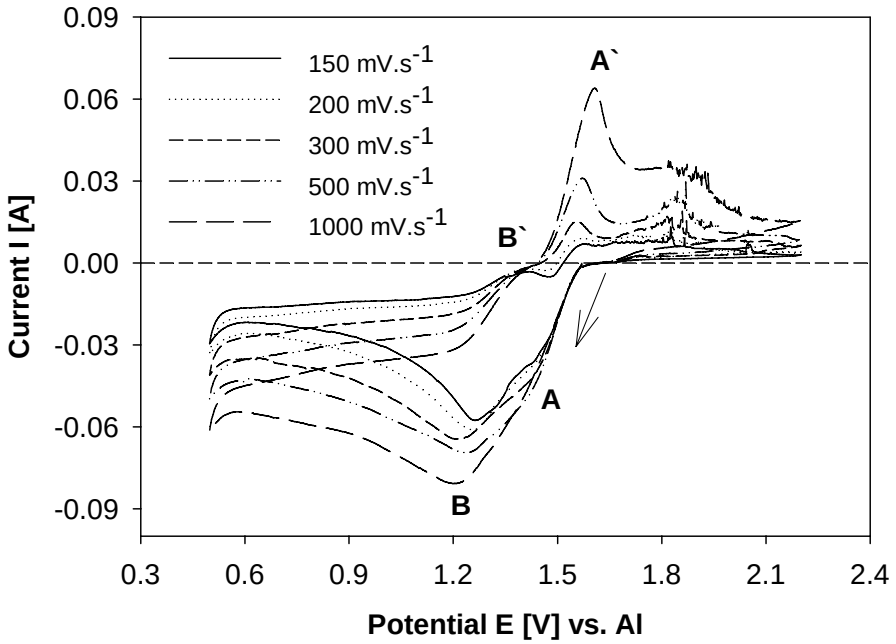

Figure 4.77 Voltammograms of $4.58 \cdot 10^{-5}$ mol.cm^{-3} Na_2SO_4 in an alumina-saturated NaF-40 mol% AlF_3 mixture obtained at 850 ºC on an Au electrode.

- *Square wave voltammetry*

Square wave voltammetry (SQWV) was performed on this system at amplitudes 15, 20 and 25 mV and frequencies 8, 20, 50, 100 and 150 Hz. More information about the system was obtained after simulation of the experimentally obtained SQWV curves. Figure 4.78 shows an example of the curves obtained and the simulated peaks at 100 Hz. The grey solid line represents the curve obtained experimentally after sulphate addition to the fluoride mixture. The best fit was reached assuming a quasi-reversible system exchanging four electrons (dotted line) at 1.5 V corresponding to signal A on the CV and three electrons (dashed line) at 1.3 V matching to peak B.

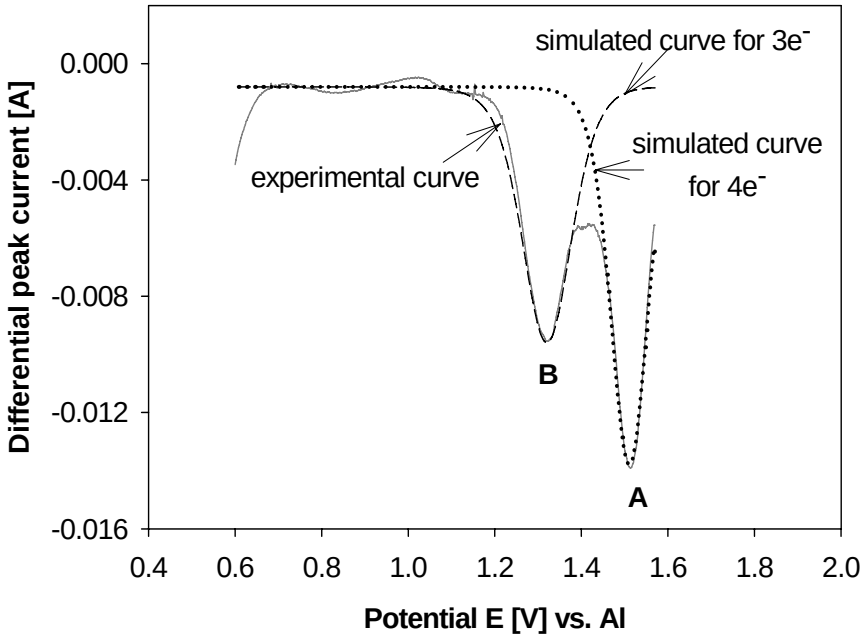

Figure 4.78 Square wave voltammogram experimentally obtained and simulated in an alumina-saturated NaF-40 mol% AlF_3 mixture containing $2.12 \cdot 10^{-5}$ mol.cm^{-3} Na_2SO_4 (added) at A = 15 mV and f = 50 Hz (corresponding to a sweep rate approximately 97 mV.s^{-1}), T = 850 ºC.

SQWV results has thus revealed that the reduction process of the sulphate anions probably involves more electrons in the cathodic steps in a very acidic electrolyte than in the melts with CR = 3 and 2. The final products might be S (0) or S (-II) formation. CVs showed also that the volatile species are formed at these experimental conditions. If S (0) (volatile at 850 ºC) is produced, this could be also an explanation why no sulphide was detected by iodimetric titration of the solidified samples of the electrolyte.

4.4.5 Molten Na_2SO_4-NaF-AlF_3 with CR = 1.2 saturated by Al_2O_3

The second eutectic point in the binary phase diagram of NaF-AlF_3 shown in Figure 4.79 lies around 45 mol% of AlF_3 with the melting point 700 ºC. Such a melt rich in AlF_3 has a CR = 1.2 and was used as a supporting electrolyte for the investigation of sulphate ions in the set of experiments presented in this chapter. The temperature of the electrolyte was kept at 755 ºC and because the melt was held in Alsint crucibles, a small amount of Al_2O_3 was added in order to saturate the melt and to prevent a chemical attack of the equipment. Also in this case gold and platinum were used as the working and counter electrodes respectively, and the potential refers to the aluminium electrode.

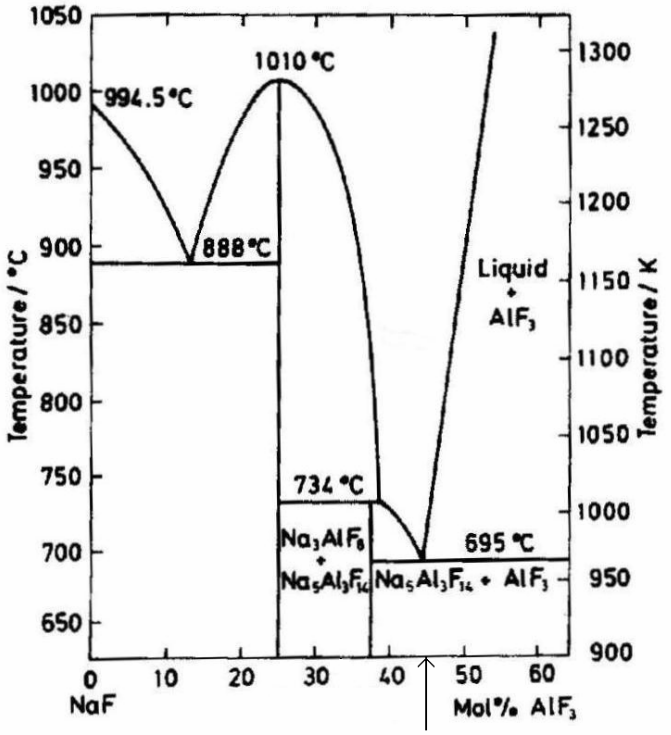

Figure 4.79 The binary phase diagram of NaF-AlF_3 [114]. The arrow indicates the melt composition of CR = 1.2.

Because density data for the electrolyte of a such composition were not available, the concentration of added sulphate ions is thus given only as weight percent. The CV of the electrolyte, shown in Figure 4.80, does not differ substantially from those presented in the previous chapters. Small amounts of Na_2SO_4 gave rise to a complex system of signals. Two main reduction peaks A and B located at potentials around 1.48 V and 1.2 V respectively and one small cathodic wave C at around 0.95 V can be observed in the voltammetric curves. Each of them is associated with one oxidation signal A` (~ 1.6 V), B` (~ 1.37 V) and C` (~ 1 V) respectively. Additionally a system of anodic peaks marked by an ellipse between 1.7-1.9 V indicating gas formation is also present in this system.

When the varying cathodic potentials were applied starting from 1.6 V in 0.1 V steps ending at 0.5 V, a set of voltammograms was recorded where the peak couples could be identified. These CVs are presented in Figure 4.81 documenting that the signals A-A`, B-B` and C-C` are the redox couples of the electrochemical behaviour of sulphur containing species. Moreover, changing the second vertex potential revealed that the anodic signals resulting in gas formation could be associated with the cathodic process taking place at the potential of peak B.

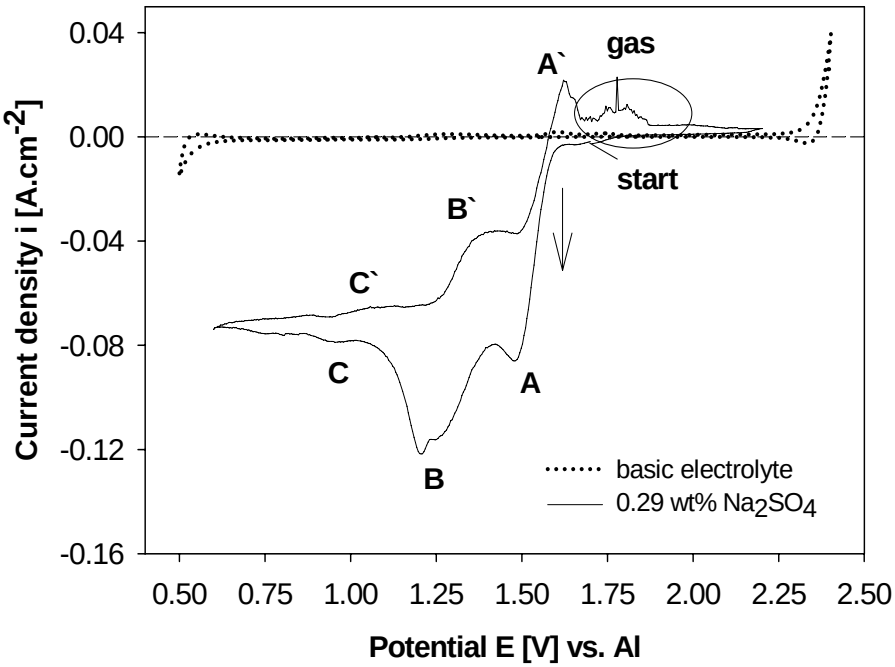

Figure 4.80 Cyclic voltammograms of the supporting electrolyte of NaF - 45 mol% AlF_3 saturated by alumina (dotted line) and containing 0.29 wt% of Na_2SO_4 (solid line). T = 755 ºC, v = 300 $mV.s^{-1}$.

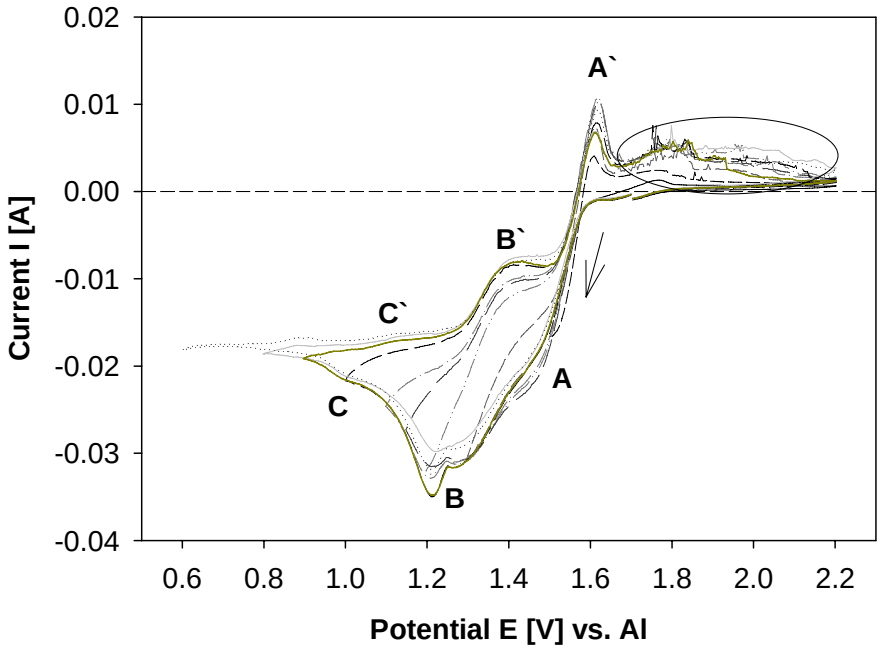

Figure 4.81 Voltammograms of NaF-45 mol% AlF_3 saturated by Al_2O_3 with addition of 0.4 wt% Na_2SO_4 (added concentration) obtained at 300 $mV.s^{-1}$ and at different cathodic vertex potentials.

The same difficulties found in the study described in previous chapter were also found in this electrolyte. The actual concentration of sulphate ions in this melt seemed to differ somewhat from the concentration of added sulphate and the reason is again probably due to the escaping volatile species of one of the sulphur compounds formed in the electrolyte. Besides, the increase of sulphate amount in the melt with each addition caused another phenomenon. Increasing sulphate concentration in the melt led to current increase in the voltammograms and apparently causes also a shift of the whole system to the more negative current values as it can be observed from the CVs in Figure 4.82. If the cathodic process is dominating over the anodic one this might lead to such a shift of the whole system to more negative current values.

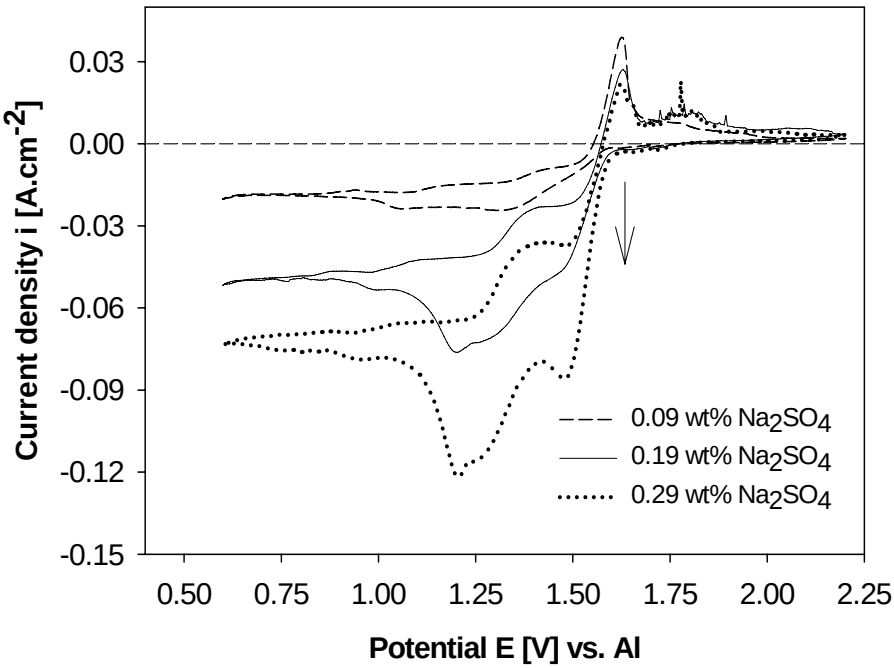

Figure 4.82 CVs of the NaF-45 mol% AlF_3 system saturated by Al_2O_3 at different concentrations of Na_2SO_4, T = 755 ºC, v = 300 $mV.s^{-1}$.

As in the previous system, the peak A is visible only at sweep rates up to 500 $mV.s^{-1}$. At higher sweep rates it merges with peak B to one wave as it is documented in Figure 4.83.

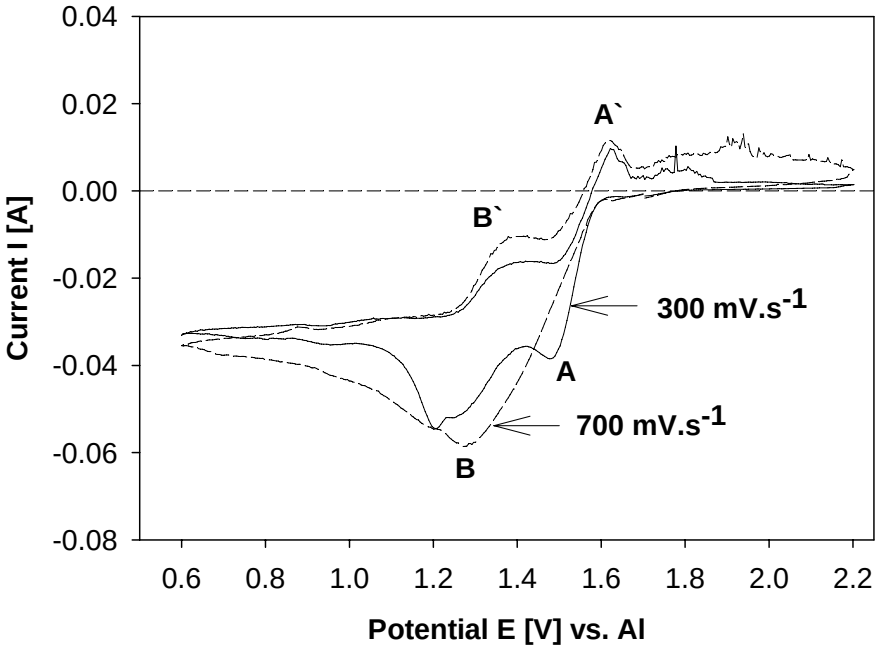

Figure 4.83 CV of 0.29 wt% Na_2SO_4 in alumina-saturated mixture of NaF-45 mol% AlF_3 at 300 and 700 $mV.s^{-1}$ and temperature 755 ºC.

To check whether the rate of the electron transfer dominates over mass transport, the current data were normalised and plotted as $i/v^{1/2}$ as a function of E. This is a useful way how to detect a change in the rate of diffusion. For a reversible system such normalised voltammograms superimpose at all sweep rates. Any variation from the reversible behaviour leads to increasing peak separation with increasing sweep rate and the peak height is also affected and reduces compared to that of a reversible system. Such normalised voltammograms are presented in Figure 7.84 for sweep rates ranging from 1000 – 3000 $mV.s^{-1}$. In the case of peak B it is clearly shown how the peak separation increases and the peak current decreases with increasing sweep rate. This indicates that the reduction process at the potential of peak B is probably changing from reversible to quasi-reversible and at high sweep rates ($\geq$1000 $mV.s^{-1}$) it becomes irreversible. Because peak A cannot be distinguished at such high sweep rates, the Figure 4.84 does not say anything about the reversibility character of peak A.

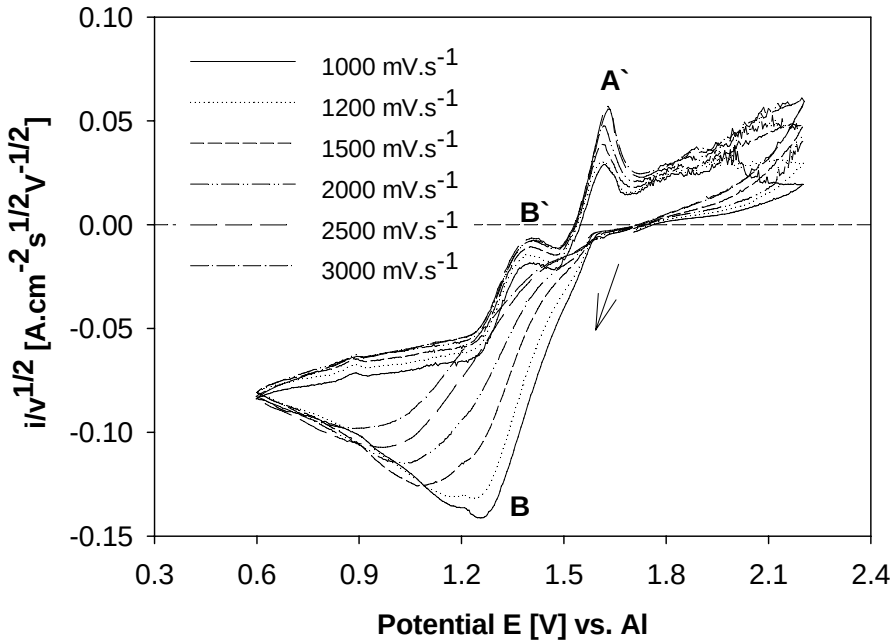

Figure 4.84 Normalised CVs of 0.29 wt% Na_2SO_4 in the alumina-saturated mixture of NaF-45 mol% AlF_3 at 755 ºC.

To confirm the formation of an insoluble product, a potential was held at 1.25 V for 10, 30 and 60 seconds and afterwards the cyclic voltammograms were recorded in the anodic direction (see Figure 4.85). As it can be seen from the figure, the anodic peak A` in the reverse scans increases linearly with the applied time. The result supports the conclusion that an insoluble species are formed during the reduction process. Besides, the signals corresponding to gas evolution in the anodic scan increased also with the retention time.

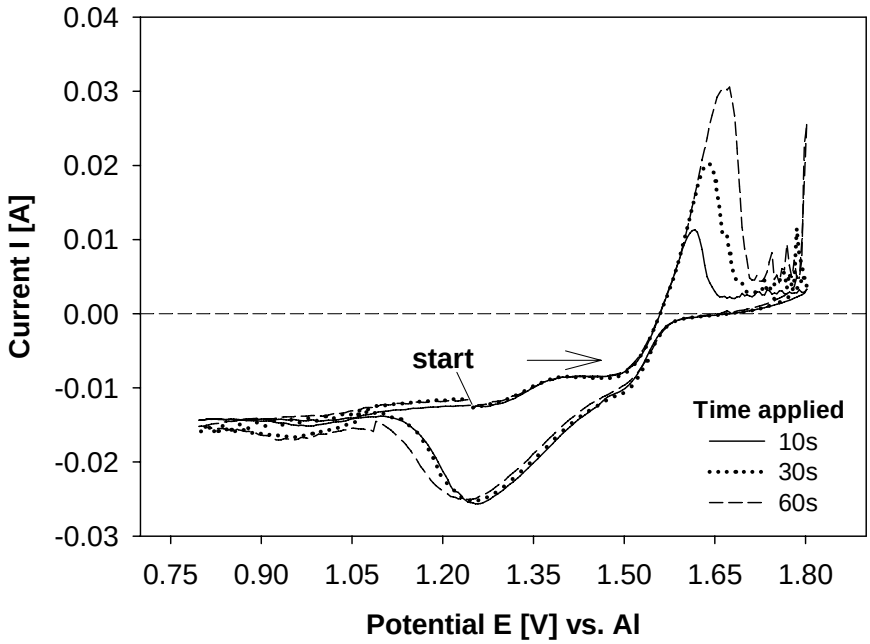

Figure 4.85 Voltammograms of 0.09 wt% Na_2SO_4 recorded on an Au electrode in the alumina-saturated mixture of NaF-45 mol% AlF_3 after applying a potential of 1.25 V for various period of time. T = 755 ºC, v = 300 $mV.s^{-1}$.

- *Square wave voltammetry*

SQWV was also performed on this system at amplitudes of 15, 20 and 25 mV and frequencies of 8, 20, 50, 100 and 150 Hz. More information about the system was obtained after simulation of the experimentally obtained SQWV curves. Figure 4.86 shows the experimentally obtained and simulated voltammograms at 100 Hz. The solid line represents the curve obtained experimentally after sulphate addition to the electrolyte. When a quasi-reversible system was assumed, the best fit was found for the curves describing a reduction step involving four electrons at 1.45 V (dashed line) which corresponds to the signal A on the CV. The simulation of the second cathodic step was more complicated and is questionable. However, it appears that a certain fit was reached for two electrons (dotted curve) at the potential 1.3 V matching to peak B. This could mean that the sulphate anions are probably reduced also in this system to the low oxidation states in spite of the fact, that the presence of sulphide anions was not confirmed by iodimetric titrations of the electrolyte samples.

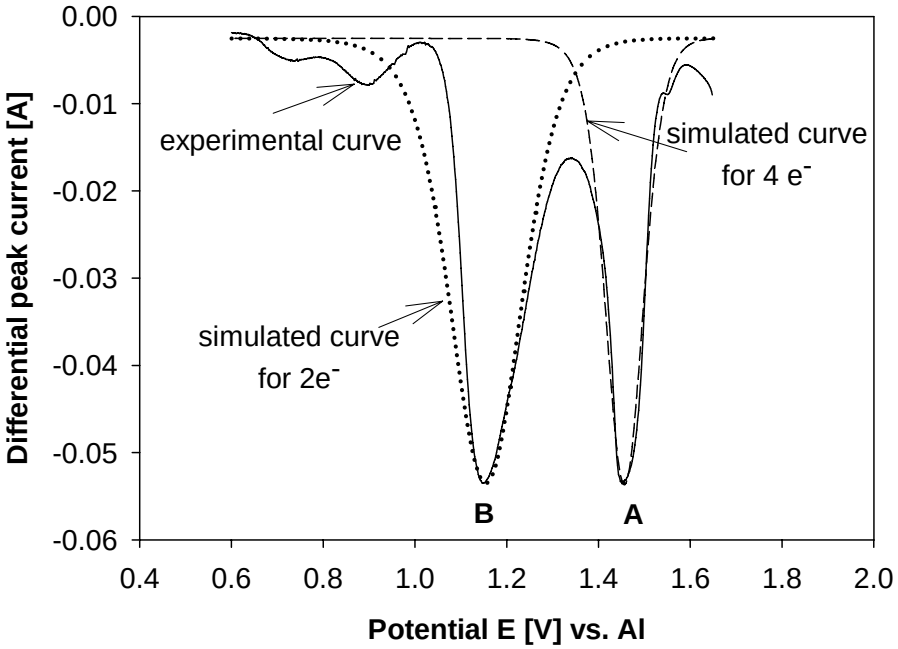

Figure 4.86 SQWVs experimentally obtained and simulated in alumina-saturated NaF-45 mol% AlF_3 mixture containing 0.29 wt% Na_2SO_4 at A = 25 mV and f = 100 Hz (corresponding to a sweep rate approximately 195 $mV.s^{-1}$), T = 755 ºC.

4.4.6 Conclusions

Voltammetry studies suggest that the electrochemical behaviour of the sulphate anion depends on the composition of the molten electrolyte.

For the fluoride mixture with CR = 3 two reduction waves were detected while the sulphate anions were reduced only in one cathodic step in the electrolyte with a composition similar to the industrial bath (with CR = 2). Because the temperature difference in these two systems was only 40 ºC, it is not likely that the temperature variation was responsible for the observed changes. On the other hand, the difference in the electrolyte composition was markedly greater (CR = 2 contains 8 mol% AlF_3 more than CR = 3) and it is believed that this can change the electrochemical behaviour of the sulphate anions. However, the results from the electrochemical measurements indicate that the first reduction step might be the same or very similar in both systems: a step involving three electrons with a preceding chemical reaction. The chemical step could be ascribed to thermal decomposition of Na_2SO_4 since the experimental temperature was above 900 ºC which is the temperature where the Na_2SO_4 species is destabilized.

In the electrolytes with CR = 1.5 and 1.2 the gas evolution observed in the anodic scan is the most important feature which differs from the systems with higher CR. Thus a formation of different species in the cathodic scan seems to be probable. The gaseous compounds are probably associated with the second reduction peak in both electrolytes. After comparison of the cyclic voltammograms, square wave voltammograms and their simulations, it appears that the mechanism of sulphate reduction might be similar in these two very acidic melts. It is also concluded, that more electrons involved in the two cathodic steps. S (VI) thus might be reduced to S (0) or S (-II) in spite of the fact that sulphide was not detected by iodimetric analysis in the solidified samples. However, some differences exist also in these two systems, such as an insoluble product formation in the electrolyte with CR = 1.2. The system with CR = 1.2 revealed also a shift of the cyclic voltammograms to more negative currents, for cathodic as well as anodic peaks, indicating that the reduction process dominates over oxidation. Additionally, the reduction of sulphate anions seems to undergo a transition from reversible to irreversible behaviour at sweep rates higher than 1000 $mV.s^{-1}$. When comparing the experimental parameters such as temperature (100 ºC difference) and composition (5 mol% AlF_3 difference) in both acidic melts it is difficult to say which of the two parameters is responsible for the differences in the electrochemical behaviour of sulphate ions observed in those two electrolytes.

5 Concluding remarks

The present work shows that the electrochemical behaviour of the sulphate anions is not the same in the used chloride and fluoride electrolytes.

While in the simple NaCl melt the sulphate anions are reduced in a single cathodic step involving two electrons, in a mixture of $CaCl_2$-NaCl (10-90 mol %) they undergo one-electron reduction. In both cases, a following chemical reaction seems to couple the charge transfer. In pure NaCl melt the chemical reaction is probably decomposition of sulphite to sulphur oxides while in the electrolyte modified by $CaCl_2$ the electroactive species seem to be SO_3 which is reduced to SO_3^- ions that further chemically combine together. A similar reduction process for the sulphate as in the electrolyte consisting only NaCl was revealed in the eutectic LiCl-KCl mixture. The different behaviour of the sulphate in the chloride melts was explained to be due to the variations of the oxoacidity of the supporting electrolytes. Generally the melts containing $CaCl_2$ are considered to be more oxoacidic than the NaCl or LiCl-KCl melts. The electrochemical reduction of sulphate ions appears to be diffusion controlled in all the above mentioned systems at the sweep rates where the effect of the chemical reaction can be neglected.

In the fluoride melts with CR = 3, 2, 1.5 and 1.2 the sulphate reduction seems to involve more electrons than in the chlorides. The charge transfer in these electrolytes is accompanied by a preceeding chemical reaction which seems to be the thermal decomposition of Na_2SO_4. It is probable that different reduction products respectively intermediates which take place in the electrochemical processes in these melts are formed. The reason for that can probably be explained by the increasing content of AlF_3 rather than by the temperature difference, at least for the results obtained in the electrolytes with CR = 3 and 2. In very acidic melts with CR = 1.5 and 1.2 the cyclic voltammograms showed in the reverse scan an extensive gas formation which was not detected in any of the other studied melts. From the simulations of the square wave voltammograms it also appears that sulphate ions can be reduced to very low oxidation states, S (0) or S (-II), in the bath containing high amounts of AlF_3.

Analysis of the melt samples after the experiments did not show evidence of sulphide formation in any of the used electrolytes, which could mean that sulphate was not reduced to sulphide in any of the systems. Though it must be mentioned here that it could also be due to the low concentration of sulphate which was added to the cell and even smaller amount of sulphate eventually converted to sulphide. One more reason could be the problem with unstable electrolyte or electrochemically active species which were escaping from the furnace with the gas outlet and thus decreasing their concentration.

References

1. http://www.world-aluminium.org/iai/stats/index.asp.
2. Grjotheim K. and Kvande H., Introduction to Aluminium Electrolysis 2nd ed. 1993, Aluminium-Verlag.
3. Thonstad J., Fellner P., Haarberg G. M., Híveš J., Kvande H., and Sterten Å., Aluminium Electrolysis. Fundamentals of the Hall-Héroult Process 3rd ed. 2001, Aluminium-Verlag.
4. Grjotheim K., Krohn C., Malinovský M., Matiašovský K., and Thonstad J., Aluminium Electrolysis. Fundamentals of the Hall-Héroult Process 2nd ed. 1982, Aluminium-Verlag.
5. Metson J. B., Proc. 9th Int. Symp. Light Metal Prod., 1997, Trondheim.
6. Johansen H. G., Thonstad J., and Sterten A., Light Metals, 1977, p. 253-261.
7. Goodes C. G. and Algie S. H., The partitioning of trace impurities between aluminium, cryolite and air - A laboratory study, Light Metals, 1989, p. 199-207.
8. Augood D. R., Impurities distribution in alumina reduction plants, in Light Metals, Proceedings of Sessions 109th AIME Annual Meeting, 1980, Las Vegas, Nevada.
9. Vorobyev G. M., Manina A. A., and Moiseev A. P., Tsvet. Met., 1967, 40, (3), p. 62.
10. Kerouanton A. and Badoz-Lambling J., Comportment chimique et électrochimique de composes du phosphore dans la cryolithe fondu, Rev. Chim. Min., 1974, 11, p. 223-228.
11. Solli P. A., Current Efficiency in Aluminium Electrolysis Cells. 1993, NTH Trondheim.
12. Thisted E. W., Electrochmical Properties of Phosphorus Compounds in Fluoride Melts. 2003, NTNU Trondheim.
13. Frolova E. B., Dobrokhotov V. B., and Tsyplakov A. M., Trudy VAMI, 1974, 89.
14. Tingle W. H., Petit J., and Frank W. B., ALUMINIUM, 1981, 57, p. 286.
15. Thonstad J., Nordmo F., Rolseth S., and Paulsen J. B., Light Metals, 1978, 2, p. 463-479.
16. Utne I., Paulsen K. A., and Thonstad J., The emission of carbonyl sulphide from prebake and soderberg aluminium cells, Light Metals, 1998, p. 293-301.
17. Kimmerle F. M., Noël L., Pisano J. T., and Mackay G. I., COS, CS_2 and SO_2 emissions from prebaked Hall Héroult cells, Light Metals, 1997, p. 153-158.
18. Firsanova L. A. and Belyaev A. I., Tsvet. Met., 1962, 5, (2), p. 88.
19. Hunt J., Petroleum Geochemistry and Geology 2nd ed 1996, New York, W. H. Freeman and Co.
20. Gilmore G. P. and Bullough V. L., A study on the effects of anode coke sulfur content on the operation of side pin Soderberg cells, Light Metals, 1982, p. 741-752.
21. Burnakin V. V., Polyakov P. V., Zalivnoy V. I., Popkova R. K., and Mozhayev V. M., Behaviour of sulphate ion in cryolite-alumina melts, Sov. J. Non-Ferrous Met. Res., 1982, 10, p. 279-285.
22. Bullough V. L., Marshall H. C., and McMinn C. J., Some effects of sulfur in petroleum coke on the performance of anodes in prebake alumina reduction cells,

Light Metals, 1971.
23. Barillon E. and Pinoir J., Use of high-sulphur cokes in the production of prebake anodes, Light Metals, 1977, p. 289-299.
24. Rhedey P., A review of factors affecting carbon anode consumption in the electrolytic production of aluminum, Light Metals, 1971.
25. Jones S. S., Hildebrandt R. D., and Hedlund M. C., Influence of high-sulfur cokes on anode performance, Light Metals, 1979.
26. Houston G. J. and Øye H. A., Reactivity testing of anode carbon materials, Light Metals, 1985.
27. Sørlie M., Kuang Z., and Thonstad J., Effect of sulphur on anode reactivity and electrolytic consumption, Light Metals, 1994, p. 659-665.
28. Hume S. M., Fisher W. K., Perruchoud R. C., Metson J. B., Terry R., and Baker K., Influence of petroleum coke sulphur content on the sodium sensitivity of carbon anodes, Light Metals, 1993, p. 535-541.
29. Dorreen M. M. R., Chin D. L., Lee J. K. C., Hyland M. M., and Welch B. J., Sulfur and fluorine containing anode gases produced during normal electrolysis and approaching an anode effect, Light Metals, 1998, p. 311-316.
30. Oedegard R., Roenning S., Sterten A., and Thonstad J., Sulphur containing compounds in the anode gas from aluminium cells, a laboratory investigation, Light Metals, 1985, p. 661-670.
31. Hanson D. R., Ravinshankara A. R., and Solomon S., Heterogeneous reactions in sulfuric acid aerosols; A framework of model calculations, J. of Geophys. Res., 1995, 99, p. 3515-3629.
32. http://www.slovalco.sk/web/homepage_ns.nsf/mainFrameset?OpenFrameset.
33. Frosta O. E., personal communication. 2007: Hydro Årdal
34. Harnisch J., Borchers R., and Fabian P., COS, CS_2 and SO_2 in aluminium smelter exhaust, Environ, Sel. and Pollut. Res., 1995, 2, (3), p. 161-162.
35. Sillinger N. and Horvath J., Light Metals, 1990, p. 369-376.
36. LaCamera A. F., Ray S. P., Liu X., Kozarek R. L., and Roddy J. L., Methods and Apparatus for reducing sulfur impurities and improving current efficiencies of inert anode aluminium production cells. 2004.
37. Strømmen S. O., Bjørnstad E., and Wedde G., SO_2 emission control in the aluminium industry, Light Metals, 2000, p. 351-356.
38. http://www.webelements.com/webelements/elements/text/S/biol.html.
39. Holleman A. F. and Wiberg E., Inorganic Chemistry 34th ed 2001, Walter de Gruyter.
40. Delarue G., Chemical reactions involving O^{2-} and S^{2-} ions in the molten LiCl-KCl eutectic, Bulletin de la Societe Chimique de France, 1960, p. 1654-1659.
41. Delarue G., Chemical properties of the molten LiCl-KCl eutectic. II.-Sulphur, sulphides, sulphites, sulphates, Bulletin de la Societe Chimique de France, 1960, p. 906-910.
42. Bodewig F. G. and Plambeck J. A., Electrochemical behaviour of sulfide in fused LiCl-KCl eutectic, J. Electrochem. Soc., 1969, 116, (5), p. 607-611.
43. Gruen D. M., McBeth R. L., and Zielen A. J., Nature of sulfur species in fused salt solutions, J. Am. Chem. Soc., 1971, 93, p. 6691-6693.
44. Giggenbach W., The blue solutions of sulfur in salt melts, Inorganic. Chem., 1971, 10, (6), p. 1308-1311.

45. Kennedy J. H. and Adamo F., Electrochemistry of sulfur in LiCl-KCl eutectic, J. Electrochem. Soc., 1972, 119, (11), p. 1518-1521.
46. Cleaver B., Davies A. J., and Schiffrin D. J., Properties of fused polysulphides - V. voltammetric studies on sulphur and polysulphides in fused KSCN and LiCl-KCl eutectic, Electrochimica Acta, 1973, 18, p. 747-760.
47. Weaver M. and Inman D., The sulphur-sulphide electrode in molten salts - I. Chronopotentiometric behaviour in lithium chloride - potassium chloride eutectic, Electrochimica Acta, 1975, 20, p. 929-936.
48. Marassi R., Mamantov G., and Chambers J. Q., Electrochemical behaviour of sulphur and sulphide in molten sodium tetrachloroaluminate saturated with NaCl, J. Electrochem. Soc., 1976, 123, (8), p. 1128-1132.
49. Paulsen K. A. and Osteryoung R. A., Electrochemical studies on sulfur and sulfides in $AlCl_3$-NaCl melts, J. of Am. Chem. Soc., 1976, 98, (22), p. 6866-6872.
50. Minh N. Q., Loutfy R. O., and Yao N. P., The electrolysis of aluminium sulfide in molten chlorides, Light Metals, 1982, p. 267-277.
51. Loutfy R. O., Keller R., and Yao N. P., Method of winning aluminum metal from aluminous ore. 1981.
52. Grjotheim K. and Welch B. J., Impact of alternative processes for aluminium production on energy requirements, Light Metals, 1981, p. 1037-1050.
53. Sportel H. and Verstraten C. W. F., Method and apparatus for the production of aluminium from alumina ore by aluminium sulfide process. 1999.
54. Xiao Y., Soons J., Lans S. C., van Sandwijk A., Reuter M. A., and van der Plas D. W., Sulfidation of Al_2O_3 with CS_2 gas Light Metals 2003 Métaux Légers, 2003, p. 101-117.
55. Lans S. C., Bohte J., Xiao Y., van Sandwijk A., Reuter M. A., and van der Plas D. W., The possibilities of electrowinning Al from Al_2S_3, Light Metals 2003 Métaux Légers, 2003, p. 63-75.
56. Minh N. Q., Loutfy R. O., and Yao N. P., The electrochemical behaviour of Al_2S_3 in molten $MgCl_2$-NaCl-KCl eutectic, J. Electroanalytical Chem., 1981, 131, p. 229-242.
57. Minh N. Q., Loutfy R. O., and Yao N. P., The electrolysis of Al_2S_3 in $AlCl_3$-$MgCl_2$-NaCl-KCl melts, J. of Applied Electrochemistry, 1982, 12, p. 653-658.
58. Minh N. Q. and Yao N. P., The electrolysis of aluminium sulfide in molten fluorides, Light Metals, 1983, p. 643-650.
59. Minh N. Q. and Yao N. P., The electrochemical behaviour of sulfide ions in molten cryolite, in Proceedings of the fourth international symposium on Molten Salts, 1984.
60. Minh N. Q. and Yao N. P., The anodic reaction of sulfide ions at graphite electrodes in molten cryolite, J. Electrochem. Soc., 1984, 131, (10), p. 2279-2282.
61. Xiao Y., van der Plas D. W., Bohte J., Lans S. C., van Sandwijk A., and Reuter M. A., Electrolysis of aluminium sulphide in molten salt, in 7th International Symposium on Molten Salts, Chemistry and Technology, 2005, Toulouse, France.
62. Pushkareva S. A., J. Applied Chem. U.S.S.R., 1959, 32.
63. Liu C. H., Electrode potentials in molten lithium sulpfate-potassium sulfate

eutectic, J. Phys. Chem., 1962, 66, p. 164-166.
64. Johnson K. E. and Laitinen H. A., Electrochemistry and reactions in molten Li_2SO_4-Na_2SO_4-K_2SO_4, J. Electrochem. Soc., 1963, 110, p. 314-318.
65. Senderoff S., Klopp E. M., and Kronenberg M. L., Eighth and Ninth Quarterly Technical Progress Reports, Contract NORD-18240. 1960.
66. Woodall B. and quoted by Laitinen H. A., Talanta 12, 1965.
67. Wrench D. M. and Inman D., A chronopotentiometric investigation of the dissociation of sulphate ions in molten equimolar NaCl-KCl at 750 ºC, Electrochimica Acta, 1967, 12, p. 1601-1608.
68. Burrows B. W. and Hills J. G., Electrochemical studies of molten alkali sulphates, Electrochimica Acta, 1970, 15, p. 445-458.
69. Burrows B. W. 1965: Southampton.
70. Hoa T. K. and Welch B. J., Electrolysis of molten salt solutions containing $PbSO_4$. I. Reactions associated with the deposition of lead, J. of Applied Electrochemistry, 1973, 3, p. 45-52.
71. Jenkins R. A. and Welch B. J., Electrolysis of molten salt solutions containing $PbSO_4$. II. Products formed when using a carbon anode, J. of Applied Electrochemistry, 1973, 3, p. 53-60.
72. Sequeira C. A. C. and Hocking M. G., Polarization measurements on solid platinum-molten sodium sulphate-sodium chloride interfaces, Electrochimica Acta, 1978, 23, p. 381-388.
73. Rapp R. A. and Goto K. S., Proceedings of the Second International Symposium on Molten Salts, 1978, Pittsburg, USA.
74. Fang W. C. and Rapp R. A., Electrochemical reactions in a pure Na_2SO_4 melt, J. Electrochem. Soc., 1983, 130, (12), p. 2335-2341.
75. Park C. O. and Rapp R. A., Electrochemical reactions in molten Na_2SO_4 at 900 ºC, J. Electrochem. Soc., 1986, 133, (8), p. 1636-1641.
76. Tilquin J.-Y., Duveiller P., Gilbert J., and Claes P., Electrochemical behaviour of sulfate in sodium silicates at 1000 ºC, Electrochimica Acta, 1997, 42, (15), p. 2339-2346.
77. Rasmussen S. B., Eriksen K. M., and Fehrmann R., Sulfate solubility and sulfato complex formation of V(V) and V(IV) in pyrosulfate melts, in Proceedings of the Jondal 2000 International Symposium 2001, Norway.
78. Wartena R., Winnick J., and Pfromm P. H., Recycling wood pulping chemicals by molten salt electrolysis: cyclic voltammetry of mixtures containing $Na_2CO_3$and Na_2SO_4, J. of Applied Electrochemistry, 2002, 32, p. 415-424.
79. Baimakov Y. V. and Vetyukov M. M., Electrolysis of Fused Salts 1966, Metallurgiya, Moscow, 410-412.
80. Mashovets V. P. and Grjotheim c. b., Elektrometallurgiya alyuminiya 1938, ONTI, Moscow.
81. Abramov G. A., Vetyukov M. M., Gupalo I. P., Kostyukov A. A., and Lozhkin L. N., Teoreticheskie osnovy elektrometallurgii alyuminiya, Metallurgizdat 1953, Moscow.
82. Burnakin V. V., Zalivnoy V. I., Polyakov P. V., Mozhayev V. M., and Tsyplakov A. M., Study of the dependence of anode overvoltage on the sulfur content in the anode mass, Sov. J. Non-Ferrous Met., 1979, 9, p. 57-58.
83. Burnakin V. V., Zalivnoy V. I., Polyakov P. V., Arskaya L. P., and Bagaev Y. I.,

Study of the electrochemical behaviour of carbon anodes under conditions involving the use of high-sulfur coke in the aluminium industry, Fiz. Chim. Electrochim. Rasplavl., 1980.
84. Burnakin V. V., Arskaya L. P., Zalivnoy V. I., Polyakov P. V., and Ofitserov V. F., The use of high-sulfur cokes in the production of anode paste, Sov. J. Non-Ferrous Met., 1981, 6, p. 68-70.
85. Burnakin V. V., Popkova R. K., Zalivnoy V. I., Polyakov P. V., and Kolosova V. I., Behaviour of sulphate ion during the electrolysis of aluminium, Sov. J. Non-Ferrous Met. Res., 1983, 2, (4), p. 282-285.
86. Ambrová M., The reaction of sulphur compounds during aluminium electrowinning. 2006, Slovak technical University, Bratislava.
87. Stern K. H., High Temperature Properties and Thermal Decomposition of Inorganic Salts with Oxyanions 2001, CRC Press LLC.
88. Lee S. W., Hong K. S., Condrate R. A., Hapanowicy R. P., and Spezer R. F., J. Mater. Sci., 1992, cited by Tilquin, 27.
89. Castro M. A., Faulds K., Smith W. E., Aller A. J., and Littlejohn D., Identification of condensed-phase species on the thermal transformation of alkaline and alkaline earth metal sulphates on a graphite platform, Spectrochimica Acta Part B, 2004, 59, p. 827-839.
90. Warner N. A. and Ingraham T. R., Decomposition pressures of ferric sulphate and aluminum sulphate, Can. J. of Chem., 1960, 38, p. 2196-2202.
91. Gabčová J. and Malinovský M., Experimental determination and thermodynamic analysis of the phase diagram of the systems NaCl-Na_2SO_4 and NaCl-NaF, Chem. Papers, 1986, 40, (2), p. 201-213.
92. Grjotheim K., Halvorsen T., and Urnes S., The phase diagram of the system Na_3AlF_6-Na_2SO_4, Can. J. of Chem., 1959, 37, p. 1170-1175.
93. Matiašovský K. and Malinovský M., Chem. Zvesti, 1965, 19, p. 41-45.
94. Koštenská I. and Malinovský M., Chem. Zvesti, 1982, 36, p. 159.
95. Neumann B. and Bergve E., Z. Elektrochem., 1915, cited by Sequeira and Hocking 21.
96. FactSage. p. software for thermodynamic calculations, www.factsage.com.
97. Noel M. and Vasu K. I., Cyclic Voltammetry and the Frontiers of Electrochemistry 1990, Aspect Publications Ltd.
98. Pletcher D., Greef R., Peat R., Peter L. M., and Robinson J., Instrumental Methods in Electrochemistry 2001, Horwood Publishing.
99. Bard A. J. and Faulkner L. R., Electrochemical Methods. Fundamentals and Applications 2001, John Wiley & Sons, Inc.
100. http://www.epsilon-web.net/Ec/manual/Techniques/Pulse/pulse.html.
101. Ramaley L. and Krause M. S., Theory of square wave voltammetry, Analytical Chemistry, 1969, 41, (11), p. 1362-1369.
102. Chamelot P., Lafage B., and Taxil P., Using square-wave voltammetry to monitor molten alkaline fluoride baths for electrodeposition of niobium, Electrochimica Acta, 1997, 43, p. 607-616.
103. Wilson C. L. and Wilson D. W., Comprehensive Analytical Chemistry. Classical Analysis, Vol. 1B, 1960, Elsevier.
104. Tomíček O., Kvantitative Analysis 1950, Prague.
105. Čakrt M., Practicum of Analytical Chemistry 1989, Bratislava, Alfa.

106. Wilson C. L. and Wilson D. W., Comprehensive Analytical Chemistry. Classical Analysis, Vol. 1C, 1962, Elsevier.
107. Inman D. and Weaver M. J., Electrochemical studies of thin oxide films formed on platinum molten LiCl-KCl containing oxide ions, Electroanal. Chem. and Interfacial Electrochem., 1974, 51, p. 45-56.
108. Asakura A. and Mukaibo T., Anodic behaviour of platinum in the LiCl-KCl eutectic melt, Electrochimica Acta, 1968, 13, p. 881-890.
109. Haan A. and van de Poorten H. V., C. r. hebd. Séanc. Acad. Sci., Paris, 1965 cited by Asakura, 261.
110. Nicholson R. S. and Shain I., Theory of stationary electrode polarography. Single scan and cyclic methods apllied to reversible, irreversible, and kinetic systems. Analytical Chemistry, 1964, 36, (4), p. 706-723.
111. Nadjo I. and Savéant J. M., Linear sweep voltammetry: kinetic control by charge transfer and/or secondary chemical reactions., Electroanalytical Chem. and Interfacial Electrochem., 1973, 48, p. 113-145.
112. Picard G. S., Three-dimensional reactivity diagrams for reaction chemistry in molten chlorides, Molten Salt Forum, 1993/94, 1-2, p. 25-40.
113. Duruz J. J., Stehle G., and Landolt D., On the role of the electrode material during cathodic deposition of Na and Al from molten fluorides., Electrochimica Acta, 1981, 26, (6), p. 771-779.
114. Holm J. L. and Holm B. J., Acta Chem. Scand., 1973, 27, p. 1410.
115. Sadoway D. R., Inert anodes for the Hall-Héroult cell: the ultimate materials challenge, JOM, 2001, 53, (5), p. 34-35.